^{142}Pr GLASS SEEDS

FOR THE BRACHYTHERAPY OF PROSTATE CANCER

A Dissertation

by

JAE WON JUNG

Submitted to the Office of Graduate Studies of
Texas A&M University
in partial fulfillment of the requirements for the degree of

DOCTOR OF PHILOSOPHY

May 2007

Major Subject: Nuclear Engineering

^{142}Pr GLASS SEEDS

FOR THE BRACHYTHERAPY OF PROSTATE CANCER

A Dissertation

by

JAE WON JUNG

Submitted to the Office of Graduate Studies of
Texas A&M University
in partial fulfillment of the requirements for the degree of

DOCTOR OF PHILOSOPHY

Approved by:

Chair of Committee,	Warren D. Reece
Committee Members,	Leslie A. Braby
	John Ford
	Michael A. Walker
Head of Department,	John W. Poston Sr.

May 2007

Major Subject: Nuclear Engineering

ABSTRACT

^{142}Pr Glass Seeds for the Brachytherapy of Prostate Cancer.

(May 2007)

Jae Won Jung, B.S.; M.S., Hanyang University, Korea

Chair of Advisory Committee: Dr. Warren D. Reece

A beta-emitting glass seed was proposed for the brachytherapy treatment of prostate cancer. Criteria for seed design were derived and several beta-emitting nuclides were examined for suitability. ^{142}Pr was selected as the isotope of choice. Seeds 0.08 cm in diameter and 0.9 cm long were manufactured for testing. The seeds were activated in the Texas A&M University research reactor. The activity produced was as expected when considering the meta-stable state and epi-thermal neutron flux. The MCNP5 Monte Carlo code was used to calculate the quantitative dosimetric parameters suggested in the American Association of Physicists in Medicine (AAPM) TG-43/60.

The Monte Carlo calculation results were compared with those from a dose point kernel code. The dose profiles agree well with each other. The gamma dose of ^{142}Pr was evaluated. The gamma dose is 0.3 Gy at 1.0 cm with initial activity of 5.95 mCi and is insignificant to other organs. Measurements were performed to assess the 2-dimensional axial dose distributions using Gafchromic radiochromic film. The radiochromic film was calibrated using an X-ray machine calibrated against a National Institute of Standards and Technology (NIST) traceable ion chamber. A calibration

curve was derived using a least squares fit of a second order polynomial. The measured dose distribution agrees well with results from the Monte Carlo simulation. The dose was 130.8 Gy at 6 mm from the seed center with initial activity of 5.95 mCi. AAPM TG-43/60 parameters were determined. The reference dose rate for 2 mm and 6 mm were 0.67 and 0.02 cGy/s/mCi, respectively. The geometry function, radial dose function and anisotropy function were generated.

DEDICATION

To God, my parents, my wife, Sook Youn and my daughter & son, Dahee and Sungwook.

ACKNOWLEDGEMENTS

I would first like to thank my Lord and Savior Jesus Christ through whom all things are sustained and held together. May He receive all the honor and glory due Him.

I would also like to express my best appreciation to Dr. Warren D. Reece for his kind guidance, priceless encouragement and support throughout my graduate study. I would like to thank Dr. Leslie A. Braby, Dr. Michael A. Walker and Dr. John Ford for their advice and for sharing their time for the research.

I would like to thank my other colleagues and friends, Dr. Siyoung Jang, Dr. Sang Hyun Cho and Jinkai Wang. I also wish to thank the staff of the Nuclear Science Center for their kindness and help provided during my studies at Texas A&M University. Their advice, help and friendship are greatly appreciated. Special thanks go to Ms. Myradel DuBard for reviewing preliminary manuscripts and assisting my English grammar. I wish to thank Mr. David J. Harrington who allowed me to use VariSeed 7.1 for my research.

I am grateful to my parents for their love and encouragement. I also thank my wife, Sook Youn for her endless help, my daughter Dahee for her delight and my son Sungwook for his passion.

TABLE OF CONTENTS

CHAPTER Page

CHAPTER Page

LIST OF FIGURES

Page

Page

LIST OF TABLES

Page

CHAPTER I

INTRODUCTION

I-1 Background

Over the last few decades, worldwide interest in the treatment of prostate cancer continually increased. A remarkable number of prostate cancers threatening men's lives have been reported in many countries including the United States. Prostate cancer is the most common cancer, shown in Figure I-1 (American Cancer Society 2006), after skin cancer, and the second leading cause of cancer-related death in men in the United States. Between 1988 and 1992, prostate cancer incidence rates increased dramatically due to earlier diagnosis with prostate-specific antigen (PSA) blood testing approved by Food and Drug Administration (FDA) in 1986 after already increasing steadily from 1975 to 1988. In contrast incidence rates for both lung and colorectal cancers in men have declined in recent years. Figure I-2 shows the prostate cancer incidence rates for men correlated with race in the United States (National Cancer Institute 2005). The incidence rate in African-Americans is the highest. Those of Asian and American Indians are the lowest. But considering the small population fractions of Asian and American Indians in the United States, the incidence risk for them is not small.

The dissertation style and format follow that of *Physics in Medicine and Biology*.

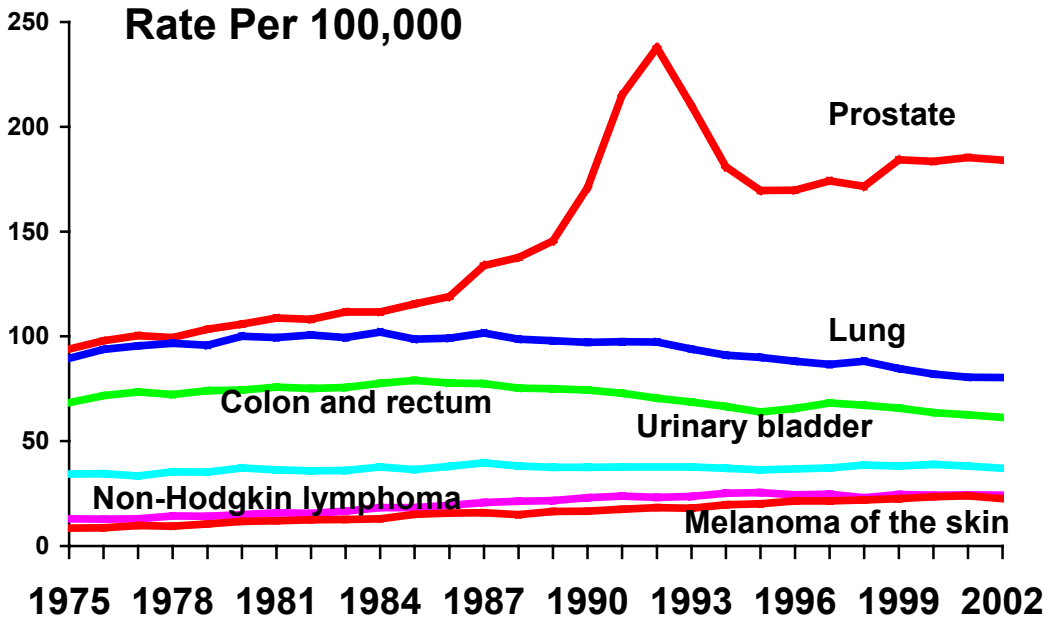

Source: Surveillance, Epidemiology, and End Results Program, 1975-2002, Division of Cancer Control and Population Sciences, National Cancer Institute, 2005.

Figure I-1. Cancer incidence rates for men in the United States

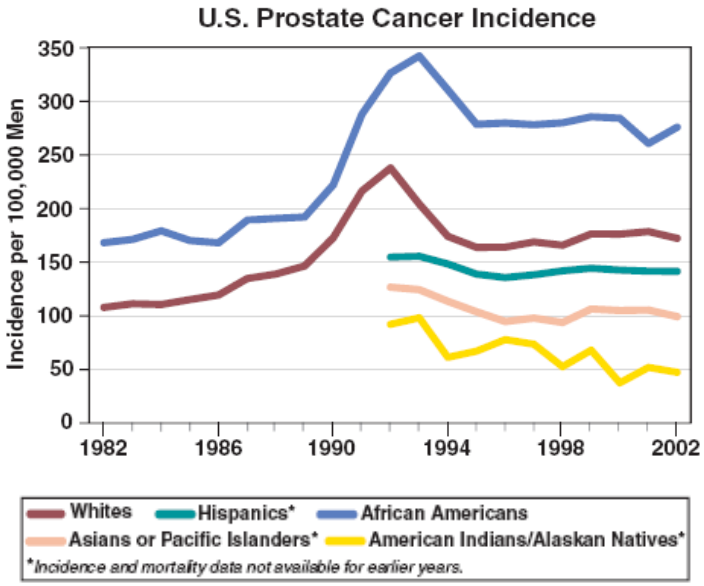

Source: Surveillance, Epidemiology, and End Results Program and the National Center for Health Statistics.

Figure I-2. Prostate cancer incidence rates for men in the U.S. with race

PSA blood testing enables doctors to find prostate cancer earlier and more easily. Early stage prostate cancer should be treated effectively with recurrence-free survival as the goal. Even though it is a slow growing cancer, optimized treatments should be selected considering quality of life after treatment. Several options for the treatment of prostate cancer exist, such as radical prostatectomy, watchful waiting, or radiation treatment (external beam radiation therapy or prostate brachytherapy). Surgical removal of the prostate can cause side effects such as erectile dysfunction or urinary incontinence. Intensity modulated radiation therapy or 3D conformal therapy can give at most 85~90 Gy to a prostate tumor, while brachytherapy can deliver about 150 Gy to a tumor. Considering the small α/β ratio reported in the literature (King and Fowler 2001), higher doses to the tumor are preferred.

The most promising treatment option is prostate brachytherapy, also known as a radioactive seed implant. Prostate brachytherapy can be used effectively for early stage prostate cancers before metastasis. A cross-sectional survey conducted by Wei *et al.* (2002) shows, in Figure I-3, that even though the brachytherapy is known for low morbidity and high recurrence-free survival, the current method of the brachytherapy treatment of prostate cancer is not preferred in terms of quality of life issues. As reported by Wallner *et al.* (1995), the dose to the urethra and rectal wall from conventional brachytherapy could be more than 360 Gy and 90 Gy respectively. This undesirable dose to adjacent organs is not insignificant and can cause not only deterministic effects but also the probabilistic effects such as a radiation-induced second cancer. Brenner *et al.* (2000) reported a pattern of radiation-induced second cancer after the radiotherapy of

prostate cancer. Brenner *et al.* reported that 10-year survival patients of prostate cancer after radiotherapy showed 34% risk increase of a radiation-induced second cancer. About 50 % of the radiation-induced second cancers were bladder and rectal cancer. For these reasons, the undesirable dose to other organs should be minimized during radiotherapy.

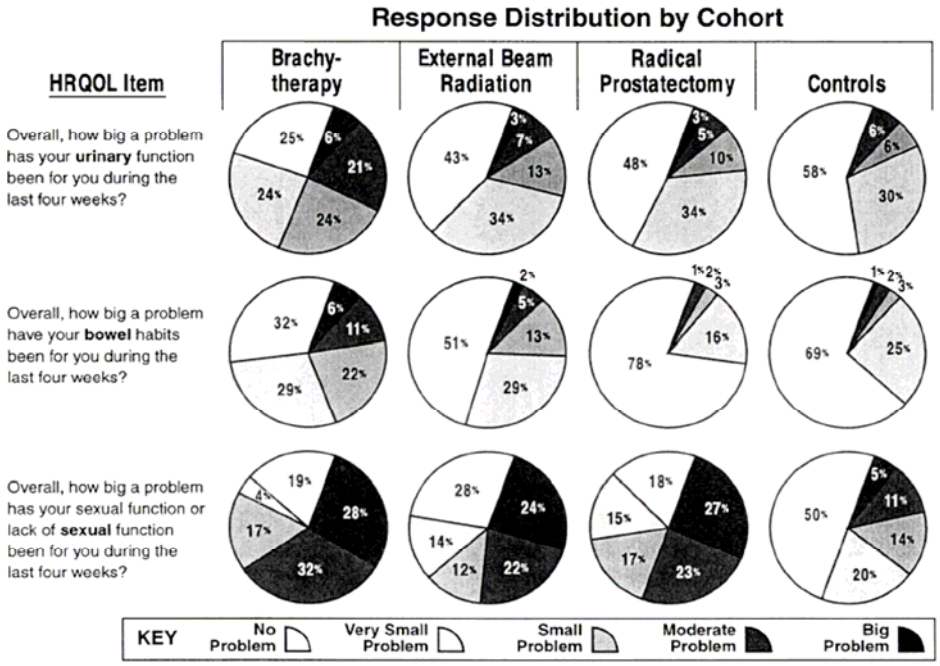

Figure I-3. Cross-sectional survey for health-related quality-of-life (Wei *et al.* 2002)

I-2 Previous work

I-2-1 Beta sources for intravascular brachytherapy

Beta sources such as ^{90}Y or ^{32}P have been used primarily for vascular brachytherapy. A dose rate table was presented for a 27 mm long, Guidant ^{32}P, intravascular brachytherapy source using Monte Carlo calculation (Bohm *et al.* 2001).

Measurements were reported for the $^{90}Sr/^{90}Y$ beta-emitter source trains used in the Novoste Beta-Cath system to determine the dosimetric characteristics of the sources at millimeter distances and to provide the necessary TG-60 dosimetry parameters for mapping the dose distributions (Roa *et al.* 2002).

I-2-2 REAS glass

Rare earth aluminosilicate (REAS) glasses have been used as radioactive material vehicles because they can contain 25 to 70 weight percent of beta emitting rare earth isotopes, e.g. ^{90}Y, ^{166}Ho, ^{153}Sm, ^{165}Dy, or ^{142}Pr (White and Day 1994). REAS glasses are chemically durable and biologically inert *in vivo*. REAS glasses exhibit no measurable weight loss (>0.1mg) for up to 6 weeks in distilled water. REAS glasses can be easily prepared as seeds for *in vivo* use or as microspheres of controlled size. REAS glasses are harder than window glass or vitreous silica. Vickers hardness is a measure of the hardness of a material, calculated from the size of an impression produced under load by a pyramid-shaped diamond indenter. The Vickers hardness of REAS glasses is 6~8 GPa, while those of window glass and vitreous silica are less than 6 GPa. One application of REAS glasses is the treatment of primary hepatocellular carcinoma (liver cancer) with radioactive (^{90}Y) yttria aluminosilicate (YAS) glass microspheres (TheraSphere^{TM}). YAS microspheres are injected into the liver via the hepatic artery to deliver a therapeutic dose of beta radiation to the tumors (Salem *et al.* 2002). Injection of ^{142}Pr glass microspheres into arteriovenous malformation (AVM) feeding arteries was suggested by Mawad and Reece (Reece 2005) to treat arterial diseases and save healthy

tissues from undesirable exposure from high-dose radiation. Microspheres 53 μm in diameter were injected into the kidney of pigs. The microspheres occluded the arteries well while sparing healthy cells in the kidney. ^{142}Pr microspheres have been studied for the treatment of arteriovenous malformations, and the effects of the arterial size and microsphere size to dose profile were evaluated (Lee and Reece 2005).

I-2-3 Biological factors

Several biological factors such as α/β ratio or biological effective dose (BED) have been extensively studied. One study (Brenner *et al.* 2002) suggested that external beam therapy with hypofractionation or high dose rate (HDR) brachytherapy is more effective in tumor control and late sequelae in the treatment of prostate cancer. The dose delivery time is closely related to the half-life of the radionuclide used in the brachytherapy seeds, but the tumor growth rate should be considered. To deliver dose to tumor effectively, the effect of half-life of the nuclide for permanent seed implants has been studied. Armpilia *et al.* (2003) suggested the optimum half-life as 4 ~ 17 days. This was based on the effectiveness of dose transfer considering initial dose rate, tumor repopulation factors or other biological factors.

After radioactive seeds are implanted in the prostate, tumor cells and normal tissue will be killed. The death of cells near seeds induces shrinkage of prostate volume. This causes migration of seeds resulting in differences from pre-planned dose distribution in the prostate. The shrinkage rate is known to be 3.9×10^{-3} day^{-1} (Dale and Jones 1999), so shrinkage effects are not significant for short half-life radioisotopes. A

clinical investigation showed that post-implant edema increased the volume of the prostate by factors which ranged from 1.33 to 1.96 (mean: 1.52). The edema half-life varied from 4 to 25 days (Waterman *et al.* 1998).

I-2-4 AAPM TG reports

The AAPM TG has suggested some practical guidelines for clinical physicists. The updated AAPM TG-43 report (Rivard *et al.* 2004) recommended a dosimetry protocol for interstitial brachytherapy sources and proposed standardized dosimetry parameters such as air-kerma strength, dose-rate constant, and geometry function. TG-43 parameters are explicitly for low energy photon emitters such as ^{125}I and ^{103}Pd and beta-emitting sources were not included. TG-43 recommends that at least one experimental measurement and one Monte Carlo determination should be required for clinical application of the seed. The AAPM TG-60 report (Nath *et al.* 1999) addressed intravascular brachytherapy physics and included dosimetry recommendations for beta emitters. The AAPM Task Group Report No. 55 (TG-55) generally addresses radiochromic film dosimetry and suggests specific procedures for using radiochromic films. The AAPM Task Group Report No. 64 (TG-64) gives an overall description of permanent prostate seed implant brachytherapy including dose uniformity and conformity in the prostate.

I-3 Research need

I-3-1 Conventional method

The conventional treatment method is to implant many tens of ^{125}I or ^{103}Pd seeds into the prostate. To insert seeds into the prostate, ultrasound-guided transperineal template implant procedures are used shown in Figure I-4. The typical template has a 13 by 13 matrix with 5 mm spacing. The needle for seed insertion is 21 cm long. The ultrasound probe usually enables doctors to guide the needle.

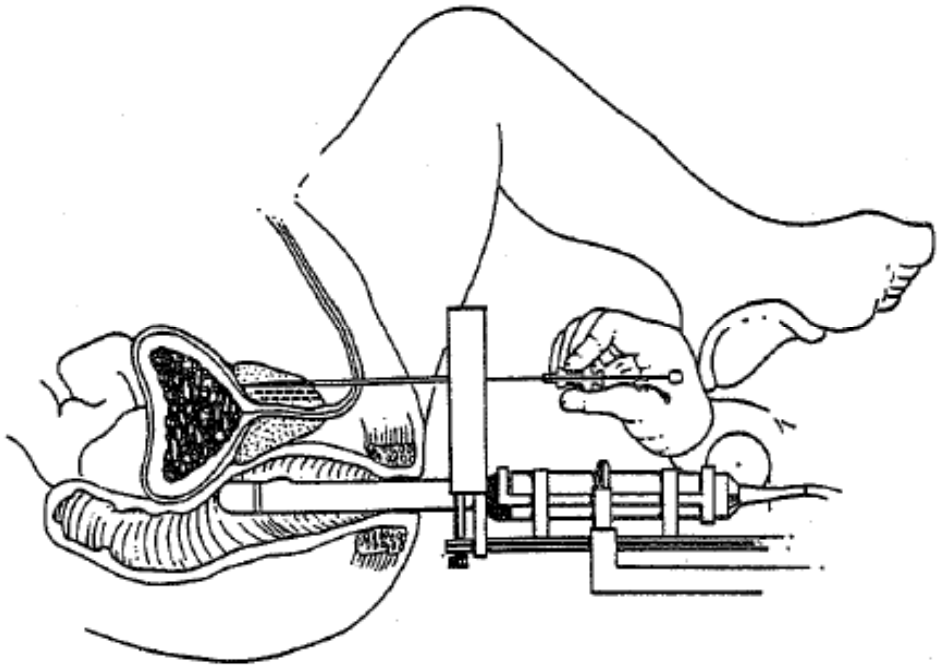

Figure I-4. Ultrasound-guided transperineal template implant (Khan 2003)

Considering that the mean free path of 22 and 28 keV photons in tissue is ~ 1.5 and 2.5 cm, respectively, some seeds can contribute significant doses to the urethra and

rectal walls. Although low energy photon sources such as ^{125}I and ^{103}Pd have a long history, side effects such as painful urination and damage to the rectal and bladder walls are common. To reduce undesirable dose to adjacent organs, we propose using a beta source for the brachytherapy treatment of prostate cancer.

I-3-2 Beta sources

While beta sources such as ^{90}Y, ^{188}Re, and ^{32}P have been used for vascular brachytherapy, beta sources have not been widely used for cancer therapy. Nevertheless beta sources offer several advantages over photon sources. Beta particles have short range and are easily shielded, lowering extraneous dose to medical staff as well as the patient. They can give a lower dose to the rectum and urethra than low energy photons from ^{125}I and ^{103}Pd. Knowing the continuous distribution in energy of the emitted electrons during beta-decay, the range and energy deposited in water or tissue can be determined using the electron stopping power relations. The range of a 2-MeV electron is 100 cm in air and 0.95 cm in water. The range R in g cm^{-2} in low-Z material for electrons (Turner 1995) can be expressed as

For $0.01 \leq T \leq 2.5$ MeV (1-1)

$$R = 0.412 \cdot T^{1.27 - 0.0954 \ln T}$$

For $T > 2.5$ MeV (1-2)

$$R = 0.530 \cdot T - 0.106$$

Figure I-5 shows the comparisons of radial dose function, *g(r)* of ^{125}I (Rivard 2002) and ^{90}Sr/^{90}Y (Roa *et al.* 2002). The radial dose function, *g(r)* suggested in AAPM Task Group Report No. 43 (TG-43) accounts for dose fall-off on the transverse-plane. The radial dose function for ^{125}I is flat to 2 cm and decreases gradually to 10% at 10 cm, while the radial dose function for ^{90}Sr/^{90}Y falls off to 0.1% at 0.8 cm. They are both normalized to 2 mm.

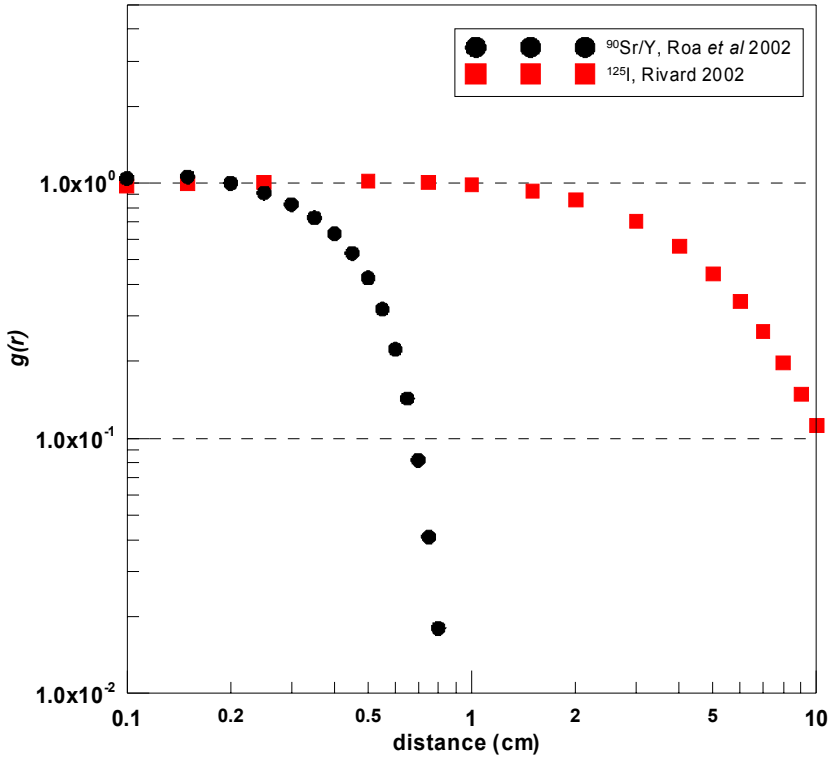

Figure I-5. Radial dose functions of ^{90}Sr/^{90}Y and ^{125}I seed

I-4 Objectives

The present study is to develop a detailed brachytherapy scheme for prostate cancer using beta emitting glass seeds. The method is to select appropriate isotopes and dimensions for brachytherapy, to produce brachytherapy seeds through glass seed design using neutron activation, to estimate dose distribution both with Monte Carlo computational calculation and experimental measurement using radiochromic films, and to provide AAPM TG-43/60 dosimetric parameters.

I-5 Outline of the study

This research was organized in four parts: isotope selection and seed design, Monte Carlo computational calculation, experimental measurement, and generation of AAPM TG-60 dosimetric parameters. As described in TG-43, one Monte Carlo calculation and one experimental measurement were performed. The results from computational dose calculation and dose measurement were compared and analyzed. Figure I-6 shows the scope of this research.

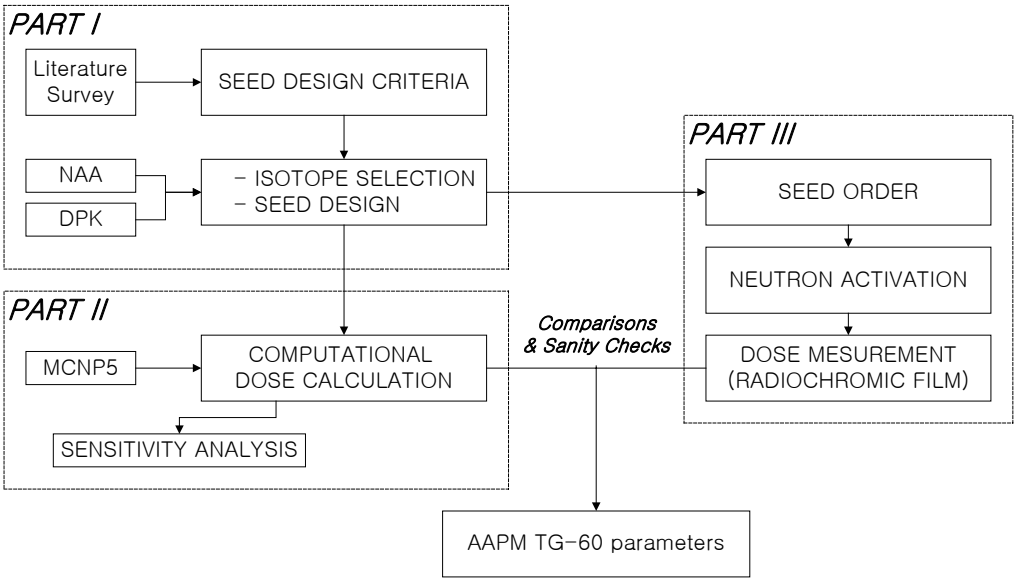

Figure I-6. Scope of research

CHAPTER II

BIOLOGICAL MODELS

II-1 Prostate anatomy and functions

The prostate is one of the male reproductive organs. The prostate produces milky fluid which is added to semen. The function of the prostate is to facilitate movement of spermatic fluid to the uterus. If the prostate is diseased and reproduction is not an issue, the prostate can be removed because it is not a life-sustaining organ. The etiological cause of prostate cancer is not well known but thought to be due to hormonal or hereditary effects. The anatomy of the prostate is shown in Figure II-1. The volume of the prostate is 30 ~ 50 cm^3 and is shaped like a chestnut. The size and shape varies each day. The organs adjacent to the prostate are the urethra, rectum, bladder, and seminal vesicles. The urethra is an approximately 4-mm diameter tube penetrating the center of prostate through which urine and semen exit. The urinary bladder is located cranial to the prostate. Seminal vesicles secrete fluid which forms part of the semen. The rectal wall is located 2 cm dorsal to the prostate.

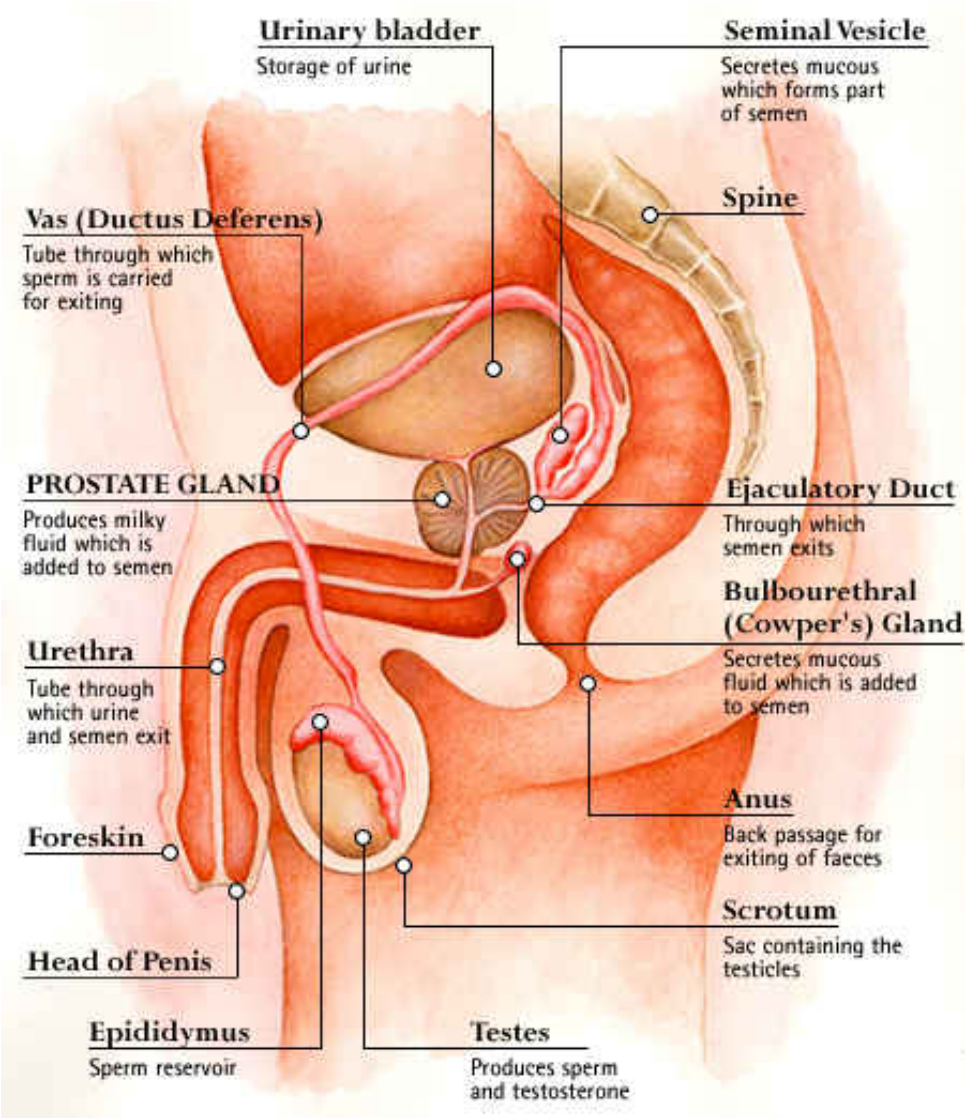

Source:http://www.dva.gov.au/media/publicat/2001/prostate/pdf/You_and_Your_Prostate2006_complete.pdf

Figure II-1. The anatomy of prostate

II-2 Prostate cancer diagnosis

Prostate cancer can be diagnosed by several tests, the most general of which is PSA blood testing. Prostate-specific antigen is an enzyme secreted by the prostate. If the

amount of secreted PSA is larger than 4 ng/ml, the prostate is suspected to be abnormal. Rectal palpation of the prostate is used to evaluate it for hardness or asymmetry. Biopsy is the most definitive test. If prostate cancer is diagnosed, Gleason scores can predict the quality of prostate cancer. Figure II-2 shows 5 different Gleason scores. A score of 1 is the least aggressive and 5 is the most aggressive. Gleason score grades the status of cancer and it is related to the tumor progression.

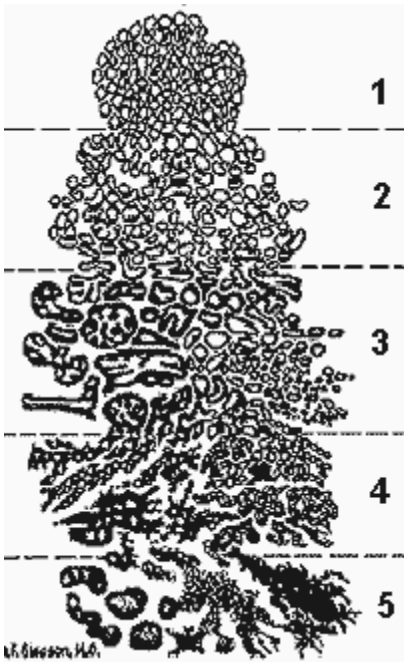

Figure II-2. Gleason Score (Gleason *et al.* 1974)

Table II-1 presents the categorization of prostate cancer. Prostate cancer is categorized as T, N, and M states. T state is primary tumor, N state is region lymph nodes invasion, and M state is distant metastasis. National Comprehensive Cancer Network (NCCN 2005) has suggested clinical practice guidelines. According to these

guidelines, if a Gleason score is small and the stage is earlier than T2, prostate brachytherapy can be used effectively. If the prostate cancer progresses further than these criteria, another treatment option should be considered.

Table II-1. Categorization of prostate cancer (NCCN 2005)

Primary Tumor (T)	
Stage	Description
TX	Primary tumor cannot be assessed
T0	No evidence of primary tumor
T1	Clinically inapparent tumor neither palpable nor visible by imaging
T2	Tumor confined within the prostate
T3	Tumor extends through the prostatic capsule
T4	Tumor is fixed or invades adjacent structures other than seminal vesicles
Regional Lymph Nodes (N)	
Stage	Description
NX	Regional lymph nodes were not assessed
N0	No regional lymph node metastasis
N1	Metastasis in regional lymph node
Distant Metastasis (M)	
Stage	Description
MX	Distant metastasis cannot be assessed (not evaluated by any modality)
M0	No distant metastasis
M1	Distant metastasis

II-3 Radiosensitivity of prostate cancer

Survival curves shown in Figure II-3 have been used for quantification of the susceptibility or sensitivity of radiation to cells or organs. The linear-quadratic (LQ) model has been used for the survival curve. The expression for the cell survival curve is

$$S = e^{-\alpha D - \beta D^2} \tag{2-1}$$

where S is the fraction of cells surviving a dose D, and α and β are constants. α is logarithmic survival constant proportional to dose and β is logarithmic survival constant proportional to the square of the dose. The ratio of α over β is used to quantify the fractionation sensitivity of a cell or organs. If the α/β ratio is small, which means β is relatively large, the survival curve bends downward quickly and the quadratic contribution is dominant (Hall and Giaccia 2006).

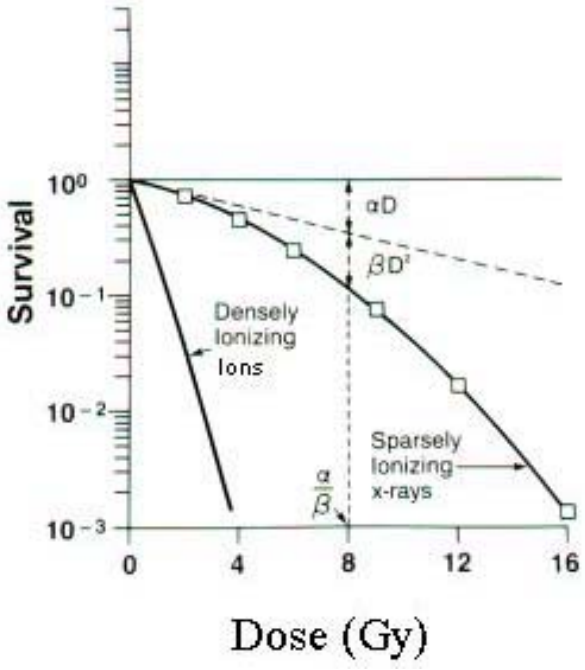

Figure II-3. Survival curve (Hall *et al.* 2006)

II-4 Biological effective dose

While the prescribed doses using ^{125}I and ^{103}Pd are known based on empirical clinical data (144 Gy and 125 Gy respectively), the prescribed dose for ^{142}Pr is not known.

Even though the same amount of total dose is deposited to a tumor or normal tissue, the biological effective dose (BED) for each radionuclide can be different from the physical dose due to the tumor doubling time, initial dose rate, tissue repair constant, relative biological effectiveness (RBE) or other biological factors. The BED based on the LQ model was expressed by Dale (1996) as

$$\text{BED} = -\ln(S)/\alpha \tag{2-2}$$

By combining Equation (2-1) and (2-2), the BED can be expressed as

$$BED = D(1+\frac{1}{\beta/\alpha}D) \tag{2-3}$$

In addition, considering the relative biological effectiveness (RBE), the BED is regarded as the prescribed dose times the relative effectiveness factor minus biological equivalent as given below in Equations (2-4) - (2-12) suggested by Antipas *et al.* (2001).

$$BED = TD \cdot RE - BRF \tag{2-4}$$

Where, *TD* is the total physical dose delivered and *RE* is the relative effectiveness factor, and *BRF* is the biological equivalent of the tumor repopulation.

$$TD = \frac{R_0}{\lambda}[1-\exp(-\lambda T_{eff})] \tag{2-5}$$

$$T_{eff} = -\frac{1}{\lambda}\ln\left(\frac{K}{RBE_{\max}R_0}\right) \tag{2-6}$$

$$RE_{tum} = RBE_{\max} + \left[\frac{2R_0\lambda}{(\mu_{tum}-\lambda)(\alpha/\beta)_{tum}}\right]A(B-C) \tag{2-7}$$

$$A = \frac{1}{1-\exp(-\lambda T_{eff})} \tag{2-8}$$

$$B = \frac{1 - \exp(-2\lambda T_{eff})}{2\lambda} \tag{2-9}$$

$$C = \frac{1 - \exp[-T_{eff}(\mu_{tum} + \lambda)]}{\mu_{tum} + \lambda} \tag{2-10}$$

$$BRF_{tum} = K \cdot T_{eff} \tag{2-11}$$

$$K = \frac{0.693}{\alpha \cdot T_{av}} \tag{2-12}$$

where,

R_0 = initial dose rate (Gy/h)

λ = radionuclide decay constant (h^{-1})

T_{eff} = effective treatment time (h)

K = tumor repopulation factor (Gy/h, Gy/day), the biologic dose required to offset each day's worth of tumor repopulation

RBE_{max} = the maximum RBE, defined as the ratio of linear sensitivity coefficient (α) with the high-LET test radiation to that for a reference (low-LET) radiation

μ_{tum} = sublethal damage repair constant (h^{-1})

$(\alpha/\beta)_{tum}$ = inverse of the fractionation factor of the tumor (Gy)

α = linear radiosensitivity coefficient (Gy^{-1})

T_{av} = average clonogen doubling time

Because the shrinkage rate is known to be small, 3.9×10^{-3} day^{-1} (Dale *et al.* 1999), shrinkage effects are not considered.

Table II-2. Tumor BEDs of several nuclides with $\alpha = 0.1$ Gy^{-1} and $T_{av} = 60$ days

μ (tumor) (h^{-1})	α/β (tumor) (Gy)	BED (^{125}I : 144 Gy)	BED (^{103}Pd : 125 Gy)	BED (^{142}Pr : 90 Gy)
Assuming $RBE_{max} = 1.0$ for all nuclides				
0.5	10	110.2	116.8	143.9
0.5	7	111.0	119.0	167.3
0.5	5	112.2	122.1	198.6
0.5	2.5	116.2	132.7	308.2
0.5	1.5	121.5	146.8	454.2
$RBE_{max} = 1.45$ (^{125}I , ^{142}Pr) and 1.75 (^{103}Pd)				
0.5	10	171.7	208.9	184.3
0.5	7	172.6	211.2	207.8
0.5	5	173.7	214.2	239.1
0.5	2.5	177.7	224.8	348.6
0.5	1.5	183.1	239.0	494.6
$RBE_{max} = 1.0$				
1.4	10	108.9	113.4	109.6
1.4	7	109.2	114.2	118.3
1.4	5	109.6	115.3	130.0
1.4	2.5	110.0	119.0	170.9
1.4	1.5	112.9	124.1	225.4
$RBE_{max} = 1.45$ (^{125}I , ^{142}Pr) and 1.75 (^{103}Pd)				
1.4	10	170.4	205.5	150.0
1.4	7	170.7	206.3	158.8
1.4	5	171.1	207.4	170.5
1.4	2.5	172.6	211.2	211.4
1.4	1.5	174.5	216.3	265.9

Table II-2 presents tumor BEDs of several nuclides. As shown in Table II-2, 90 Gy of ^{142}Pr gives the equivalent BED of 144 Gy of ^{125}I and 125 Gy of ^{103}Pd. Thus 90 Gy of ^{142}Pr is suggested as the prescribed dose based on the sensitivity analysis of dose of ^{142}Pr and the BED comparison.

Table II-3. BEDs with typical radionuclides for different parameters

K (Gy/day) / α/β (Gy) / Isotope ($T_{1/2}$)	0.01 3.5	0.1 3.5	0.1 1.5	0.6 10	0.9 10
^{142}Pr (19.12 h)	92.5	91.8	151.2	60.0	58.6
^{198}Au[a] (65 h)	95.1	93.0	129.7	67.3	63.6
^{131}Cs[a] (233 h)	96.9	90.8	107.3	62.0	53.0
^{103}Pd[a] (407 h)	97.0	87.4	98.0	52.0	40.1
^{125}I[a] (1426 h)	94.7	70.2	73.6	13.6	2.5

[a]Armpilia *et al.* 2003

Biological factors such as α/β ratio and K are not certain. The sensitivity calculation results of various factors are presented in Table II-3. The most probable parameters are used. Recent studies suggest that the α/β ratio ranges from 1.5 to 5 and K is between 0.01 and 0.9. The BEDs of ^{142}Pr are reasonable compared to other typical radionuclides.

Figure II-4 shows the sensitivity of α/β ratio. As the α/β ratio increases, the BED for ^{142}Pr decreases exponentially. The BEDs for ^{125}I and ^{103}Pd are relatively insensitive to α/β ratio because the initial dose rate greatly contributes to the BED.

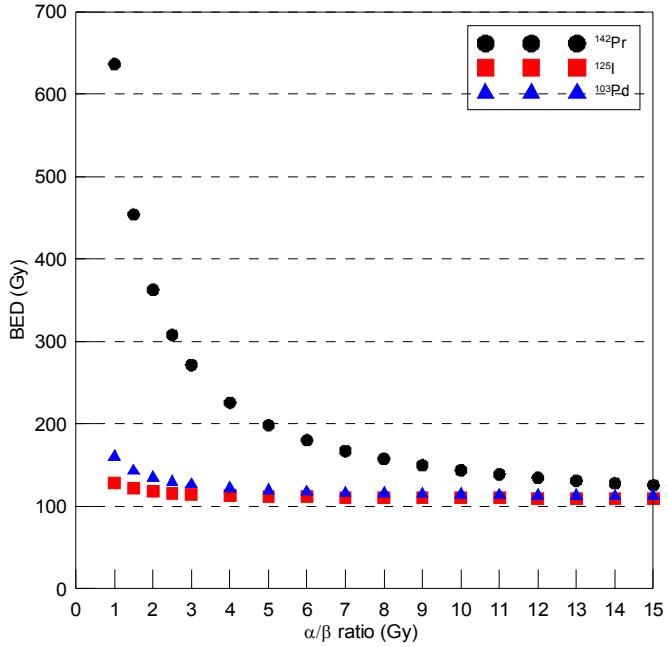

Figure II-4. Biological effective dose as a function of α/β ratio. $\mu = 0.5\ h^{-1}$, $RBE_{max} = 1$, $\alpha = 0.1\ Gy^{-1}$ and $T_{av} = 60$

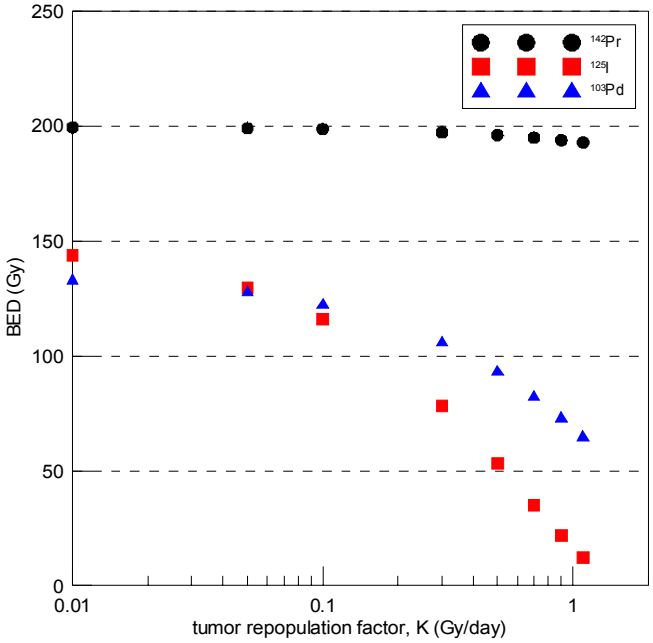

Figure II-5. Biological effective dose as a function of K with α/β ratio of 5. $\mu = 0.5\ h^{-1}$, and $RBE_{max} = 1$

As tumor repopulation factor increases, the BEDs of ^{103}Pd and ^{125}I fall off sharply because of their long half-life as shown in Figure II-5. The BED of ^{142}Pr is insensitive to tumor repopulation factor. Therefore, ^{142}Pr is acceptable for treating tumors with high K's and low α/β ratios.

CHAPTER III

ISOTOPE SELECTION AND SEED DESIGN

III-1 Conventional seed

Several seeds using ^{125}I or ^{103}Pd have been used for the treatment of prostate cancer. Several companies such Theragenics Corp., Amersham, Best Inc., and others have developed and, over time, improved brachytherapy seeds. The price of the seeds is from $50 to $150 per seed. More than 50 seeds are typically used during a single treatment. The shapes of several seeds are posted on the AAPM RPC seed registry (RPC 2006) and shown in Figure III-1. The dimensions of typical seeds are ~ 5 mm long and 0.8 mm in diameter to fit within established urologic implantation devices such as template-guided needle delivery systems. Most of them have radiation opaque markers and titanium encapsulation. The titanium cladding is 0.04 mm - 0.06 mm thick. Gold or silver is used as the radiation opaque marker. Typical seed strengths are on the order of 0.3 mCi for ^{125}I for permanent prostate implants. Some of seeds consist of several of ^{125}I or ^{103}Pd beads inside the titanium cladding.

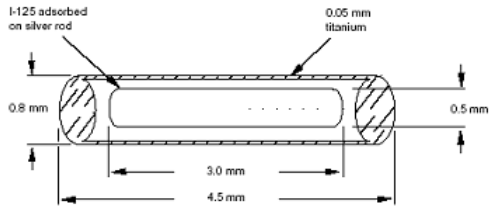

(a) Amersham OncoSeed model 6711

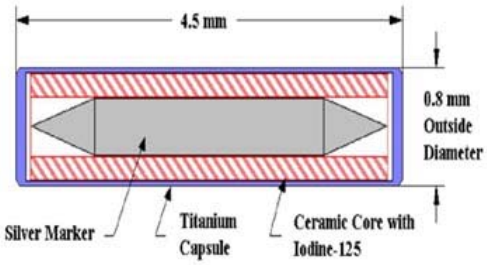

(b) I-Plant model 3500

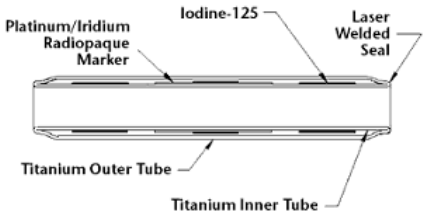

(c) Ibt Intersource125 model 1251L

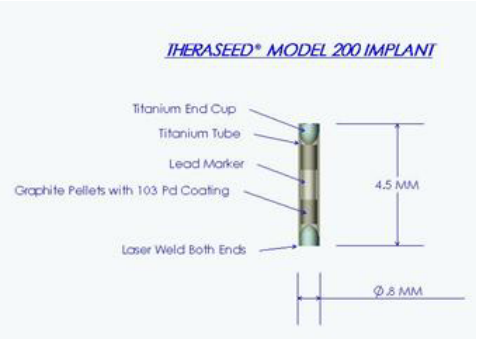

(d) THERASEED model 200

(e) Prospera Med 3633

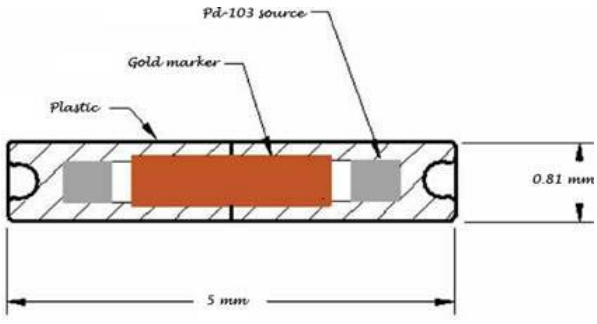

(f) OptiSeed model 1032P

Figure III-1. Brachytherapy seeds (RPC 2006)

III-2 Isotope selection criteria

Although over one hundred seeds are sometimes used to treat the prostate, we assumed fifty seeds for a typical implantation to lessen surgery time. If 50 seeds are used and the prostate is 50 g and 50 cm^3, 1 seed should cover 1 cm^3 of prostate volume and we should get the target dose at about 0.6 cm from the center. The target dose selected for this study is 150 Gy. This value is selected conservatively based on 144 Gy for ^{125}I and 125 Gy for ^{103}Pd. We seek to achieve this target dose using a radionuclide that produces high-energy beta particles because we believe that adjacent tissues can be spared unnecessary dose.

III-3 Seed design criteria

We want the seeds to be activated in a low thermal neutron fluence rates typical of research reactors so the neutron absorption cross section should be large enough to make sufficient activity easily in these neutron fields. As discussed earlier, a radionuclide with short half-life for high dose rate irradiation is acceptable. The seeds should have chemical, mechanical, and biological integrity during neutron activation and *in vivo*. The cost of manufacture of these seeds should be relatively inexpensive. Finally the seeds should be visible during seed implant and post-implant monitoring with or without radiation opaque markers.

III-4 Neutron activation analysis

The isotope ^{142}Pr will be made in a low neutron fluence reactor such as research reactor. The target activities can be easily controlled by knowing the neutron fluence rates, neutron activation time, mass of target nuclide per seed, and neutron absorption cross section. The activity at end of activation can be expressed as

$$A = \frac{m \cdot wt \cdot abun}{M} \cdot Av \cdot \sigma \cdot \phi \cdot (1 - e^{-\lambda t_0}) \tag{3-1}$$

where,

A = activity (dps, Bq)

m = total mass of seed (g)

wt = weight percent of element

$abun$ = abundance of isotope

M = atomic mass of isotope (g)

Av = Avogardo's number

σ = neutron capture cross section (barn, 10^{-24} cm^2)

ϕ = neutron flux (cm^{-2}sec^{-1})

λ = decay constant (sec^{-1})

t_0 = neutron activation time (sec)

III-5 DPK code description

To get the preliminary dose distribution, BRAIN-DOSES code was used (Dauffy 1998). BRAIN-DOSES code is based on SADDE (Reece *et al.* 1989) and VARSKIN (Traub *et al.* 1987) codes. SADDE is a code to generate input from the calculated beta spectra for VARSKIN. The following inputs for SADDE were needed.

1. the isotope name
2. whether to include multiple isotopes
3. the number of decay paths for this radionuclide
4. the atomic number of the transition nucleus
5. the atomic mass of the parent nucleus
6. the endpoint beta energy in MeV
7. the fractional yield
8. the forbiddenness for the particular decay
9. the number of internal conversion and Auger electrons for this radionuclide

The output was added to betadata.dat file for VARSKIN code. Table III-1 and III-2 present the inputs and outputs for several beta emitters.

Table III-1. Examples of input decks for SADDE Mod 2 (Reece *et al.* 1989)

^{90}Y	^{142}Pr	^{188}Re	^{32}P
Y-90	Pr-142	Re-188	P-32
N	N	N	N
1	1	1	1
40.	60.	76.	16.
90.	142.	188.	32.
2.2792	2.1622	2.120	1.709
0.99984	0.963	0.967	1.0
1	1	1	1
0	0	0	0

BRAIN-DOSES integrates the Berger point kernels over the source volume, employing the scaled point kernels tabulated by Berger in 1971. Dose point kernel (DPK) codes are fast and have good agreement in simple geometries when compared with Monte Carlo calculation. The Berger beta dose point kernel can be expressed as

$$B(\rho, E) = \frac{1}{4\pi\delta\rho^2}\int_0^{E_{\max}} \frac{EN(E)}{X_{90}} F(\frac{\rho}{X_{90}}, E)dE \qquad (3\text{-}2)$$

where, ρ is the distance between source point and dose point (cm), δ is the density of the irradiated medium (assumed to be unity for tissue) (g/cm^3), *N(E)* is the probability density of fluence, X_{90} is the radius of the sphere within which 90% of the beta energy is deposited from a point source in a finite medium (cm), and *F* is the dimensionless scaled absorbed dose distribution as a function of the modified path length and the X_{90} distance. BRAIN-DOSES was developed for 5 different source geometries: point, line, shell cylinder, solid cylinder and solid sphere. Table III-3 presents the output of BRAIN-DOSES for a ^{142}Pr glass seed.

Table III-2. Examples of output data for SADDE Mod 2

^{90}Y
Y-90 0.9367 0.5170 1.0000 1.3300 1.2900 1.2500 1.2200 1.2000 1.1800 1.1900 1.1800 1.1600 1.1300 1.1000 1.0700 1.0300 0.9900 0.9400 0.8900 0.8400 0.7900 0.7400 0.6900 0.6300 0.5800 0.5200 0.4700 0.4100 0.3100 0.2200 0.0800 0.0200 0.0000 0
^{142}Pr
Pr-142 .8375 .4878 1.0010 1.4232 1.3965 1.3698 1.3442 1.3257 1.3150 1.2706 1.2310 1.1941 1.1536 1.1117 1.0726 1.0294 .9854 .9402 .8925 .8434 .7925 .7400 .6861 .6312 .5755 .5196 .4640 .4093 .3053 .2127 .0775 .0147 .0005 1 1575. 0.325
^{188}Re
Re-188 .7186 .4370 1.0992 2.3837 2.1544 1.9251 1.6958 1.6802 1.6297 1.3599 1.3393 1.3135 1.2787 1.2365 1.1893 1.1366 1.0803 1.0234 .9634 .9018 .8395 .7767 .7137 .6512 .5895 .5291 .4705 .4143 .3108 .2218 .0930 .0266 .0038 0.0 0.0
^{32}P
P-32 .7217 .3765 1.0000 1.2678 1.2527 1.2376 1.2239 1.2185 1.2149 1.2022 1.1872 1.1712 1.1482 1.1202 1.0852 1.0459 1.0023 .9573 .9089 .8583 .8059 .7522 .6974 .6415 .5847 .5276 .4709 .4151 .3087 .2140 .0764 .0140 .0004 0.0 0.0

Table III-3. Examples of output for BRAIN-DOSES

Program BRAIN_DOSES

Pr-142 9L, 0.8D

2-D Cylindrical Source Geometry

Nuclide : Pr-142
1.8*X90 Distance : 0.878040 cm
No gamma dose calculation
Source Strength : 1.00000 uCi
Source Density : 0. g/cm^3
Diameter of Disk : 800.000 um
Relative Error : 1.00000E-04

Calculated Results:

Radial Distance (cm)	Dose Rate (rad/h)	
0.0000	9.89E+01	8.13E-02
0.0400	1.39E+01	1.33E-02
0.0800	7.68E+00	7.88E-03
0.1200	4.92E+00	5.41E-03
0.1600	3.37E+00	4.00E-03
0.2000	2.39E+00	3.09E-03
0.2400	1.73E+00	2.46E-03
0.2800	1.26E+00	2.00E-03
0.3200	9.20E-01	1.66E-03
0.3600	6.65E-01	1.39E-03
0.4000	4.74E-01	1.19E-03
0.4400	3.31E-01	1.02E-03
0.4800	2.25E-01	8.85E-04
0.5200	1.47E-01	7.73E-04
0.5600	9.19E-02	6.80E-04
0.6000	5.42E-02	6.03E-04
0.6400	2.97E-02	5.37E-04
0.6800	1.47E-02	4.80E-04
0.7200	6.34E-03	4.32E-04
0.7600	2.20E-03	3.90E-04
0.8000	5.39E-04	3.54E-04
0.8400	7.11E-05	3.22E-04
0.8800	0.00E+00	2.94E-04
0.9200	0.00E+00	2.69E-04
0.9600	0.00E+00	2.47E-04
1.0000	0.00E+00	2.28E-04

III-6 Nuclide comparison

Several candidate radionuclides were considered for seed production. Figure III-2 shows the radial dose profiles of various beta emitters from the BRAIN-DOSES code as a function of distance from the surface of the seed at seed midpoint. The dose profiles are mainly dependent on the range of the beta particles.

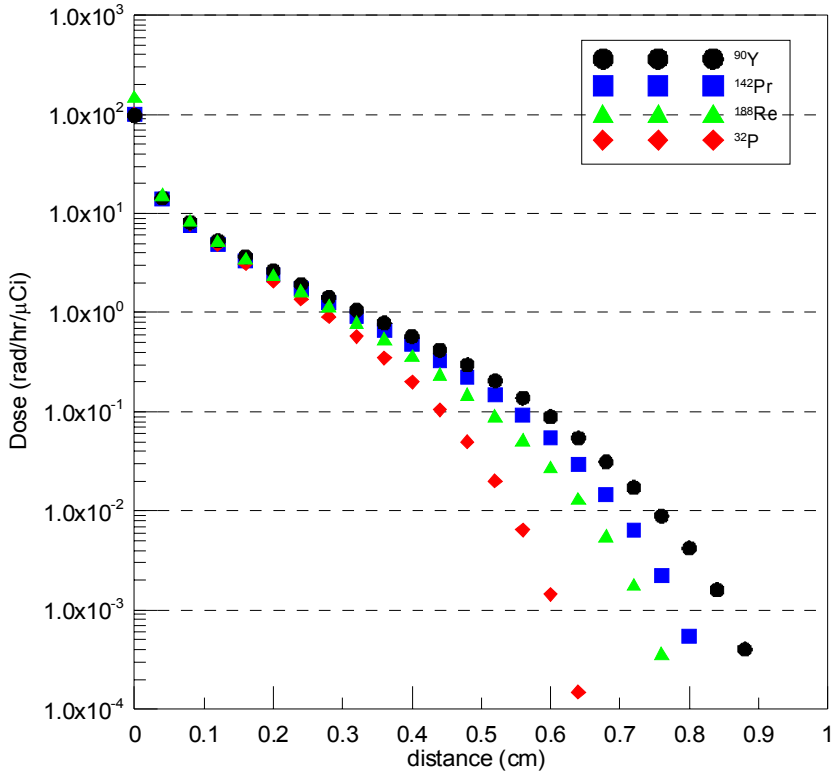

Figure III-2. Radial dose profiles of several beta emitters

Yttrium and phosphorus have been used for intravascular brachytherapy. ^{90}Y glass microspheres have been used for hepatocellular carcinoma. But ^{90}Y has a small thermal neutron absorption cross section and ^{32}P produces relatively low energy beta

particles. Rhenium has a large neutron cross section but it is not easily incorporated into glass because of its volatility. Table III-4 compares the properties of several beta emitters. Because the dose profile of ^{142}Pr decreases more rapidly than that of ^{90}Y, as seen in Figure III-2, ^{142}Pr is more useful for intravascular brachytherapy treatment in which a high localized dose is needed around the blood vessel.

Table III-4. Properties of several beta emitters

Property	**^{142}Pr**	**^{90}Y**	**^{188}Re**	**^{186}Re**	**^{32}P**
Half life	**19.12 h**	64.0 h	17.0 h	90.6 h	14.28 d
Maximum beta energy (MeV)	**2.162**	2.281	2.118	1.071	1.709
Abundance	**1.000**	1.000	0.626	0.374	1.000
Weight Percent in glass	**0.445**	0.4	0.3	0.3	0.25
Density of glass (g/cm^3)	**4.0**	3.29	2.9	2.9	3.06
Gamma emissions for imaging	**1.58 MeV, γ(3.7%)**	Brems[a]	155.0 keV, γ(15%)	137.2 keV, γ(9.5%)	Brems[a]
Thermal neutron cross section	**7.5 b (+3.9b)[b]**	1.28 b	73 b	112 b	0.17 b

[a] Bremsstrahlung.
[b] Cross section of meta-stable state.

III-7 Properties of ^{142}Pr

Based on neutron activation analysis and BRAIN-DOSES calculations, ^{142}Pr was selected as the most appropriate isotope. It is a rare earth material suitable for REAS glass and a sufficiently large cross section of 7.5 barns (+3.5 barn of meta-stable state) for activation in research reactors. ^{142}Pr is made by neutron activation of the 100% abundant ^{141}Pr, producing both the 19.12 hour ground state and 14.6 min meta-stable state. The ^{142}Pr ground state decays emitting 2.162 MeV endpoint energy beta rays 96.3 % of the time and has a 3.7% yield of 1.575 MeV gamma rays. With a 19.12 h half life, 90% of the dose (D_{90}) is deposited in 2.65 days. Figure III-3 shows the beta spectrum of ^{142}Pr. This data was obtained from http://ie.lbl.gov.

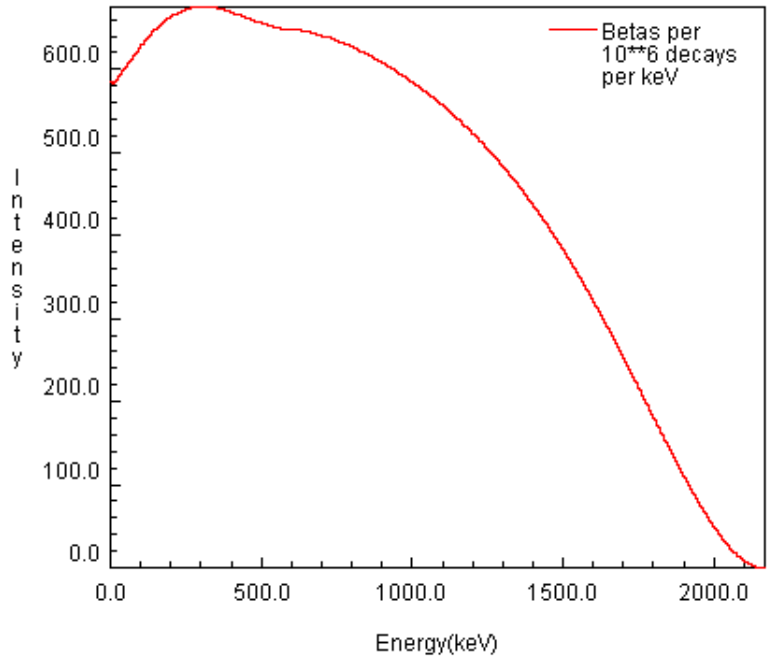

Figure III-3. Beta spectrum of ^{142}Pr

Figure III-4 shows the decay scheme of ^{142}Pr from http://atom.kaeri.re.kr/ton.

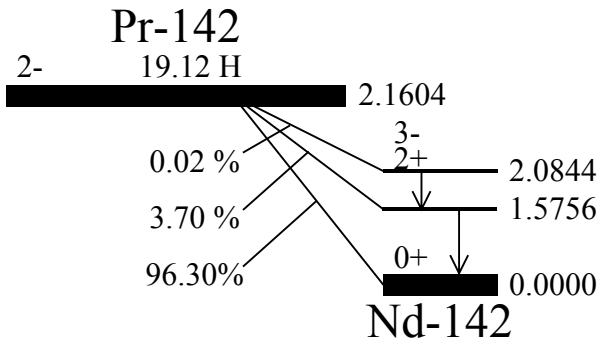

Figure III-4. Decay scheme of ^{142}Pr

III-8 ^{142}Pr REAS glass seeds

^{142}Pr REAS glass seeds have several advantages over conventional seeds. The Pr seed is economical; it costs less than 15 dollars per seed including materials and neutron activation costs. Due to the short range of beta particles, the dose to adjacent organs can be minimized with optimized implantation positions of the seeds. Because of the short half-life of ^{142}Pr, and associated high dose rate, distortion of the prostate during irradiation is less than with ^{125}I, for example, that has a D_{90} of 204 days. Pr seeds can have very high dose rates, if desired, and give doses up to thousands of Gy to tumors near seeds. Because of high density and high atomic number of Pr glass, a radio-opaque marker is not necessary. Cladding or encapsulation is not required because the seed is unreactive in water or tissue. Variable sizes and shapes of glass seeds can be made and the seed is not easily broken. The seed is reusable after a high dose rate (HDR) treatment by reactivation.

CHAPTER IV

MONTE CARLO COMPUTATIONAL MODELING

Radiation interaction is basically a stochastic process. Monte Carlo method is a statistical method to predict the behaviors of individual particles using cross sections for all interaction processes. Cross sections are randomly sampled to determine type of interaction that will occur, distance to that interaction, energy transferred, new direction of particle and distance to next interaction.

IV-1 MCNP Monte Carlo code

The MCNP5 code was used to calculate the quantitative dosimetric parameters of the Pr seeds. MCNP is a general-purpose Monte Carlo code. It can be used for neutron, photon, electron, or coupled neutron/photon/electron transport with the default modeling of secondary radiations such as positrons, K-edge characteristic x-rays, and bremsstrahlung. It can model an arbitrary three-dimensional geometry and various source types such as point, volume, and surface with user-defined source spectrums. A continuous-slowing-down model expressed as equations (4-1, 2) is used for electron transport. (X-5 Monte Carlo Team 2003).

In MCNP, the energy and path lengths of electron transport are modeled by

$$E_{n-1} - E_n = -\int_{S_{n-1}}^{S_n} \frac{dE}{ds} ds \qquad (4\text{-}1)$$

where E_n, S_n, and $-dE/ds$ are energy, the total path length, and the total stopping power in energy per unit length.

The electron collisional stopping power due to collisions between particles and atoms is from the Berger's formulation:

$$-\left(\frac{dE}{ds}\right)_{col} = NZ\frac{2\pi \cdot e^4}{m v^2}\left\{\ln[\tau^2(\tau+2)] - C2 + C3 - \beta^2 + C4\left(\frac{\tau}{\tau+1}\right)^2 - \delta\right\} \qquad (4\text{-}2)$$

where, $C2 = \ln(2I^2)$, $C3 = 1 - \ln 2$, $C4 = \frac{1}{8} + \ln 2$.

Here N is the atom density of the medium in cm^{-3}; Z is the average atomic number of the medium; m, e, and v are the rest mass, charge, and speed of the electron, respectively; t is the electron kinetic energy in units of the electron rest mass

The electrons partly lose their energy by radiative interactions with the Coulomb force field of atom. The electron radiative stopping power is modeled as

$$-\left(\frac{dE}{ds}\right)_{rad} = 10^{24} Z(Z+\bar{\eta})(\alpha r_e^2)(T+mc^2)\Phi_{rad}^{(n)} \qquad (4\text{-}3)$$

where, η is a parameter to account for the effect of electron-electron bremsstrahlung, α is the fine structure constant, r_e is the classical electron radius and $\Phi_{rad}^{(n)}$ is the scaled electron-nucleus radiative energy-loss cross section based upon evaluations by Berger and Seltzer.

As beta particles interact with matter, statistical variations occur in the amount of energy in each collision. The statistical variation of energy losses is called energy

straggling (Turner 1995). Landau/Blunck-Leisegang theory expresses energy straggling due to collisions as

$$f(s,\Delta)d\Delta = \phi(\lambda)d\lambda\,, \tag{4-4}$$

where s is the length of the substep, Δ is energy loss, and $\phi(\lambda)$ is a universal function of a single scaled variable.

The angular deflection is sampled for each substep. The Goudsmit-Saunderson theory is used for precalculation and tabulation of multiple scattering distributions at the initiation of a run.

$$F(s,\mu) = \sum_{l=0}^{\infty}\left(l+\frac{1}{2}\right)\exp(-sG_l)P_l(\mu)\,, \tag{4-5}$$

where s is the length of the substep, $\mu = cos\ \theta$ is the angular deflection from the direction at the beginning of the substep, $P_l(\mu)$ is the l^{th} Legendre polynomial, and G_l is

$$G_l = 2\pi N\int_{-1}^{+1}\frac{d\sigma}{d\Omega}\left[1-P_l(\mu)\right]d\mu\,, \tag{4-6}$$

in terms of the microscopic cross section $d\sigma/d\Omega$, and the atom density N of the medium.

The sampling of bremsstrahlung photons produced is simulated along electron substeps. The radiative energy loss uses the average energy of all the bremsstrahlung photons sampled. Such a scheme conserves energy more closely but becomes more like a continuous-slowing-down approximation energy-loss model.

Beta particles lose their energy through several processes at the same time or with a slight time difference. For the computation sequence, the transport data of particles in each substep may not be equal to the actual data in a substep. To compensate for this discrepancy, MCNP adopts the two energy indexing algorithms: MCNP energy-indexing algorithm and ITS energy-indexing algorithm. The MCNP energy-indexing algorithm uses the precalculated transport data from the initial energy group, while the ITS energy-indexing algorithm assigns the data from the average energy group. Schaart *et al.* (2002) compared computational results of two energy indexing algorithms with experimental results. ITS electron energy-indexing algorithm agreed with the experimental results more closely.

The detailed modeling not addressed here is described in MCNP5 manual (X-5 Monte Carlo Team 2003).

IV-2 Code modeling

The MCNP5 base model for the glass seed was developed consisting of 3 cells, 181 surfaces, and 177 detector cells. The *F8 tally (an energy deposition tally, with units of MeV) in a 0.01 cm radius spherical water receptor was used to calculate dose per unit activity at varying distances. Dose can be calculated as *F8 tally divided by mass of detector cells. An “ITS-style” energy-indexing algorithm (Jeraj *et al.* 1999) was used and the number of source electron histories was chosen so that there was less than 1% of statistical error at the reference point. Mode P E was used with default modeling of

bremsstrahlung. Figure IV-1 shows the MCNP drawings denoting the seed and detectors in water on x-y plane, and y-z plane.

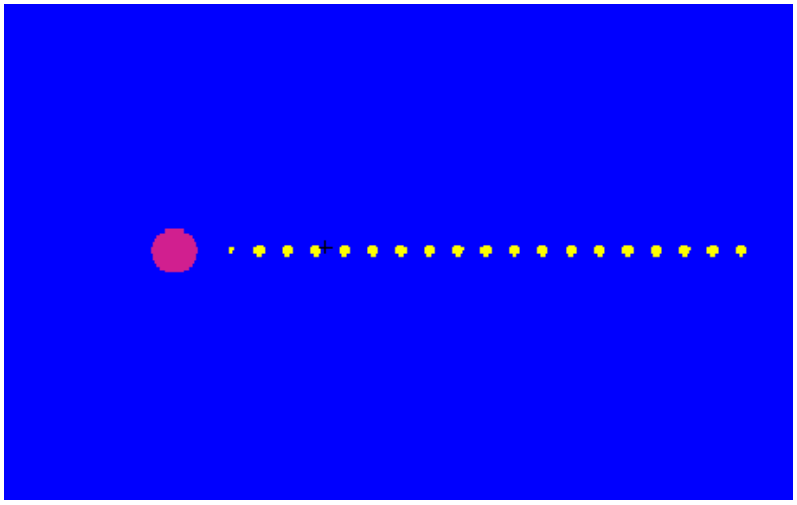

a) x-y plane

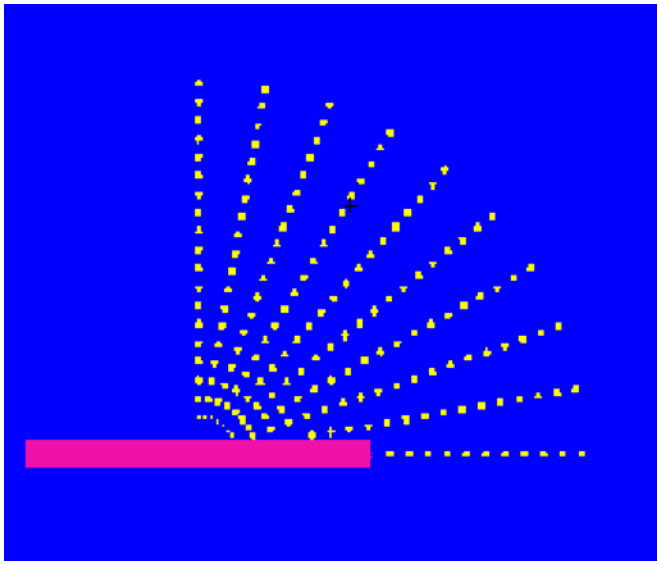

b) y-z plane

Figure IV-1. MCNP drawings

IV-3 Calculation results

The MCNP5 Monte Carlo code was used to calculate dose rate distributions in water. Dosimetry data in water were calculated in radial distances from the glass seed from 1 mm to 10 mm, and over angles ranging from 0^o to 90^o using *F8 tally in a 0.02 cm diameter water receptor. Figure IV-2 shows radial dose profiles of DPK and MCNP5 calculation. The profiles have a good agreement up to 0.6 cm but beyond 0.6 cm, the DPK code underestimates the dose.

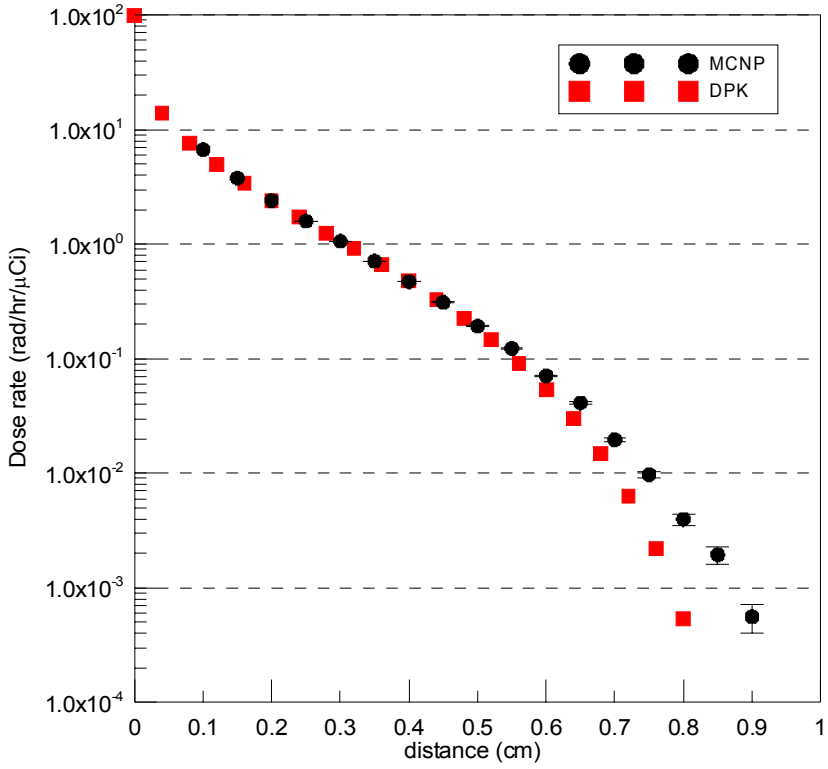

Figure IV-2. Radial dose profiles of DPK and MCNP5 calculation

Figure IV-3 shows the comparison of radial dose profiles of various seeds. Even though the design and dimensions of the seeds are different, note that the dose profile of ^{142}Pr is in a reasonable range compared with those of other beta-emitting seeds. For ^{90}Sr/^{90}Y, the dose within 0.2 cm is much higher than with other seeds because of the dose contribution of ^{90}Sr and the effects of the different seed dimensions.

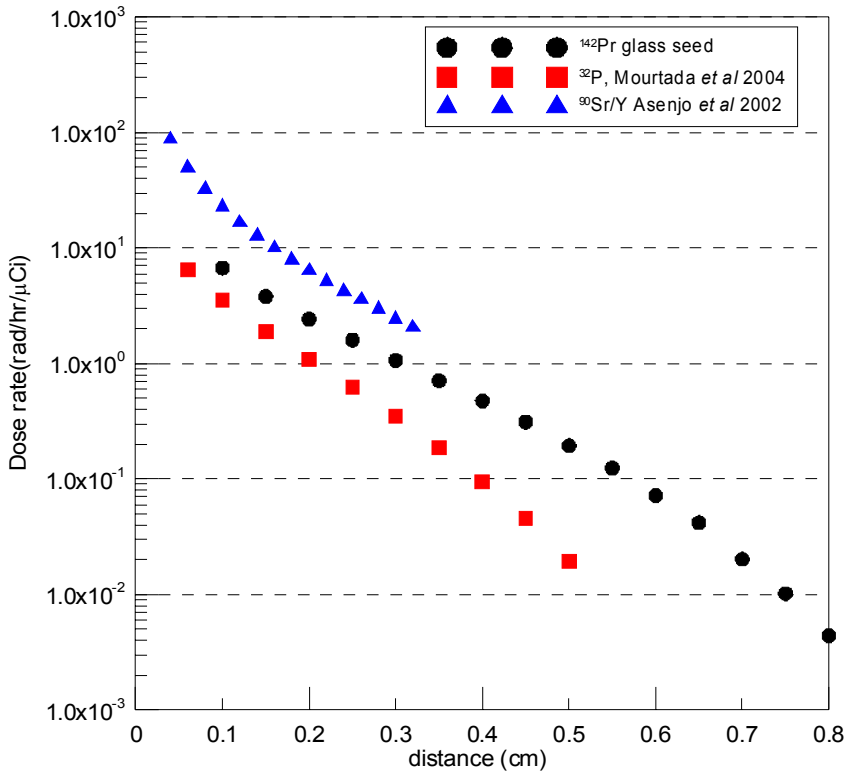

Figure IV-3. Comparison of radial dose profiles of various beta emitters

Figure IV-4 shows the radial dose profiles of beta and gamma dose from Pr seeds. The dose profile from beta decreases gradually to 0.6 cm because of low-energy part of the spectrum of beta particles and drops sharply after 0.6 cm (the range of average beta

energy). The dose profile is obviously also controlled by the inverse-square distance effects. The dose profile of gamma rays decreases gradually and the gamma dose is dominant beyond 0.9 cm. Calculations suggest that the dose at 1.0 cm from the source with initial activity of 5.95 mCi is 2.7×10^{-4} Gy/h.

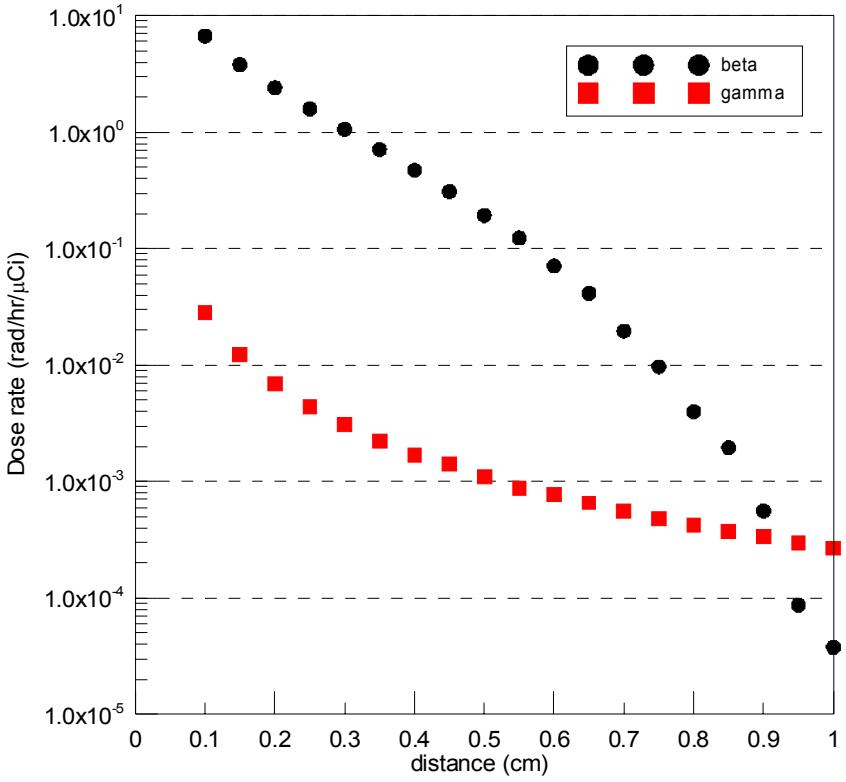

Figure IV-4. Radial dose profiles of beta and gamma dose of ^{142}Pr

IV-4 Uncertainty analysis

Table IV-1 presents an uncertainty analysis for the calculations performed. On the transverse-plane the statistical uncertainties in water at 0.2 cm and 0.6 cm were 0.3 % and 1.0 % respectively.

Table IV-1. Uncertainty assessment for Monte Carlo calculations

Monte Carlo uncertainties		
Component	r = 0.2 cm	r = 0.6 cm
Statistics	0.3 %	1.0 %
Cross-sections (2.3 %)		
Seed geometry	2.0 %	2.0 %
Source energy spectrum	1.56 %	1.56 %
Quadrature sum	3.4 %	3.6 %

For the electron calculation, MCNP5 uses mcplib04 and el03 cross section libraries. They have 2.3% uncertainty in the cross-sections. Even though the energy spectrum is modeled using the A option in which the entries are monotonically increasing or decreasing between the points selected as the energy spectrum, it cannot be modeled exactly as the curve of energy spectrum. The average energy of the input is 1.56% less than that of energy spectrum. The total quadrature sum uncertainty was estimated to 3.4 % for 2 mm and 3.6 % for 6 mm respectively.

IV-5 Sensitivity analysis

A sensitivity analysis was performed to find the optimum size of the detector in MCNP calculations, the impact of seed length, and the effect of "ITS-style" energy indexing algorithm. Figure IV-5 shows the comparison of dose rate as a function of radius of detector. The output shows no significant differences below 0.01 cm radius. A smaller detector needs more computation time to get the same statistical uncertainty. The 0.01 cm radius detector was selected for most calculations based on the resolution of the output and computation time.

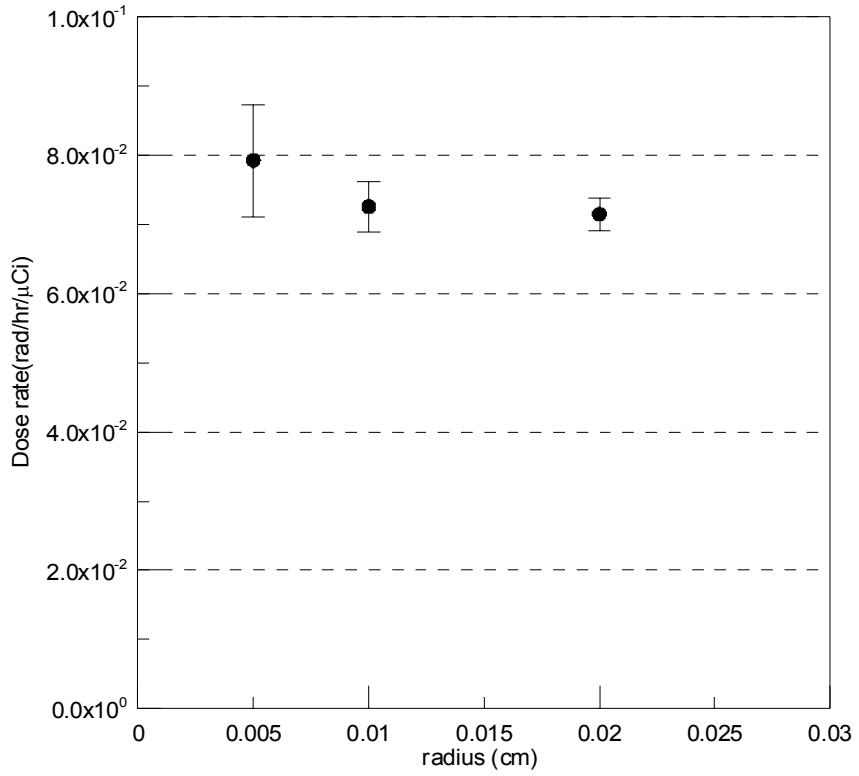

Figure IV-5. Comparison of dose rate for different radii of the detectors

Figure IV-6 shows the radial dose profiles as a function of seed length with initial activity of 5.95 mCi. The radial dose profile does not vary significantly with the length of seed.

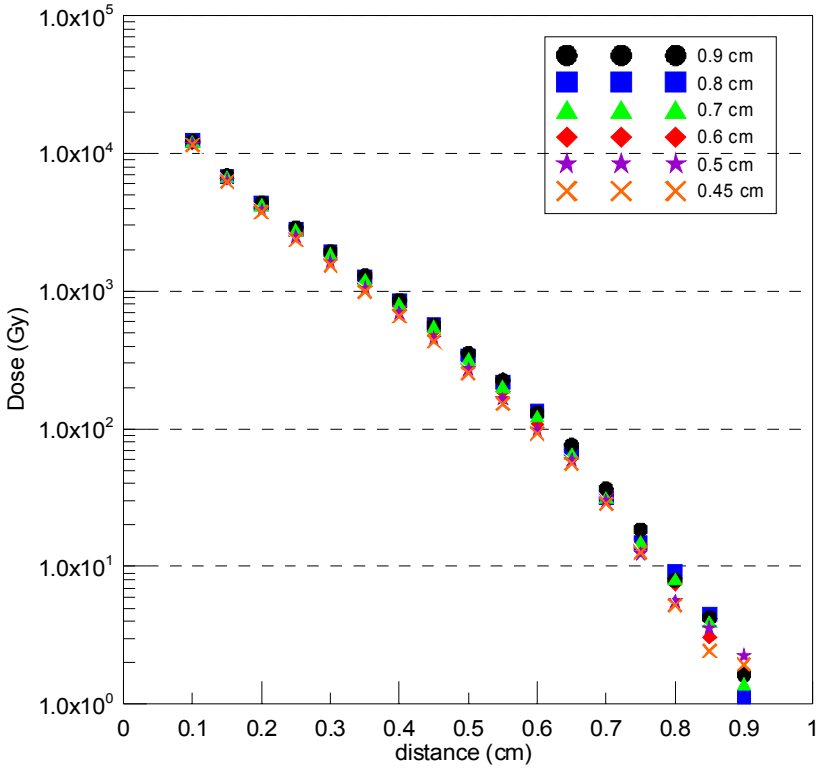

Figure IV-6. Radial dose profiles of different lengths of the seed

Figure IV-7 shows the axial dose profiles as a function of seed length with initial activity of 5.95 mCi. The axial dose profile decreases as the seed length is shortened. If a 0.45-cm length of seed is used, the radial and axial dose at 0.6 cm is expected to be same meaning that the dose profile of the seed is similar to an isotropic source. From this analysis, we may predict the dose distributions of longer seeds. The radial dose profile

will be about the same at the transverse-plane at any length longer than 4.5 cm length and the axial dose profile will be increased proportional to the length.

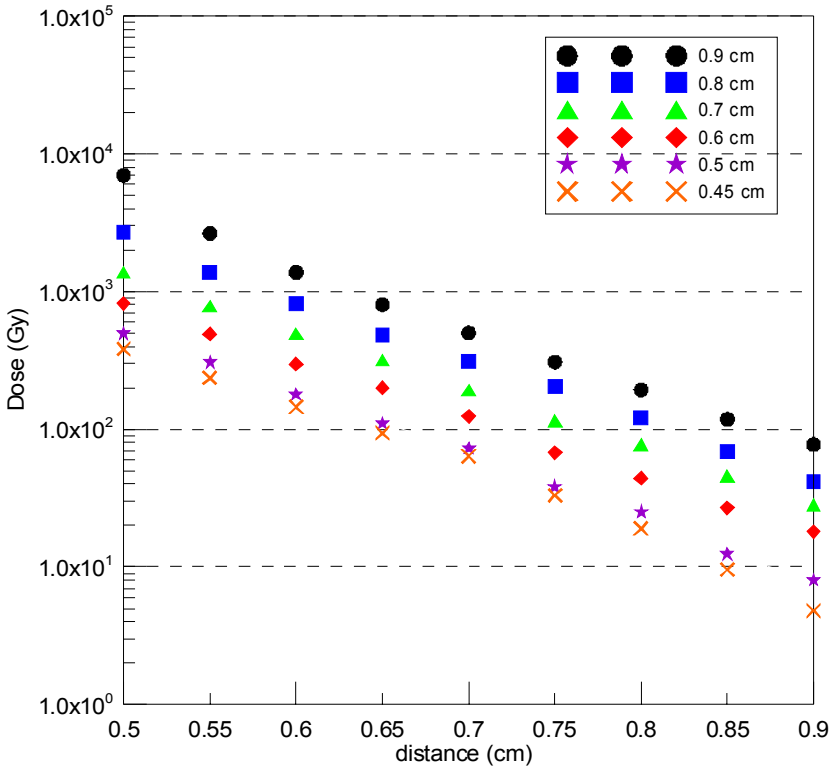

Figure IV-7. Axial dose profiles of different lengths of the seed

CHAPTER V

EXPERIMENTAL MEASUREMENT

V-1 Preparation of experiment

The Pr Glass was manufactured by MO-SCI Corporation (Rolla, MO 65402). The glass comes in about 15.0 cm long rods as shown in Figure V-1. The rod diameter is 0.08 ± 0.001 cm, the same as the typical ^{125}I seeds. Because the rod is extruded from bulk glass, it may bend and be uneven. It is recommended that the glass rod be drawn to get more uniform diameter of the seeds. To cut the rods, a specially designed cutting tool was made using a DREMEL® tool which can cut the glass to the same length as shown in Figure V-2. The edges of the seed were smoothed with sandpaper. Figure V-3 shows the seed dimensions and coordinate system based on AAPM TG-43. The length is twice that of the typical ^{125}I seeds to achieve the target dose at the edges of the field and to shorten surgery time. The density of Pr glass is 4.0 g/cm^3 and the weight percent of Pr is 44.5%. The refractory index of Pr glass is 1.705 ~ 1.715. Table V-1 presents the compositions of ^{142}Pr REAS glass. The detailed material test sheet is listed in Appendix I.

Figure V-1. Raw ^{142}Pr REAS glass seed

Figure V-2. Specially designed DREMEL tools

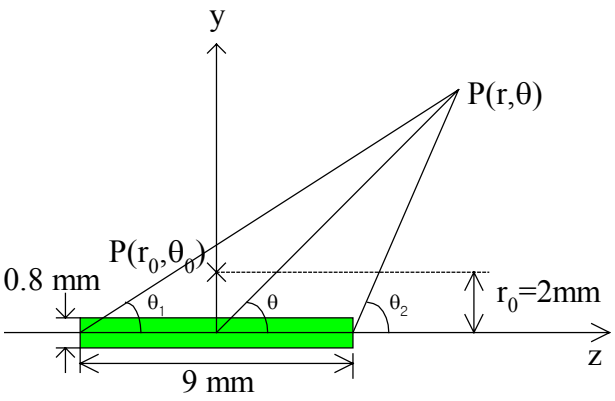

Figure V-3. Seed dimensions and coordinate system

Table V-1. Compositions of ^{142}Pr REAS glass seed

Element	Weight %	Mass in seed (mg)
Si	0.153	2.754
Al	0.081	1.458
Pr	0.445	8.010
O	0.321	5.778
Total	1.000	18.000

V-2 Nuclear Science Center Reactor (NSCR)

The Pr glass seeds were activated in a TRIGA (Teaching, Research, and Isotopes, General Atomic) reactor. The TRIGA reactor at Nuclear Science Center (NSC 2003) in Texas A&M University, College Station, Texas is a one-megawatt (MW) pool type nuclear reactor. Each location in the grid supports a fuel bundle with 4 positions for either fuel elements, control rods or other non-fueled elements. Figure V-4 shows the TRIGA core configuration including regular fuel elements, an instrumented fuel element, shim safety rods, a transient rod and a regulating rod.

The fuel elements and control rods are contained in bundle assemblies which are positioned and supported by an aluminum grid plate containing a 6 by 9 array of holes. The grid plate accommodates graphite blocks, detectors, pneumatic devices and various experiments. The grid locations in column A on the grid plate are available for positioning various irradiation objects. The grid locations D3 and D7 are reserved for experiments that require fast neutrons or higher neutron flux. Pneumatic irradiation devices are installed for the production of short-lived radioisotopes. The irradiation cell located at the west end of the reactor pool is used to irradiate large objects. In this configuration, samples can be easily loaded and unloaded for long and short irradiations. The reactor operates at a maximum steady-state power level of 1 MW. At this level, the thermal neutron flux at various sample irradiation locations ranges from about 1.0×10^{12} neutrons$\cdot$cm^{-2}s^{-1} to a maximum of 1.5×10^{13} neutrons$\cdot$cm^{-2}s^{-1}. The information of research reactors worldwide is available at www.iaea.or.at/worldatom/rrdb.

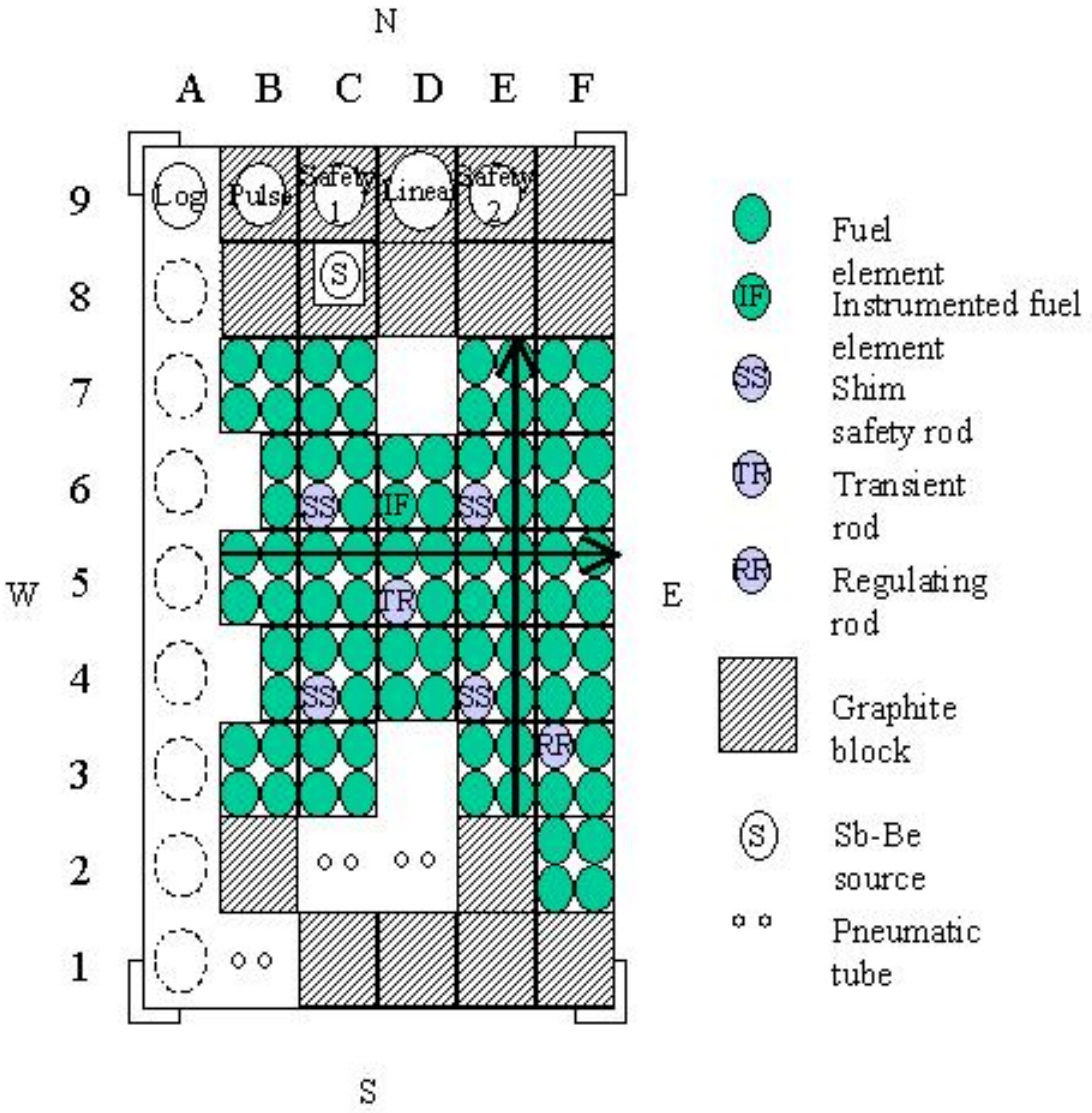

Figure V-4. Current NSCR core configuration

V-3 Neutron activation

For this experiment, the D7 location was used for neutron activation. Si and Al as well as Pr were activated in the reactor. However ^{28}Al has a 2.24 minute half-life and ^{31}Si has 2.62 hours half-life with 0.07% yield of gamma rays. Table V-2 presents several isotopes that are made during a one hour neutron activation of ^{142}Pr REAS glass at the D7 location.

Table V-2. Isotopes from neutron activation of ^{142}Pr REAS glass

Isotope	Activity	Half-life	Radiation	Yield
^{31}Si	17.9 μCi	2.62 h	γ 1.266 MeV β 1.48 MeV	0.07 % 100 %
^{28}Al	3.05 mCi	2.25 min	γ 1.778 MeV β 2.863 MeV	100 % 100 %
^{142}Pr	**4.384 mCi**	**19.12 h**	**γ 1.575 MeV** **β 2.162 MeV**	**3.7 %** **96.3 %**
^{142m}Pr	**1.675 mCi**	**14.6 min**	**IT**	**100 %**
^{19}O	2.59 μCi	26.9 sec	γ 1.365 MeV β 4.623 MeV	50.4 % 45.4 %

Cd-covered gold foils and bare gold foils were used to measure the neutron fluence rate at the activation location. Because Cd has a high thermal neutron cross section, essentially all of the thermal neutrons are absorbed in Cd. The Cd-covered Au-foil was almost solely activated by the epi-thermal neutron. The activities of Au-foils

were measured using a HPGe detector and the fluence rate of the thermal (2200 m/s) and epi-thermal neutrons was estimated to 1.481×10^{13} and 6.976×10^{11} $cm^{-2}s^{-1}$, respectively.

Based on the neutron fluence rate measured with the gold foils, the activities of ^{142}Pr were calculated using neutron activation equations and measured with a HPGe detector. The HPGe detector is the most popular for evaluating a photon source because of its high resolution. A semiconductor detector acts as a solid-state ionization chamber. The ionizing particle-beta ray, alpha particle, etc.-interacts with atoms in the sensitive volume of the detector to produce electrons by ionization. The collection of these ions leads to an output pulse. In contrast to the relatively high mean ionization energy of 30 to 35 eV for most counting gases, a mean energy expenditure of only 3.5 eV is required to produce an ionizing event in a semiconductor detector.

Radiation spectroscopy is the analysis of radiation sources or radioisotopes by measuring the energy distribution of the source. A spectrometer is an instrument that separates the output pulses from a detector, usually a scintillation detector or a semiconductor detector, according to size. Since size distribution is proportional to the energy of the detected radiation, the output of the spectrometer provides detailed information that is useful in identifying unknown radioisotopes and in counting one isotope in the presence of others. This technique has found widespread application in X-ray and gamma-ray analysis using NaI(Tl) scintillation detectors and semiconductor detectors, in beta-ray analysis using liquid scintillation detectors, and in alpha analysis using semiconductor detectors. Nuclear spectrometers are available in two types, either a single-channel instrument or a multichannel analyzer (MCA). The essentials of a single-

channel spectrometer consist of the detector, a linear amplifier, a pulse-height selector, and a readout device, such as a scaler or a ratemeter.

A multichannel analyzer has an analog-to-digital converter (ADC) instead of a pulse-height selector to sort all the output pulses from the detector according to height. The MCA also has a computer-type memory for storing the information from the ADC or from another source. This feature allows automated data processing operations such as background subtraction and spectrum stripping.

Although ^{142}Pr is mainly a beta source, HPGe detectors can detect ^{142}Pr using gamma spectroscopy because it has a 3.7 % yield of 1.5 MeV photons. As shown in Figure V-5, the ^{142}Pr glass seeds has prominent peak at 1.5 MeV after several half-lives of ^{142}Pr. Table V-3 compares the calculated and measured activities. The activity was measured about 5 half-lives of ^{142}Pr after end of neutron activation for 20 minutes with 1.21% of dead time. The epi-thermal neutron flux was considered for the calculation. The induced activity of the ^{142}Pr glass seeds was as predicted.

Table V-3. Activity from measurement and calculation

	Measurement (HPGe)	Calculation (NAA)
Activity	235.88 μCi	236.5 μCi

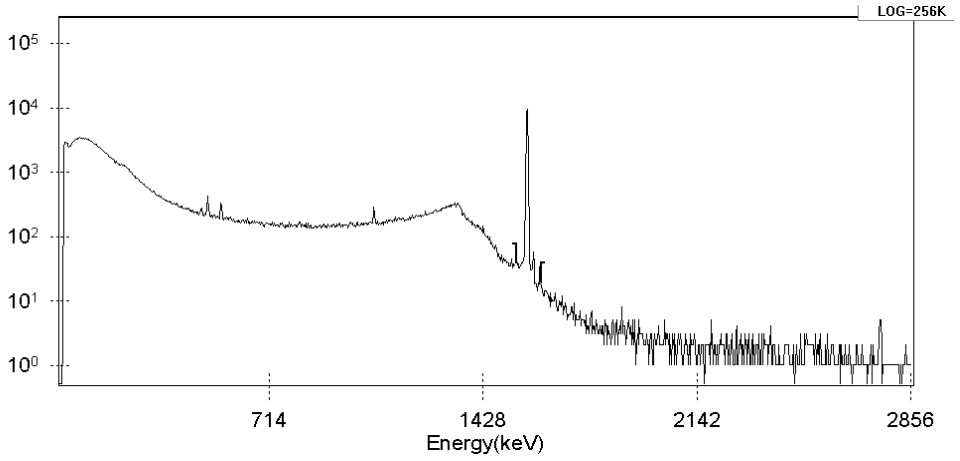

Figure V-5. Energy spectrum of ^{142}Pr at HPGe detector

Figure V-6 shows the relative activity as a function of time after activation. The square is ^{142}Pr activity from ground-state. The triangle is the activity from meta-stable state. The circle is the total activity. After about 3 half lives of ^{142m}Pr, the total activity is at maximum. After meta-stable decay, 36% of total activity is derived from the meta-stable state. Immediately after activation, the ^{142}Pr seed is too active to measure on the HPGe detector. We measured the activity after several half-lives of ^{142}Pr passed and calculated the activity back to the end of neutron activation.

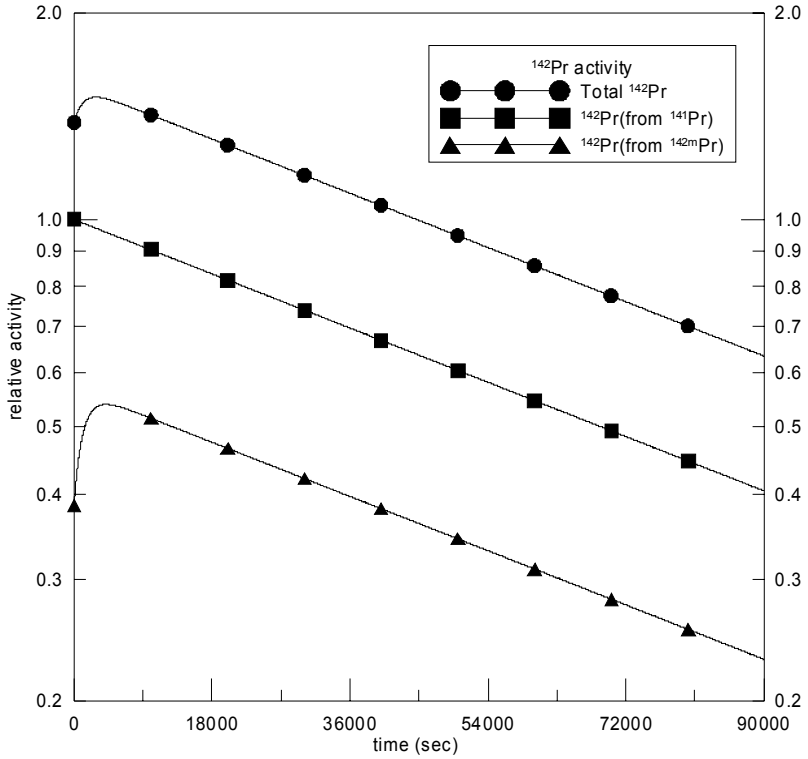

Figure V-6. Relative activity of ^{142}Pr and ^{142m}Pr after end of neutron activation

The activity of ^{142}Pr and ^{142m}Pr can be expressed as

i) $0 < t < t_0$

$$\frac{dN_1}{dt} = R - \lambda_1 N_1 \tag{5-1}$$

$$\frac{dN_2}{dt} = \lambda_1 N_1 - \lambda_2 N_2 \tag{5-2}$$

$$R = \phi \cdot \Sigma_{act} \cdot V \tag{5-3}$$

where, t_0 is neutron activation time, ϕ is neutron flux, Σ_{act} is activation cross section, V is volume, N_1 and N_2 are the number of atoms of ^{142}Pr and ^{142m}Pr, and λ_1 and λ_2 are decay constant of ^{142}Pr and ^{142m}Pr, respectively.

Integrating Eq. (5-1) and (5-2) give

$$N_1(t) = \frac{R}{\lambda_1}(1 - e^{-\lambda_1 t}) \tag{5-4}$$

$$A_1(t) = N(t) \cdot \lambda_1 = R(1 - e^{-\lambda_1 t}) \tag{5-5}$$

$$N_2(t) = R\left(\frac{1 - e^{-\lambda_2 t}}{\lambda_2} - \frac{e^{-\lambda_1 t} - e^{-\lambda_2 t}}{\lambda_2 - \lambda_1}\right) \tag{5-6}$$

$$A_2(t) = \lambda_2 N_2(t) = R\left(1 - e^{-\lambda_2 t} - \frac{\lambda_2}{\lambda_2 - \lambda_1}(e^{-\lambda_1 t} - e^{-\lambda_2 t})\right) \tag{5-7}$$

where, A_1 and A_2 are the activity of ^{142}Pr and ^{142m}Pr, respectively.

ii) $t > t_0$

$$\frac{dN_1}{dt} = -\lambda_1 N_1 \tag{5-8}$$

$$\frac{dN_2}{dt} = \lambda_1 N_1 - \lambda_2 N_2 \tag{5-9}$$

$$A_1(t) = A_{10}(1 - e^{-\lambda_1 t}) \tag{5-10}$$

$$N_2(t) = \frac{A_{10}}{\lambda_2 - \lambda_1} \cdot e^{-\lambda_1 t} + \left(N_{20} - \frac{A_{10}}{\lambda_2 - \lambda_1}\right) \cdot e^{-\lambda_2 t} \tag{5-11}$$

$$A_2(t) = \lambda_2 N_2(t) \tag{5-12}$$

The above equations are strictly true if the neutron flux and cross section are constant and the number of ^{141}Pr atoms during and after neutron activation is constant. As shown Table V-3, the calculation result has excellent agreement with the measurement result.

V-4 Radiochromic film dosimetry

To verify the Monte Carlo calculation, we measured the two-dimensional dose distribution around the seed. The conventional dosimetries such as TLD, polymer gels, plastic scintillators, and radiochromic films were surveyed. BANG gel was considered for dosimetry measurements, but because of high refractory index of ^{142}Pr REAS glass and asymmetric two-dimensional dose distributions of the seed, BANG gel was not used. We used radiochromic dye films for measuring the spatial 2-D dose distributions mostly because of the very steep gradients around beta sources. Radiochromic film is easy to use, dose-rate independent, insensitive to normal room light, self-developing with no other processing, and tissue-equivalent. Its color is stable with time after the stabilization time of 24 hours. GAFCHROMIC® MD-55-2 (Nuclear Associates) is doubly layered and water resistant except for the edge of the films (Butson *et al.* 2001).

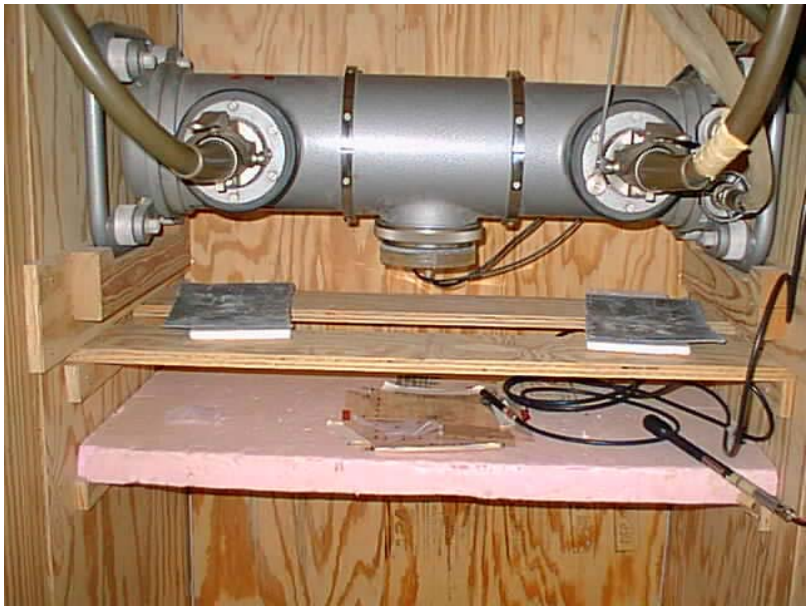

Figure V-7. X-ray machine (Norelco MG300) of the Nuclear Science Center

The radiochromic films were calibrated using an X-ray machine (Norelco Model MG-300) at the Nuclear Science Center shown in Figure V-7. They were cut to about 1 cm × 3 cm strips and taped onto the holder for exposure. They were carefully managed to prevent exposure from direct sunlight because they are sensitive to ultra-violet. The radiochromic films were exposed to known doses of X-rays calibrated against a NIST traceable ion chamber. The operating parameters of the X-ray machine were 250 kVp and 10 mA. After each exposure the color changes of the films were read using an Epson Perfection 2480 PHOTO scanner and converted to 8 bit numbers in MATLAB software. The MATLAB commands are listed in Appendix III. From the data acquired in Table V-4, optical densities were generated. The optical density (OD) can be expressed as

$$OD = \log\left(\frac{I_0}{I}\right) \tag{5-13}$$

where I_0 is the amount of light transmitted through an unexposed film, and I is the amount of light transmitted through irradiated film.

A calibration curve shown in Figure V-8 was derived and fit based on the optical density (OD) of the known doses. The calibration curve can be used to measure the dose of 2 MeV beta particles without correction. From these data, optical densities were generated and 2-dimensional dose profiles were derived.

Table V-4. Calibration film image and 8 bit numbers

0 Gy		2 Gy	
Color	Pixel value (0~256)	Color	Pixel value (0~256)
	203		192
5 Gy		10 Gy	
Color	Pixel value (0~256)	Color	Pixel value (0~256)
	179		162
20 Gy		50 Gy	
Color	Pixel value (0~256)	Color	Pixel value (0~256)
	133		90
70 Gy			
Color	Pixel value (0~256)	Color	Pixel value (0~256)
	70		

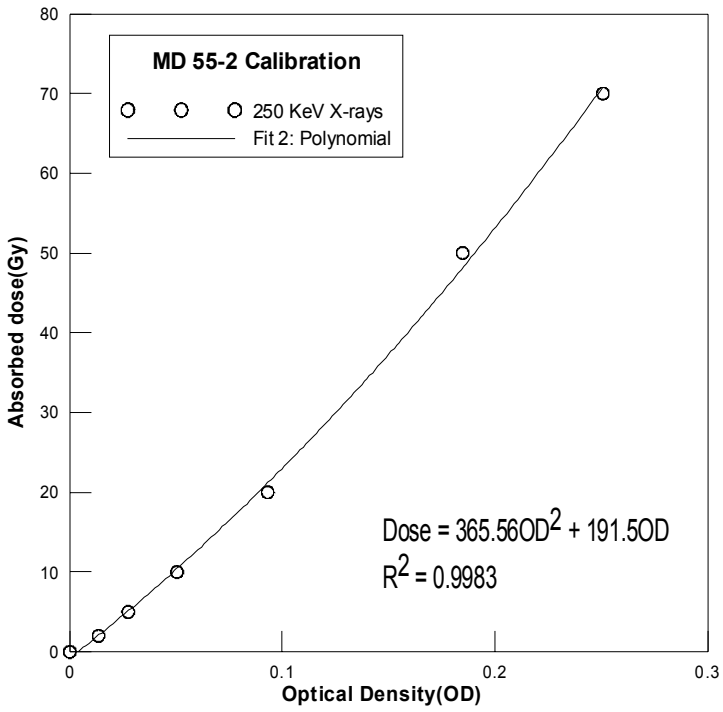

Figure V-8. Calibration data and fitted curve of MD-55-2

V-5 Experiment procedures

Table V-5. The experiment time sequence

No.	Sequence (start time)	Duration	Time	^{142}Pr activity	Comments
1	Activation	1 h	0:00:00	0 mCi	D7TI device
2	Decay time	30 min	1:00:00	5.53 mCi	Decay time (short-lived radionuclides)
3	Handling	30 min	1:30:00	5.94 mCi	
4	Film Irradiation	1 half-life of ^{142}Pr (19.12 h)	2:00:00	5.95 mCi	
5	Film Stabilization	1 day	21:07:12	-	
6	Film Scan	-	-	-	
7	Activity Measurement	4 day after EOI (5 half-life, ~1/32)	-	214.50 μCi	

First of all, the seed was cut to the precise length and smoothed with sandpaper and weighed. After that, the seed was put in a plastic container with a cushion. The container was sealed in an aluminum can. The can was placed in special equipment for installation at reactor core location D7. The equipment was moved to D7 location with full power operation following operation procedure (NSC 2003). After a given time, the equipment was removed from the core and stored in the pool for 30 minutes to allow decay of short half-life radionuclides such as ^{28}Al. The activated seed was removed and placed in an experimental set-up. The seed irradiated the radiochromic film for a given time (19.12 h, one half-life of ^{142}Pr). After that, the seed was stored in lead-shielded storage to decay. The radiochromic film was stored in light-shielded area for stabilization. After 1 day of film stabilization time, the film was scanned. After several

half-lives of ^{142}Pr, the activity of seed was measured with a HPGe detector. Table V-5 presents the time sequence of the experiments. The activities are estimated assuming that the experiment is conducted in the exact time sequence.

V-6 Experiment I – Radial dose profile

Experiment I was conducted to measure radial dose distribution at the axial center. Figure V-9 shows a schematic diagram of the source-film arrangement in a solid water phantom. The solid water phantom (manufactured by Gammex®) simulated water or tissue equivalent medium. The Solid Water™ phantom material is designed to have the same electron density as water. The hole above the glass seed was filled with TLD rods. The electron density of TLD chips has a little more than that of tissue or pure water, but this effect is negligible.

Figure V-10 shows the film image and dose contour for 19.12 hour exposure with an initial activity of 5.51 mCi. The center of the film was removed during drilling so the dose at surface was not measured. The radial dose profile is axisymmetric as expected. Figure V-11 shows the comparisons of radial dose profiles. MCNP calculation results agree well with film measurement results from 0.4 cm to 0.65 cm. Beyond 0.65 cm, MCNP5 underestimates the dose.

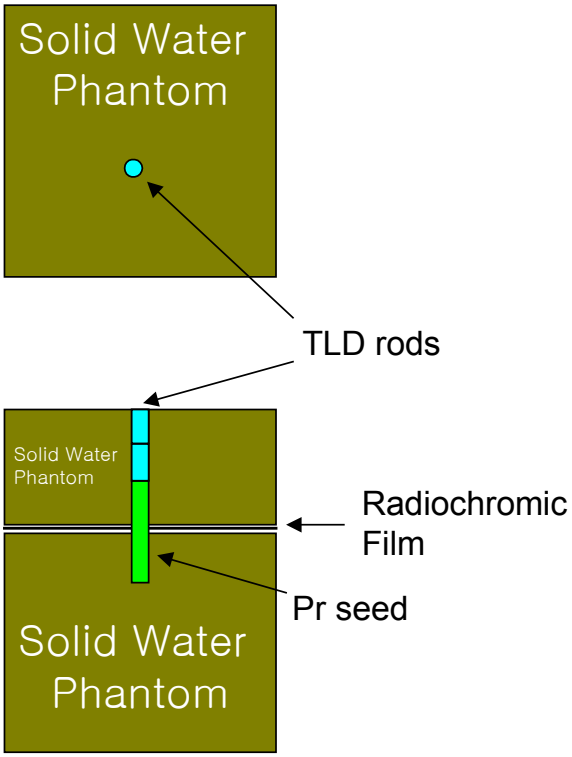

Figure V-9. Experiment setup for radial dose distribution

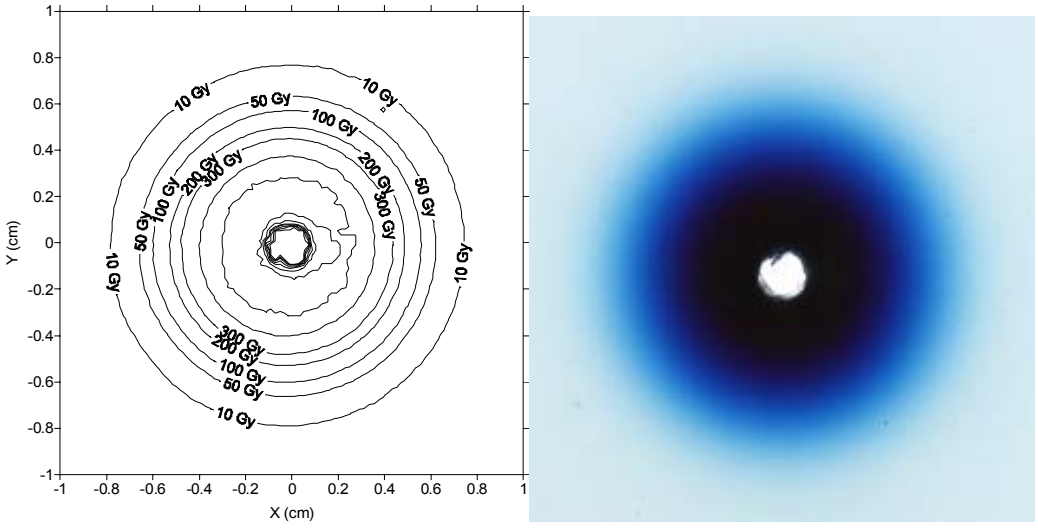

Figure V-10. (a) transverse-plane isodose plots of radiochromic film, (b) radiochromic film image of ^{142}Pr seeds

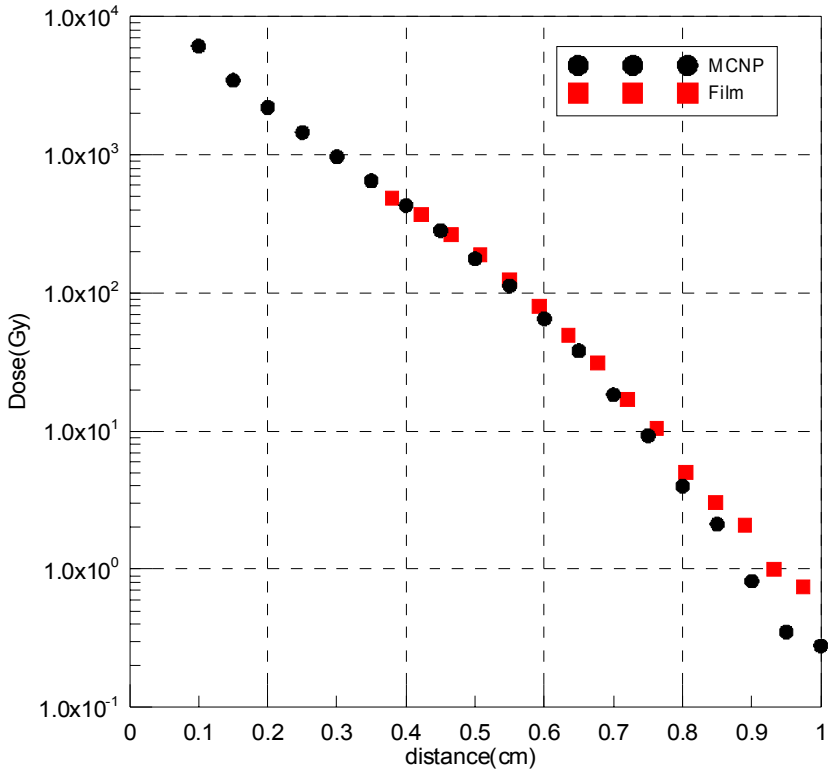

Figure V-11. Radial dose distribution

V-7 Experiment II – Axial dose profile

As shown in Figure V-12, a solid water phantom was used to provide full backscattering conditions during measurements. The radiochromic film was placed on the top of the solid water phantom. Distilled water inside a thin plastic film (Reynolds®) was put in a plastic cup with bottom removed. The thin plastic film prevented the distilled water from wetting the radiochromic film. The activated Pr glass seed was

placed in the middle of the bottom of a container of distilled water and the radiochromic film exposed for known times.

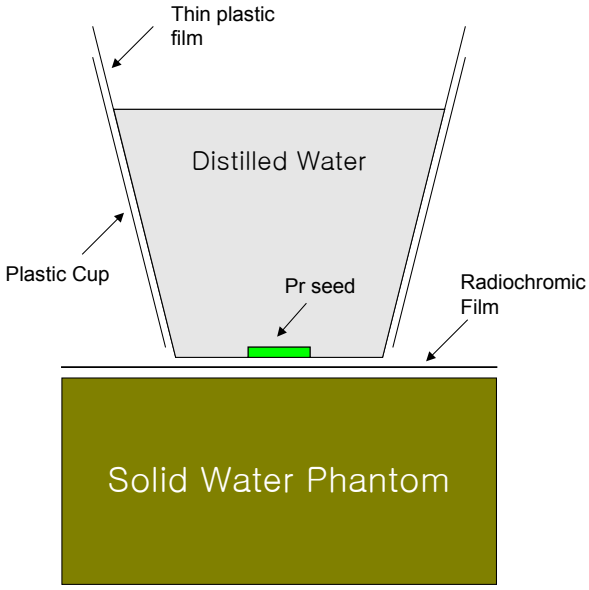

Figure V-12. Experiment setup for two-dimensional dose distributions

Radiochromic film was exposed one hour post-irradiation for 19.12 hours (one half life of ^{142}Pr). Figure V-13 shows the two-dimensional dose profiles from Monte Carlo simulation and film measurement. The interpolation was performed using the kriging algorithm in the SURFER® program. The calculated and measured dose distributions were in excellent agreement. The sensitivity of the radiochromic film is from 3 to 100 Gy, so the doses above 200 Gy are not shown for film measurement.

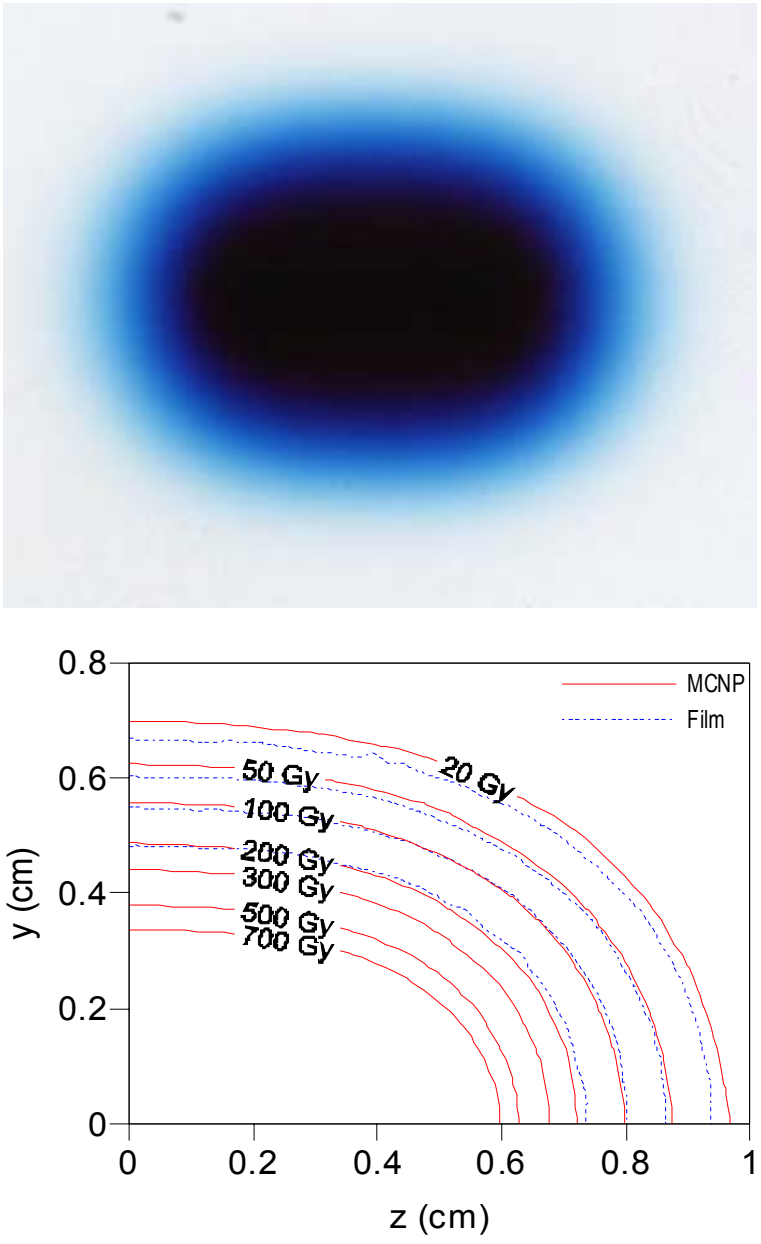

Figure V-13. (a) two-dimensional dose profiles of radiochromic film for 19.12 hour exposure with 5.95 mCi seed, (b) comparison of isodose plots of Monte Carlo calculation (solid lines) and radiochromic film measurement (dotted lines)

The total doses at r = 6 mm and $\theta = 90^{o}$ and at r = 6 mm and $\theta = 0^{o}$ were calculated to be 130.8 Gy and 192.7 Gy respectively. Considering that a second seed positioned on a 1.2 cm center to center grid would double the dose at this point shown in Figure V-14, the dose at r = 6 mm and $\theta = 90^{o}$ can be equal to 261.6 Gy. The results show that the seed can achieve the target dose and meet the seed design criteria.

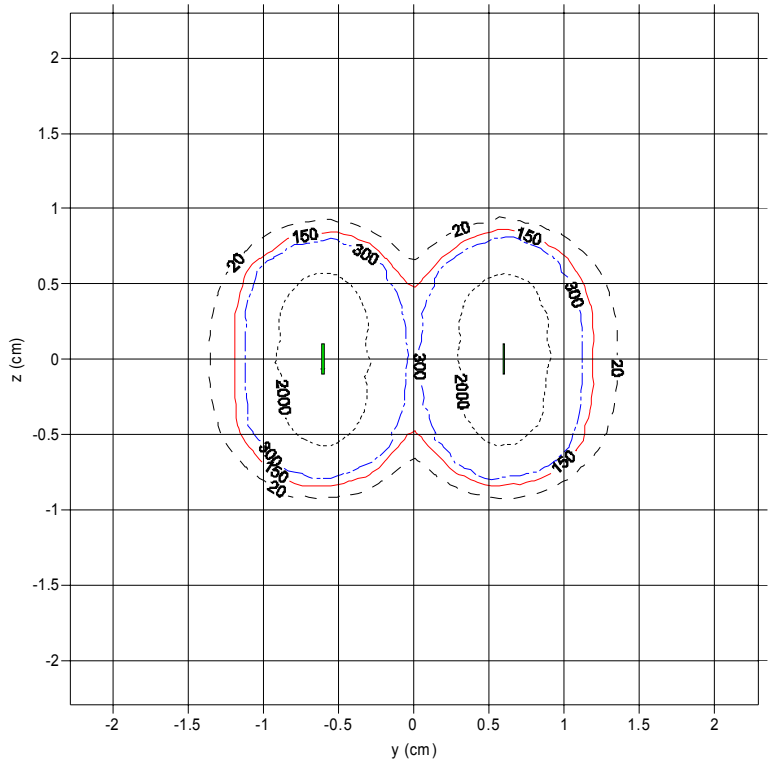

Figure V-14. Two-dimensional dose profiles using radiochromic film for two seeds (in Gy)

CHAPTER VI

AAPM TG-60 DOSIMETRIC PARAMETERS

VI-1 Dosimetry parameters

The dosimetric parameters defined in AAPM TG-60/TG-43 were determined using the Monte Carlo calculations, including: reference dose rate, geometry function, radial dose function and anisotropy function. The coordinate system can be seen in Figure V-3. The dose at a point can be expressed as

$$D(r,\theta) = D(r_0,\theta_0)\cdot[G(r,\theta)/G(r_0,\theta_0)]\cdot g(r)\cdot F(r,\theta) \qquad (6\text{-}1)$$

where r is radial distance from the source, θ is angle between the line segment from point of interest to center of source, $G(r,\theta)$ is geometry function resulting from spatial distribution of the radioactivity within the source, $g(r)$ is radial dose function, $F(r,\theta)$ is anisotropy function describing the dose variation and $D(r_0,\theta_0)$ is the dose rate in water at the reference point. The reference point suggested in AAPM TG-60 is r_0 = 2 mm and θ_0 = 90^0. Table VI-1 presents the lookup dose rate table.

Table VI-1. Lookup dose rate table in rad/h/μCi

θ, deg r, mm	90	80	70	60	50	40	30	20	10	0
0.10	6.71E+0	6.90E+0	7.22E+0	7.88E+0	9.19E+0	1.15E+1	1.57E+1			
0.15	3.80E+0	3.89E+0	4.17E+0	4.64E+0	5.47E+0	6.89E+0	9.35E+0	1.52E+1		
0.20	2.41E+0	2.46E+0	2.67E+0	3.03E+0	3.66E+0	4.62E+0	6.50E+0	1.05E+1		
0.25	1.59E+0	1.63E+0	1.77E+0	2.05E+0	2.51E+0	3.29E+0	4.76E+0	7.79E+0		
0.30	1.06E+0	1.10E+0	1.21E+0	1.42E+0	1.76E+0	2.41E+0	3.55E+0	6.00E+0	1.45E+1	
0.35	7.11E-1	7.36E-1	8.32E-1	9.80E-1	1.25E+0	1.72E+0	2.59E+0	4.61E+0	1.15E+1	
0.40	4.73E-1	4.95E-1	5.50E-1	6.75E-1	8.82E-1	1.23E+0	1.87E+0	3.27E+0	8.69E+0	
0.45	3.11E-1	3.26E-1	3.70E-1	4.57E-1	6.11E-1	8.48E-1	1.28E+0	2.16E+0	4.65E+0	
0.50	1.94E-1	2.06E-1	2.42E-1	3.10E-1	4.15E-1	5.83E-1	8.63E-1	1.34E+0	2.19E+0	3.84E+0
0.55	1.24E-1	1.26E-1	1.49E-1	2.03E-1	2.76E-1	4.00E-1	5.75E-1	8.24E-1	1.16E+0	1.45E+0
0.60	7.16E-2	7.74E-2	9.54E-2	1.29E-1	1.75E-1	2.65E-1	3.70E-1	5.32E-1	6.65E-1	7.57E-1
0.65	4.18E-2	4.10E-2	5.33E-2	8.04E-2	1.16E-1	1.73E-1	2.46E-1	3.38E-1	4.17E-1	4.42E-1
0.70	2.01E-2	2.25E-2	3.21E-2	4.71E-2	7.35E-2	1.10E-1	1.61E-1	2.14E-1	2.56E-1	2.75E-1
0.75	1.02E-2	1.09E-2	1.68E-2	2.63E-2	4.30E-2	6.59E-2	9.95E-2	1.34E-1	1.63E-1	1.69E-1
0.80	4.39E-3	5.32E-3	9.14E-3	1.35E-2	2.59E-2	4.15E-2	6.36E-2	8.49E-2	1.01E-1	1.06E-1
0.85	2.33E-3	2.40E-3	4.73E-3	7.54E-3	1.40E-2	2.27E-2	3.85E-2	5.25E-2	6.20E-2	6.48E-2
0.90	9.01E-4	1.27E-3	1.59E-3	3.02E-3	6.87E-3	1.20E-2	2.08E-2	3.15E-2	3.91E-2	4.26E-2

VI-2 The reference dose rate for ^{142}Pr source $D(r_0, \theta_0)$

The dose rate at reference dose point $D(r_0, \theta_0)$ and a target point $D(r=6mm, \theta_0)$ derived based on two-dimensional dose distributions in water is presented in Table VI-2.

Table VI-2. The reference dose rate

Dose point	Dose rate (rad/h/μCi)
r = 2 mm, θ = 90°	2.412 ± 0.0099
r = 6 mm, θ = 90°	0.072 ±0.0017

VI-3 The geometry function, G(r, θ)

From the definition in TG-43, the geometry function can be expressed as

$$G(r,\theta) = 1/r^2 \quad \text{for point source approximation} \quad (6\text{-}2)$$

$$= \frac{\theta_2 - \theta_1}{Lr\sin\theta} \quad \text{for line source approximation} \quad (6\text{-}3)$$

Because the seed has no cladding nor radio-opaque markers and the active length is relatively long to get larger coverage, the line source approximation was used. The geometry function at the edges of the seed should be higher than that of isotropic source. Table VI-3 presents the geometry function times r^2 at various angles and distances.

Table VI-3. Geometry function, $G(r,\theta)$ times r^2

θ, deg r, mm	90	80	70	60	50	40	30	20	10	0
1.00	0.301	0.306	0.323	0.354	0.406	0.493	0.647	-	-	-
1.50	0.416	0.424	0.448	0.494	0.570	0.698	0.928	1.409	-	-
2.00	0.512	0.522	0.552	0.610	0.707	0.872	1.172	1.806	-	-
2.50	0.591	0.602	0.638	0.704	0.817	1.011	1.369	2.143	-	-
3.00	0.655	0.667	0.705	0.777	0.900	1.112	1.510	2.392	5.272	-
3.50	0.708	0.720	0.759	0.833	0.960	1.178	1.588	2.512	5.693	-
4.00	0.750	0.763	0.802	0.876	1.000	1.212	1.602	2.474	5.549	-
4.50	0.785	0.797	0.836	0.907	1.025	1.222	1.571	2.296	4.524	-
5.00	0.814	0.826	0.863	0.930	1.040	1.217	1.514	2.065	3.278	5.263
5.50	0.838	0.849	0.884	0.947	1.047	1.204	1.450	1.853	2.499	3.025
6.00	0.858	0.868	0.901	0.959	1.050	1.187	1.390	1.686	2.062	2.286
6.50	0.875	0.884	0.915	0.968	1.051	1.170	1.338	1.559	1.799	1.920
7.00	0.889	0.898	0.926	0.975	1.050	1.153	1.293	1.463	1.629	1.704
7.50	0.901	0.909	0.935	0.980	1.047	1.139	1.256	1.389	1.510	1.563
8.00	0.911	0.919	0.943	0.984	1.044	1.125	1.224	1.332	1.425	1.463
8.50	0.920	0.927	0.949	0.988	1.042	1.113	1.198	1.287	1.360	1.389
9.00	0.927	0.934	0.955	0.990	1.039	1.102	1.176	1.251	1.311	1.333

VI-4 The radial dose function, g(r)

The radial dose function, *g(r)* is calculated as

$$g(r) = \left(\frac{D(r,\theta_0)}{D(r_0,\theta_0)} \right) \left(\frac{G(r_0,\theta_0)}{G(r,\theta_0)} \right) \tag{6-4}$$

The radial dose function can be expressed using a least squares fit of a fifth order polynomial as

$$g(r) = a_0 + a_1 r + a_2 r^2 + a_3 r^3 + a_4 r^4 + a_5 r^5 \tag{6-5}$$

Table VI-4 presents the radial dose function g(r) 5^{th} order polynomial coefficients valid from 1.0 mm to 10 mm. The coefficient of determination is 0.999.

Table VI-4. 5^{th} order polynomial coefficients

Coefficient	Value
a_0	1.2623376
a_1	-0.0187000
a_2	-0.0735998
a_3	0.0087016
a_4	-0.0000594
a_5	-0.0000183

VI-5 The 2D anisotropy function, F(r,θ)

The 2D anisotropy function, *F(r,θ)*, is defined as

$$F(r,\theta)=\left(\frac{D(r,\theta)}{D(r,\theta_0)}\right)\left(\frac{G(r,\theta_0)}{G(r,\theta)}\right) \tag{6-6}$$

The 2D anisotropy function describes the variation of the dose rate around the seed, in the r distance and θ direction. The maximum value of the anisotropy function was estimated to 32.863. This is because the isodose profile is elliptical as seen in Figure VI-1. Most conventional seeds have a significant cold spots at the ends of the seed due to self-attenuation through the seed and encapsulation welds at the edges, while the Pr seed has no cold spots near the source ends as shown in Figure VI-1. Table VI-5 presents the anisotropy function values.

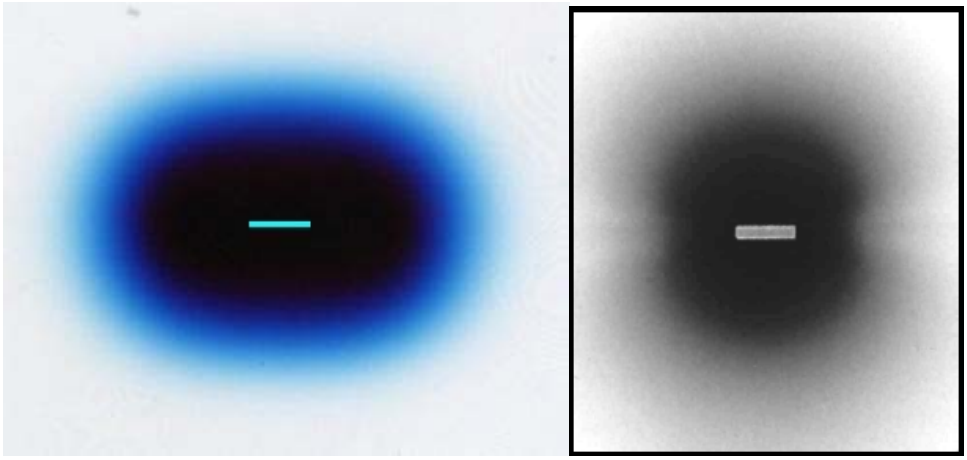

Figure VI-1. (a) radiochromic film image of ^{142}Pr seeds, (b) autoradiograph of ^{131}Cs Seed, available at http://www.isoray.com/assets/InvestorPresentation9606lw.pdf ("seed" superimposed and scaled for illustration)

Table VI-5. Aniostropy function

θ, deg r, mm	90	80	70	60	50	40	30	20	10	0
1.0	1.000	1.010	1.002	0.997	1.014	1.048	1.083			
1.5	1.000	1.006	1.020	1.030	1.053	1.083	1.106	1.187		
2.0	1.000	1.000	1.025	1.056	1.100	1.124	1.179	1.234		
2.5	1.000	1.002	1.028	1.079	1.138	1.205	1.289	1.349		
3.0	1.000	1.021	1.058	1.125	1.203	1.334	1.449	1.547	1.701	
3.5	1.000	1.017	1.090	1.169	1.298	1.455	1.625	1.823	2.009	
4.0	1.000	1.030	1.088	1.222	1.399	1.610	1.847	2.096	2.485	
4.5	1.000	1.030	1.118	1.273	1.502	1.751	2.057	2.373	2.597	
5.0	1.000	1.047	1.180	1.399	1.677	2.012	2.393	2.732	2.801	3.062
5.5	1.000	1.005	1.139	1.451	1.781	2.250	2.683	3.011	3.149	3.250
6.0	1.000	1.068	1.269	1.609	1.992	2.674	3.192	3.785	3.870	3.969
6.5	1.000	0.971	1.220	1.738	2.313	3.098	3.847	4.541	4.847	4.814
7.0	1.000	1.105	1.533	2.132	3.093	4.212	5.484	6.455	6.947	7.118
7.5	1.000	1.061	1.590	2.373	3.640	5.128	7.021	8.531	9.551	9.594
8.0	1.000	1.202	2.014	2.852	5.155	7.669	10.800	13.231	14.655	15.050
8.5	1.000	1.022	1.971	3.018	5.323	8.064	12.720	16.118	18.026	18.430
9.0	1.000	1.395	1.712	3.142	6.807	11.207	18.183	25.897	30.750	32.863

CHAPTER VII

CLINICAL PLANNING

VII-1 Treatment planning

To treat a patient effectively, treatment planning should be based on the health condition of patient, shape and place of the prostate, PSA level, Gleason score, and other factors. There are two types of seed implants, permanent seed implants and temporary seed insertion. For permanent seed implants, the half-life of the radionuclide is less than 100 days and beta emitters or low energy photon emitters are often used to reduce the dose to other organs. For temporary seed insertion, the seeds will stay for a certain time and will be then removed. There is no half-life limitation for temporary seed insertion. The ultrasound-guided transperineal template is used for permanent seed implants, while the loader is used for to reduce the dose to medical staff during the operation.

There are two kinds of treatment planning: pre-operational planning, intraoperation planning. Images of the prostate should be prepared for treatment planning. Since the shape and place of prostate changes daily, real-time planning has come to be preferred. The pre-operational planning is required to predict how many seeds and what activity would be needed. Precise digital imaging enables real-time planning. During the operation, the image of the seeds in the prostate and real-time software should be used to save operation time.

Post-implant dosimetry should be performed to find the effects of seed displacement and migration. Figure VII-1 shows the process flow diagram suggested in AAPM TG-64 report.

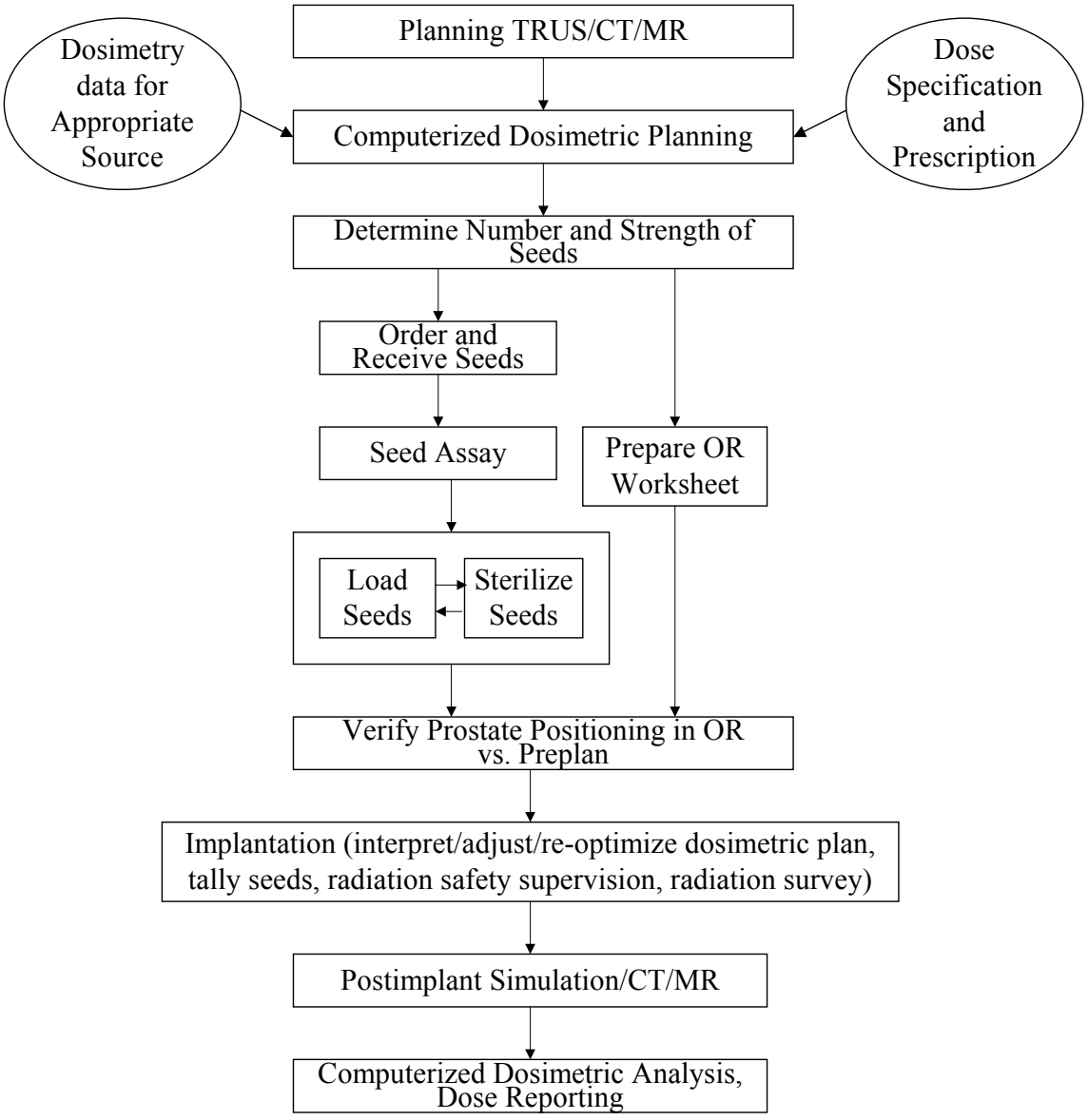

Figure VII-1. Process flow diagram for a pre-planned prostate seed implant

VII-2 High dose rate (HDR) brachytherapy

As described in Chapter II, the effect of dose rate is remarkable. In the case of permanent seed implant, dose rate is mostly determined by the half-life of seed isotope. For HDR, the half-life is not a factor to be considered because the seeds should be removed after a certain time. HDR has several advantages over LDR. The total dose is delivered to tumor cells in a short period such as 2 hours or less. The effects of seed migration, prostate distortion, or edema are very small. However, much higher activity is required generally. In case of ^{142}Pr glass seeds, a high fluence rate reactor having more than 10^{15} $cm^{-2}sec^{-1}$ is generally needed to get the desired activity. One-hour neutron activation in 10^{15} $cm^{-2}sec^{-1}$ can get about 361 mCi of ^{142}Pr. Within an hour, more than 150 Gy can be delivered at 0.6 cm from seed center with initial activity of 361 mCi.

VII-3 Dose coverage

Several tens of seeds are used for the treatment of prostate brachytherapy. The three-dimensional dose distributions at prostate can be drawn using juxtaposition of dose profile of a single seed. We can use a commercial software such as VariSeed^{TM} or CMS software to optimize seed position and dose distribution. From the calculation results, the dose point can be expected to satisfy the target dose. The dose coverage per seed is presented in Table VII-1.

Table VII-1. Dose coverage per seed

Prescribed dose	90 Gy	150 Gy
Volume	1.9 cm^3	1.65 cm^3

The three-dimensional dose profile of a seed can be obtained by interpolation of the dose rate table presented in Table VI-1. A fortran program code listed in Appendix D using Monte Carlo sampling was developed to find the overall three-dimensional dose distributions of prostate. The dose coverage can be determined by the program code. One million random positions were sampled to assess dose coverage. AAPM TG-64 recommends the evaluation of dose uniformity and conformity.

Figure VII-2 shows the isodose distributions of x-y plane and y-z plane based on Monte Carlo calculation results with the initial activity of 5.95 mCi. Ideally 40 seeds can cover the entire prostate.

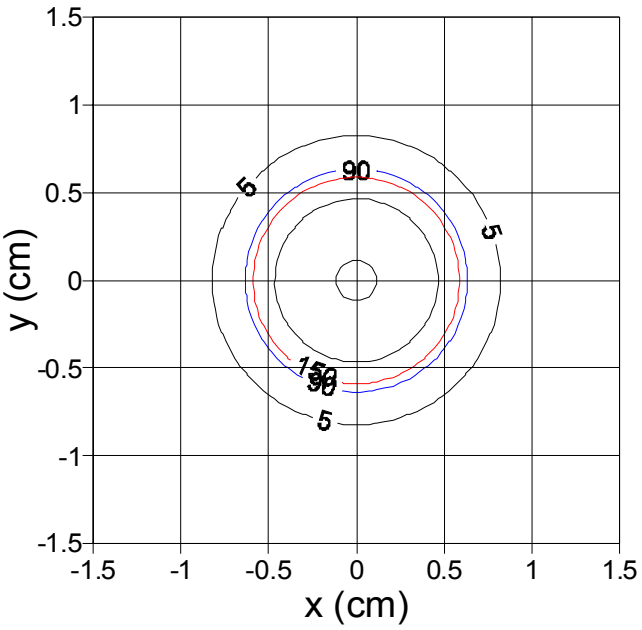

a) x-y plane (in Gy)

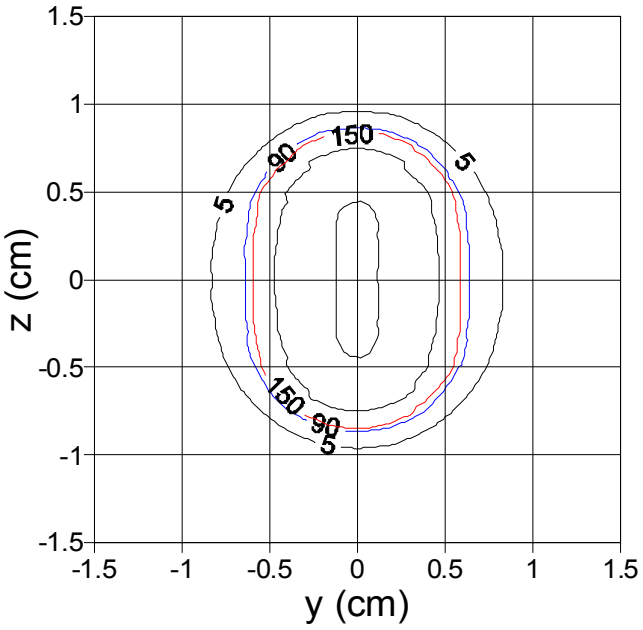

b) y-z plane (in Gy)

Figure VII-2. Two-dimensional isodose curve based on Monte Carlo calculation

VII-4 Seed positioning

To deliver the prescribed dose to the prostate, seed positioning is critical. This can be achieved by the proper dose planning and accurate delivery of the seeds. Two of the major factors for the proper dose planning are coverage and conformity. Coverage can be defined as the percent of volume in the prostate receiving the prescribed dose or more. Even if the prescribed dose is delivered to most of the prostate, cold spots can leave viable tumor cells. Cold spots can be of two kinds. One is from a seed's self-attenuation which is insignificant for ^{142}Pr glass seed. The other is from the seed position which can be caused by inadequate planning of seed position, imprecise implantation, by seed migration, or, by the change of prostate volume. During planning and implantation, all the expected factors that can cause the cold spots should be considered. The ideal is to place the seeds to produce a uniform prescribed dose, which may cause closer placement of seeds. The pre-operation treatment planning and positioning was commonly used in the past, however, the real time planning and image-guided positioning is preferred because the imaging technique of the prostate has advanced and the shape and size of the prostate can vary day to day.

Two loading patterns have been used: uniform loading and peripheral loading. Uniform loading places the seeds with uniform spacing which gives more dose to the center of the prostate, and especially high doses along the urethra. Peripheral loading is nonuniform loading so as to spare the urethra. For ^{142}Pr glass seeds, even for uniform loading, doses do not peak at the center of the prostate along the urethra.

VII-5 VariSeed™

A commercial software package, Variseed 7.1, has been used in a one-year research version for case study of seed placement. The VariSeed software is a brachytherapy treatment planning package for transperineal ultrasound-guided implants (VariSeed 2005). The features of the software are as follows:

- SeedFinder™ automatically locates seeds in a CT data series, dramatically reducing the time needed to create post-operation plans
- Rules-based Dose Optimization logic creates the ideal pre-plan
- Dynamic interpolation of contour entries for faster planning
- Image Fusion for targeted therapies or to compare pre- and post- plans
- Instantly auto-traces solid line contours from ultrasound images
- Modifies pre-plan dosimetry as seeds are placed using the Implant View (link) real time dosimetry module
- Twister™ (link) 3D offers volume acquisition without prostate distortion
- Exports data to all available automatic needle loading systems.

VariSeed software packages allow pre-operative planning, intra-operative planning, and post-operative evaluation of prostate cancer treatment courses. 2-D or 3-D images of patients' prostate from CT or ultra-sound video are used for real-time planning and the images are processed with needles and seeds in place. The VariSeed software adopts the inverse planning algorithm and tries to spare adjacent critical organs such as urethra and rectum wall through an optimized planning system. The real-time planning

and isodose contours enable modification of the pre-operative planning and to manually correct incorrect insertion of a seed in real time. SourceEdit is one of the VariSeed software packages to incorporate a seed characteristics. The user-defined source allows us to describe the ^{142}Pr glass seed in addition to the existing ^{125}I and ^{103}Pd seeds. I load all the dosimetric parameters such as dose-rate constant, source strength, half-life of isotope, radial dose function and anisotropy functions as well as seed dimension and geometry using SourceEdit.

The SourceEdit is designed for the AAPM TG-43 parameters. As ^{142}Pr seed is a beta source, the dosimetric parameters should be modified to TG-43 to be incorporated to the software. The equation (7-1) is expressed the dose rate in the form of AAPM TG-43.

$$D(r,\theta) = S_K \cdot \Lambda \cdot [G(r,\theta)/G(r_0,\theta_0)] \cdot g(r) \cdot F(r,\theta) \tag{7-1}$$

where S_K is the air-kerma strength and Λ is the dose rate constant in water.

Equating TG-60 to TG-43, dose rate is expressed as the air-kerma strength times dose rate constant.

$$D(r_0,\theta_0) = S_K \cdot \Lambda \tag{7-2}$$

VII-6 Case study

A case study was performed to assess the feasibility of the ^{142}Pr seed and to model the seed using VariSeed. The main work was the description of the seed, optimized planning, and comparison of the planning with the conventional seeds. From the case study, we may find how many ^{142}Pr seeds can be used, what the coverage of the prostate is, and how much dose is delivered to adjacent organs. A prostate was selected that had 49 cm^3 of prostate volume as shown in Figure VII-3. The image of the prostate includes urethral and rectal walls.

With the dose-optimized placement method, the system finds the best arrangement of sources that most closely satisfies the dose constraint rules we specify. For this study, 50 seeds were set for the maximum number of sources per needle. The implant volume was set to include the prostate and exclude the urethra for seed placement. The dose rules required that the prostate volume be above 100.0% of the prescribed dose with 10 as a weighting factor, that the rectal surface be below 45.0 Gy with 5 as a weighting factor, and that the urethral surface be below 180.0 Gy with 5 as a weighting factor which was the half of the maximum dose described in TG-64 report. The prescribed dose for ^{142}Pr seed was set to 90 Gy. Figure VII-3 shows the sagittal, coronal, and transverse views with two-dimensional isodose distributions in the prostate which should be identical on Monte Carlo calculation results shown in Figure VII-2. The yellow, blue and green lines delineate the periphery of the prostate, rectum and urethra. The pink line shows the isodose curve of 90 Gy.

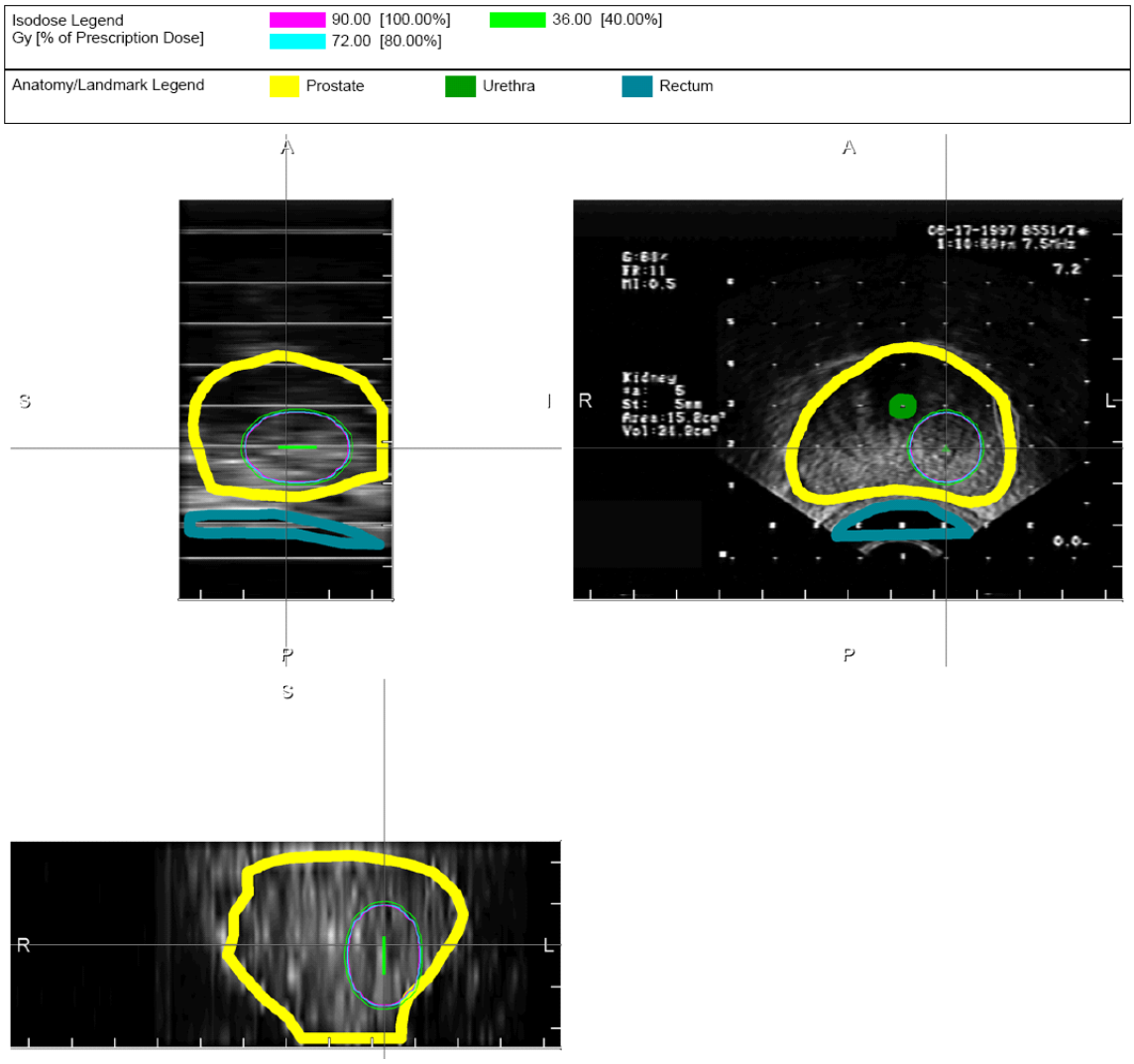

Figure VII-3. Two-dimensional isodose curve at midplane of prostate for a single ^{142}Pr glass seed

Figure VII-4 shows the ultrasound-based computer image of transverse section of midprostate showing planned seed positions. The optimum seed configuration will administer a minimal prescribed dose to the periphery of the prostate while sparing uninvolved normal structures. The picture enables easy seed loading for quality control.

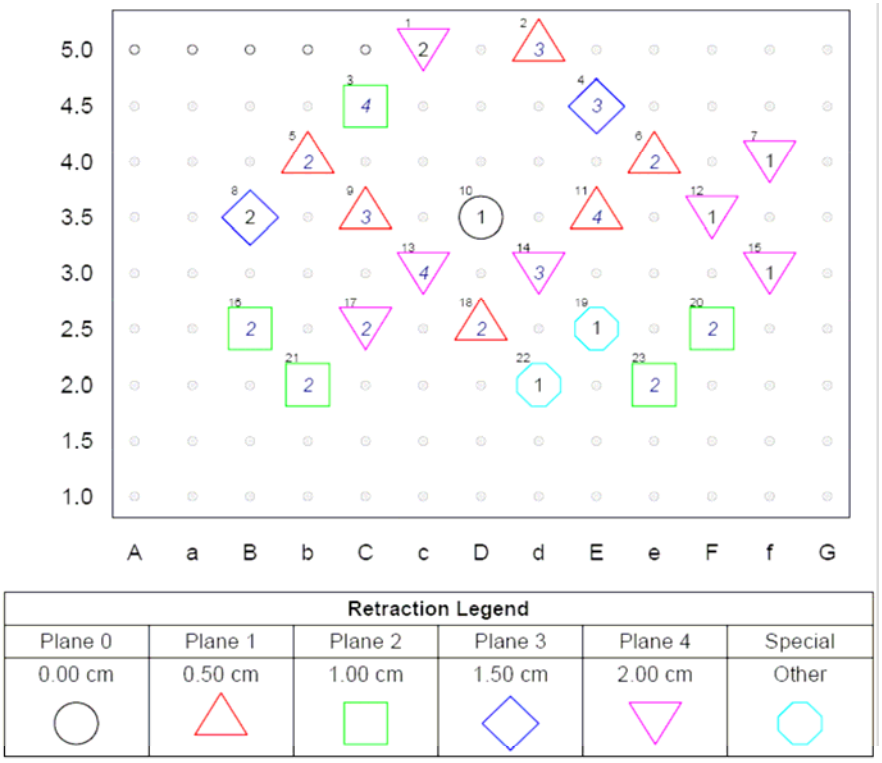

Figure VII-4. Ultrasound-based computer image of transverse section of midprostate showing planned seed positions

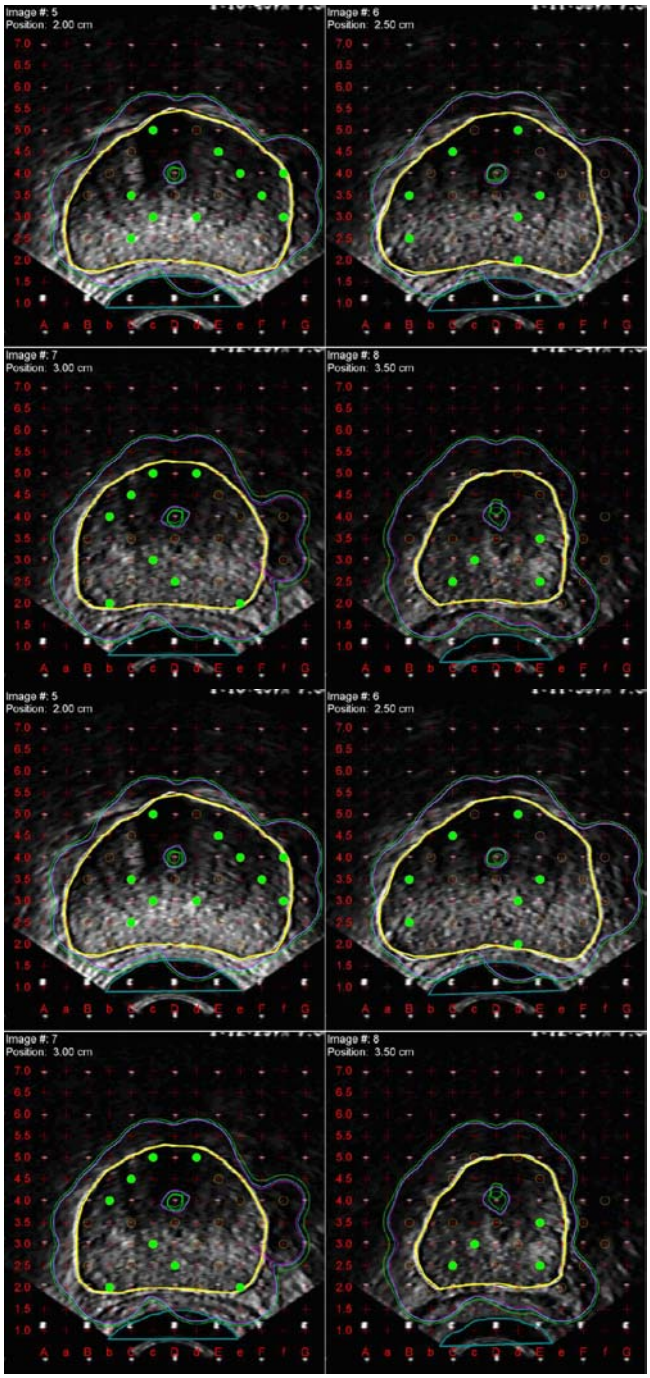

Figure VII-5. Planned seed positions and resultant isodose coverage with different heights

Figure VII-5 shows the planned seed positions and resultant isodose coverage with different heights after automatic source placement. Figure VII-6 shows the needle loading patterns after dose-optimization planning.

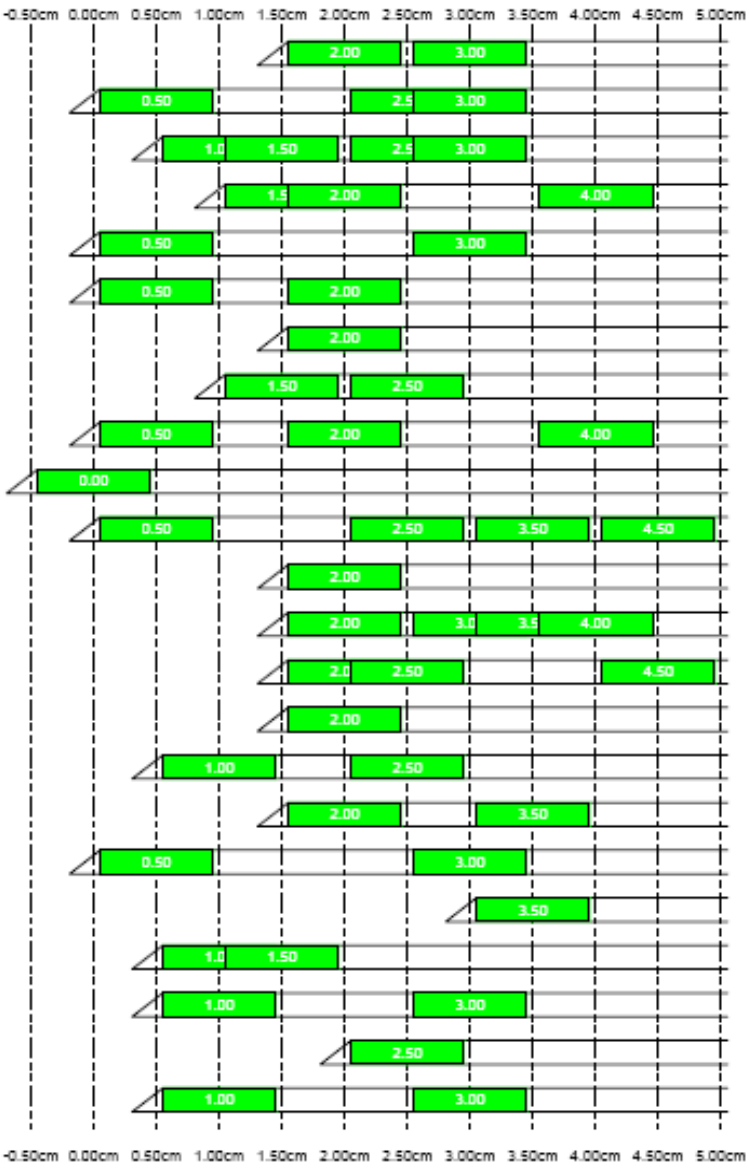

Figure VII-6. Needle loading patterns after dose-optimization planning

Based on the dose-optimization planning, the best arrangement of seeds, dose coverage, and isodose contours were found. A study was conducted for ^{125}I seeds with the same prostate and dose-optimization parameters except that the prescribed dose for ^{125}I was set to 144 Gy. Table VII-2 presents the comparison of the number of seed, dose coverage and undesired dose to adjacent organs of ^{142}Pr glass seed and typical ^{125}I seeds.

Table VII-2. Comparisons of dose-optimization of ^{125}I and ^{142}Pr

	^{125}I (6733)	^{142}Pr
Number of Seeds	79	50
Fraction of the prostate volume above the prescribed dose	79.4 %	89.3 %
Fraction of the rectum surface below 45.0 Gy	56.9 %	100.0 %
Fraction of the urethra surface below 180.0 Gy	95.6 %	100.0 %

Fifty ^{142}Pr seeds can deliver the prescribed dose to about 90% of the prostate volume, while 20% of the prostate volume is less than the prescribed dose for ^{125}I seeds. In this comparison, the coverage by ^{142}Pr glass seeds is higher than that of typical ^{125}I seeds. The surface area of the rectal wall exposed by ^{142}Pr glass seeds is less than that by ^{125}I seeds. ^{142}Pr glass seeds can deliver the prescribed dose to larger volume of prostate and the undesirable doses to adjacent organs are less.

CHAPTER VIII

SUMMARY AND CONCLUSIONS

A beta-emitting glass seed is proposed for the brachytherapy treatment of prostate cancer. While beta sources have been used for vascular brachytherapy, beta sources have not been widely used for cancer therapy. Nevertheless beta sources have several desirable properties. Beta sources have short range and are easily shielded, lowering extraneous dose to the medical staff as well as the patient. They can give a lower dose to the adjacent organs than the low energy photons from ^{125}I or ^{103} Pd.

Seed design criteria were developed as follows. The seeds should have chemical, mechanical, and biological integrity during neutron activation and *in vivo*. The cost of manufacture of these seeds should be relatively inexpensive. The seeds should be visible during seed implants and post implant monitoring with or without radiation opaque markers. Finally a target dose should be established at about 0.6 cm from seed's center. A 90 Gy dose for ^{142}Pr is selected as the prescribed dose based on the sensitivity analysis of dose from ^{142}Pr and the BED comparison.

Several beta-emitting nuclides were examined for suitability using DPK methods for dose calculation and considering neutron cross sections. Yttrium and phosphorus have been used for intravascular brachytherapy. ^{90}Y glass microspheres have been used for hepatocellular carcinoma. But ^{90}Y has a small thermal neutron absorption cross section and ^{32}P produces relatively lower energy beta particles. Rhenium has large

neutron cross section but it is not easy to incorporate into glass because of its volatility. ^{142}Pr was selected as isotope of choice. ^{142}Pr is made by neutron activation of the 100% abundant ^{141}Pr, producing both the 19.12 hour ground state and 14.6 min meta-stable state. The ^{142}Pr ground state decays emitting 2.162 endpoint energy beta rays 96.3 % of the time and has a 3.7% yield of 1.575 MeV gamma rays. Seeds 0.08 cm in diameter and 0.9 cm long were manufactured for testing. The seeds were activated in the Texas A&M research reactor. The activity produced was as predicted considering the meta-stable state and epi-thermal neutron flux.

^{142}Pr REAS glass seeds have several advantages over the conventional seeds. The seed is economical; it costs less than 15 dollars per seed including materials and neutron activation costs. Due to the short range of beta particles, the dose to adjacent organs can be minimized with the optimized implantation positions of the seeds. Because of the short half-life of ^{142}Pr, and the associated high dose rate, distortion of the prostate during irradiation is less than with ^{125}I, for example, that has a D_{90} of 204 days. Pr seeds can have very high dose rates, if desired, and give doses up to thousands of Gy to tumors near seeds. Because of high density and high atomic number of Pr glass, a radio-opaque marker is not necessary. Cladding or encapsulation is not required because the seed is unreactive in water or tissue. Variable sizes and shapes of glass seeds can be made and the seed is not easily broken. The seed is reusable after a high dose rate (HDR) treatment by reactivation.

The MCNP5 Monte Carlo code was used to calculate the quantitative dosimetric parameters suggested in AAPM TG-43/60. The Monte Carlo calculation results were

compared with those from a dose point kernel code. The dose profiles have a good agreement with each other out to 0.6 cm from the seed. The gamma dose is 0.3 Gy at 1.0 cm with initial activity of 5.95 mCi and therefore contributes insignificantly to adjacent organs. The total uncertainty in dose was estimated to be 3.4 % at 2 mm and 3.6 % at 6 mm.

A sensitivity analysis was performed to find the optimum size of the detector in the MCNP calculations, the impact of the length of the seed, and the effect of "ITS-style" energy indexing algorithm. A 0.01 cm radius detector was selected as detector size considering associated error and computation time. The radial dose profile will be about the same at the transverse-plane at any length longer than 4.5 cm length and the axial dose profile will be increased proportional to the length increment.

Measurements were performed to assess the 2-dimensional axial dose distributions using Gafchromic radiochromic films. The radiochromic film was calibrated using an X-ray machine calibrated against a NIST-traceable ion chamber. A calibration curve was derived using a least squares fit of a second-order polynomial. The measured dose distribution agreed well with results from the Monte Carlo simulation.

The dose at 6 mm from the seed center with initial activity of 5.95 mCi was 130.8 Gy. AAPM TG-43/60 parameters were determined. The reference dose rate for 2 mm and 6 mm were 0.67 and 0.02 cGy/s/mCi, respectively. The geometry function, radial dose function and anisotropy function were generated. Most conventional seeds have significant cold spots at the ends of the seed due to self-attenuation through the

seed and encapsulation welds at the edges, while Pr seed has no cold spots near the source ends.

The Pr seed is applicable to HDR. HDR has several advantages over LDR. The total dose is delivered to tumor cells in a short period such as 1 or 2 hours. The effect of seed migration, prostate distortion, or edema is very small. However, much higher activity is required. In case of ^{142}Pr glass seeds, a high fluence rate reactor having more than 10^{15} $cm^{-2}sec^{-1}$ is needed to get the desired activity. One-hour neutron activation in 10^{15} $cm^{-2}sec^{-1}$ can produce 361 mCi of ^{142}Pr. Within an hour, more than 150 Gy can be delivered at 0.6 cm from seed center with initial activity of 361 mCi.

A case study was performed to assess the feasibility of the ^{142}Pr seed and to model the seed using the VariSeed software package. The main work was the description of the seed, optimized planning, and comparison of the planning with the conventional seeds. With the dose-optimized placement method, the system finds the best arrangement of sources that most closely satisfies the dose constraint rules. From the case study, we found that ^{142}Pr seeds can deliver the prescribed dose to almost all the prostate with less dose to adjacent organs than conventional seeds.

These seeds can be used for prostate brachytherapy, for permanent breast seed implants, and for head and neck cancers. If Pr glass is made in the form of microspheres, it can be applicable to hepatocellular carcinoma.

REFERENCES

American Cancer Society 2006 Cancer Statistics http://www.cancer.org/downloads/STT/Cancer_Statistics_2006_Presentation.ppt last accessed October 1, 2006.

Antipas V, Dale R G and Coles I P 2001 A theoretical investigation into the role of tumour radiosensitivity, clonogen repopulation, tumour shrinkage and radionuclide RBE in permanent brachytherapy implants of ^{125}I and ^{103}Pd *Phys. Med. Biol.* **46** 2557-2569

Armpilia C I, Dale R G, Coles I P, Jones B and Antipas V 2003 The determination of radiobiologically optimized half-lives for radionuclides used in permanent brachytherapy implants *Int. J. Radiat. Oncol. Biol. Phys.* **55** 378-385

Asenjo J, Fernandez-Varea J M and Sanchez-Reyes A 2002 Characterization of a high-dose-rate ^{90}Sr-^{90}Y source for intravascular brachytherapy by using the Monte Carlo code PENELOPE *Phys. Med. Biol.* **47** 697-711

Bohm T D, Mourtada F A and Das R K 2001 Dose rate table for a ^{32}P intravascular brachytherapy source from Monte Carlo calculations *Med. Phys.* **28** 1770-1775

Brenner D J, Curtis R E, Hall E J and Ron E 2000 Second malignancies in prostate carcinoma patients after radiotherapy compared with surgery *Cancer* **88** 398-406

Brenner D J, Martinez A A, Edmundson G K, Mitchell C, Thames H D and Armour E P 2002 Direct evidence that prostate tumors show high sensitivity to fractionation

(low α/β ratio), similar to late-responding normal tissue *Int. J. Radiat. Oncol. Biol. Phys.* **52** 6-13

Butson M J, Cheung T and Yu P K 2001 Radiochromic film dosimetry in water phantoms *Phys. Med. Biol.* **46** N27-N31

Dale R G 1996 Dose-rate effects in targeted radiotherapy *Phys. Med. Biol.* **41** 1871-1884

Dale R G and Jones B 1999 Enhanced normal tissue doses caused by tumour shrinkage during brachytherapy *Br. J. Radiol.* **72** 499-501

Dauffy L 1998 Calculation of dose to soft tissue from implanted beta sources A thesis for Master of Science, Texas A&M University, College Station, Texas

Gleason D F, Mellinger G T, and the Veterans Administration Cooperative Urological Research Group 1974 Prediction of prognosis for prostatic adenocarcinoma by combined histologic garding and clinical staging *J. Urol.* **111** 58-64

Hall E J and Giaccia A J 2006 *Radiobiology for the Radiologist* (Philadelphia: Lippincott Williams & Wilkins)

Jeraj R, Keall P J and Ostwald P M 1999 Comparisons between MCNP, EGS4 and experiment for clinical electron beams *Phys. Med. Biol.* **44** 705-717

Khan F M 2003 *The Physics of Radiation Therapy* (Philadelphia: Lippincott Williams & Wilkins)

King C R and Fowler J F 2001 A simple analytic derivation suggests that prostate cancer α/β ratio is low *Int. J. Radiat. Oncol. Biol. Phys.* **51** 213-214

Lee S-W and Reece W D 2005 Dose calculation of ^{142}Pr microspheres as a potential treatment for arteriovenous malformations *Phys. Med. Biol.* **50** 151-166

Mourtada F, Soares C G and Horton J L 2004 A segmented ^{32}P source Monte Carlo model to derive AAPM TG-60 dosimetric parameters used for intravascular brachytherapy *Med. Phys.* **31** 602-608

Nath R, Amols H, Coffey C, Duggan D, Jani S, Li Z, Schell M, Soares C, Whiting J, Cole P E, Crocker I and Schwartz R 1999 Intravascular brachytherapy physics: Report of the AAPM Radiation Therapy Committee Task Group No. 60 *Med. Phys.* **26** 119-152

National Comprehensive Cancer Network (NCCN) Practice Guidelines for Prostate Cancer 2005 v.2.2005

National Cancer Institute 2005 Surveillance, Epidemiology, and End Results Program, 1975-2002, Division of Cancer Control and Population Sciences,

NSC (Nuclear Science Center) 2003 Safety Analysis Report (SAR) for the Nuclear Science Center of Texas A&M University. College Station, TX: Nuclear Science Center (NSC) at Texas A&M University

Reece W D 2005 Private communication (College of Engineering, Texas A&M University)

Reece W D, Miller S D and Durham J S 1989 SADDE (Scaled Absorbed Dose Distribution Evaluator) - A code to generate input for VARSKIN. NUREG/CR-5276, U.S. Nuclear Regulatory Commission, Washington D.C.

Rivard M J 2002 Comprehensive Monte Carlo calculations of AAPM Task Group Report No. 43 dosimetry parameters for the Model 3500 I-Plant ^{125}I brachytherapy source *Appl. Radiat. Isot.* **57** 381-389

Rivard M J, Coursey B M, DeWerd L A, Hanson W F, Huq M S, Ibbott G S, Mitch M G, Nath R and Williamson J F 2004 Update of AAPM Task Group No. 43 Report: A revised AAPM protocol for brachytherapy dose calculations *Med. Phys.* **31** 633-674

Roa D E, Song H, Yue N, d'Errico F and Nath R 2002 Measured TG-60 dosimetric parameters of the Novoste Beta-Cath ^{90}Sr/Y source trains for intravascular brachytherapy *Cardiovasc. Radiat. Med.* **3** 199-204

RPC (Radiological Physics Center), The M.D. Anderson Cancer Center, Houston, TX http://rpc.mdanderson.org/rpc/htm/Home_htm/Low-energy.htm last accessed October 1, 2006.

Salem R, Thurston K G, Carr B I, Goin J E and Geschwind J H 2002 Yttrium-90 microspheres: radiation therapy for unresectable liver cancer *J Vasc Intervent Radiol* **13** S223-S229

Schaart D R, Jansen J Th M, Zoetelief J and de Leege P F A 2002 A comparison of MCNP4C electron transport with ITS 3.0 and experiment at incident energies between 100 keV and 20 MeV: influence of voxel size, substeps and energy indexing algorithm *Phys. Med. Biol.* **47** 1459-1484

Traub R J, Reece W D, Scherpelz R I and Sigalla L A 1987 Dose calculation for contamination of the skin using the computer code VARSKIN. NUREG/CR-4418, U.S. Nuclear Regulatory Commission, Washington D.C.

Turner J E 1995 *Atoms, Radiation, and Radiation Protection* (New York: John Wiley & Sons, Inc)

VariSeed™ 7.1 User Guide (Charlottesville: Varian Medical Systems, Inc)

Wallner K, Roy J and Harrison L 1995 Dosimetry guidelines to minimize urethral and rectal morbidity following transperineal I-125 prostate brachytherapy *Int. J. Radiat. Oncol. Biol. Phys.* **32** 465-471

Waterman F M, Yue N, Corn B W and Dicker A P 1998 Edema associated with I-125 or Pd-103 prostate brachytherapy and its impact on post-implant dosimetry: an analysis based on serial CT acquisition *Int. J. Radiat. Oncol. Biol. Phys.* **41** 1069-1077

Wei J T, Dunn R L, Sandler H M, McLaughlin P W, Montie J E, Litwin M S, Nyquist L and Sanda M G 2002 Comprehensive comparison of health-related quality of life after comtemporary therapies for localized prostate cancer *J Clin. Oncol.* **20** 557-566

White J E and Day D E 1994 Rare earth aluminosilicate glasses for *in vivo* radiation delivery *Key Eng. Mat.* **94-95** 181-208

X-5 Monte Carlo Team 2003 MCNP - A General Monte Carlo N-Particle Transport Code, Version 5, LA-UR-03-1987, Los Alamos National Laboratory

APPENDIX A

MATERIAL TEST SHEET

A.1 Composition

SPECTRO X-LAB Job Number: R and D

Sample Name	Method	Sample State	Date of Evaluation
GL0793	Gl0793	Preβtablette	12/30/2005
GL0793_r01	Gl0793	Preβtablette	12/30/2005

Sample Name	Al_2O_3 [%]	SiO_2 [%]	Sum [%]
GL0793	15.29 ± 0.06	32.66 ± 0.06	47.95
GL0793_r01	15.22 ± 0.06	32.73 ± 0.06	47.95
Average	15.25	32.69	47.95
Standard deviation	0.05245	0.05505	0.00260

A.2 Density

Density Measurements – Ultrapycnometer 1000

GL-0793; +212 μm frit	Sample Wt. (g)	Meas. 1 (g/cc)	Meas. 2 (g/cc)	Meas. 3 (g/cc)
Test #1	21.2276	4.1009	4.0984	4.1009
Test #2	26.1264	4.0890	4.0905	4.0867
Test #3	33.9117	4.0791	4.0817	4.0752
GL-0793; +212 μm frit	Meas. 4 (g/cc)	Meas. 5 (g/cc)	Average	Std. Dev.
Test #1	4.0971	4.0946	4.0984	0.0027
Test #2	4.0867	4.0899	4.0886	0.0018
Test #3	4.0749	4.0750	4.0772	0.0031

APPENDIX B

MCNP INPUT DECK

```
Beta   particle at     water
c      Cell   Cards
c      Pr     source
c      Pr-glass4.0g/cm3
5      1     -4     -1      2 -3   imp:p,e=1
c      detector0degree
11      3     -1  -11  imp:p,e=8
12      3     -1  -12  imp:p,e=8
13      3     -1  -13  imp:p,e=8
14      3     -1  -14  imp:p,e=8
15      3     -1  -15  imp:p,e=8
16      3     -1  -16  imp:p,e=8
17      3     -1  -17  imp:p,e=8
18      3     -1  -18  imp:p,e=8
19      3     -1  -19  imp:p,e=8
20      3     -1  -20  imp:p,e=8
21      3     -1  -21  imp:p,e=8
22      3     -1  -22  imp:p,e=8
23      3     -1  -23  imp:p,e=8
24      3     -1  -24  imp:p,e=8
25      3     -1  -25  imp:p,e=8
26      3     -1  -26  imp:p,e=8
27      3     -1  -27  imp:p,e=8
28      3     -1  -28  imp:p,e=8
29      3     -1  -29  imp:p,e=8
c      detector10degree
111     3     -1  -111  imp:p,e=8
112     3     -1  -112  imp:p,e=8
113     3     -1  -113  imp:p,e=8
114     3     -1  -114  imp:p,e=8
115     3     -1  -115  imp:p,e=8
116     3     -1  -116  imp:p,e=8
117     3     -1  -117  imp:p,e=8
118     3     -1  -118  imp:p,e=8
119     3     -1  -119  imp:p,e=8
120     3     -1  -120  imp:p,e=8
121     3     -1  -121  imp:p,e=8
122     3     -1  -122  imp:p,e=8
123     3     -1  -123  imp:p,e=8
124     3     -1  -124  imp:p,e=8
125     3     -1  -125  imp:p,e=8
126     3     -1  -126  imp:p,e=8
127     3     -1  -127  imp:p,e=8
128     3     -1  -128  imp:p,e=8
129     3     -1  -129  imp:p,e=8
```

```
c      detector20degree
211      3     -1  -211  imp:p,e=8
212      3     -1  -212  imp:p,e=8
213      3     -1  -213  imp:p,e=8
214      3     -1  -214  imp:p,e=8
215      3     -1  -215  imp:p,e=8
216      3     -1  -216  imp:p,e=8
217      3     -1  -217  imp:p,e=8
218      3     -1  -218  imp:p,e=8
219      3     -1  -219  imp:p,e=8
220      3     -1  -220  imp:p,e=8
221      3     -1  -221  imp:p,e=8
222      3     -1  -222  imp:p,e=8
223      3     -1  -223  imp:p,e=8
224      3     -1  -224  imp:p,e=8
225      3     -1  -225  imp:p,e=8
226      3     -1  -226  imp:p,e=8
227      3     -1  -227  imp:p,e=8
228      3     -1  -228  imp:p,e=8
229      3     -1  -229  imp:p,e=8
c      detector30degree
311      3     -1  -311  imp:p,e=8
312      3     -1  -312  imp:p,e=8
313      3     -1  -313  imp:p,e=8
314      3     -1  -314  imp:p,e=8
315      3     -1  -315  imp:p,e=8
316      3     -1  -316  imp:p,e=8
317      3     -1  -317  imp:p,e=8
318      3     -1  -318  imp:p,e=8
319      3     -1  -319  imp:p,e=8
320      3     -1  -320  imp:p,e=8
321      3     -1  -321  imp:p,e=8
322      3     -1  -322  imp:p,e=8
323      3     -1  -323  imp:p,e=8
324      3     -1  -324  imp:p,e=8
325      3     -1  -325  imp:p,e=8
326      3     -1  -326  imp:p,e=8
327      3     -1  -327  imp:p,e=8
328      3     -1  -328  imp:p,e=8
329      3     -1  -329  imp:p,e=8
c      detector40degree
411      3     -1  -411  imp:p,e=8
412      3     -1  -412  imp:p,e=8
413      3     -1  -413  imp:p,e=8
414      3     -1  -414  imp:p,e=8
415      3     -1  -415  imp:p,e=8
416      3     -1  -416  imp:p,e=8
417      3     -1  -417  imp:p,e=8
418      3     -1  -418  imp:p,e=8
419      3     -1  -419  imp:p,e=8
420      3     -1  -420  imp:p,e=8
421      3     -1  -421  imp:p,e=8
422      3     -1  -422  imp:p,e=8
```

```
423     3    -1  -423  imp:p,e=8
424     3    -1  -424  imp:p,e=8
425     3    -1  -425  imp:p,e=8
426     3    -1  -426  imp:p,e=8
427     3    -1  -427  imp:p,e=8
428     3    -1  -428  imp:p,e=8
429     3    -1  -429  imp:p,e=8
c     detector50degree
511     3    -1  -511  imp:p,e=8
512     3    -1  -512  imp:p,e=8
513     3    -1  -513  imp:p,e=8
514     3    -1  -514  imp:p,e=8
515     3    -1  -515  imp:p,e=8
516     3    -1  -516  imp:p,e=8
517     3    -1  -517  imp:p,e=8
518     3    -1  -518  imp:p,e=8
519     3    -1  -519  imp:p,e=8
520     3    -1  -520  imp:p,e=8
521     3    -1  -521  imp:p,e=8
522     3    -1  -522  imp:p,e=8
523     3    -1  -523  imp:p,e=8
524     3    -1  -524  imp:p,e=8
525     3    -1  -525  imp:p,e=8
526     3    -1  -526  imp:p,e=8
527     3    -1  -527  imp:p,e=8
528     3    -1  -528  imp:p,e=8
529     3    -1  -529  imp:p,e=8
c     detector60degree
611     3    -1  -611  imp:p,e=8
612     3    -1  -612  imp:p,e=8
613     3    -1  -613  imp:p,e=8
614     3    -1  -614  imp:p,e=8
615     3    -1  -615  imp:p,e=8
616     3    -1  -616  imp:p,e=8
617     3    -1  -617  imp:p,e=8
618     3    -1  -618  imp:p,e=8
619     3    -1  -619  imp:p,e=8
620     3    -1  -620  imp:p,e=8
621     3    -1  -621  imp:p,e=8
622     3    -1  -622  imp:p,e=8
623     3    -1  -623  imp:p,e=8
624     3    -1  -624  imp:p,e=8
625     3    -1  -625  imp:p,e=8
626     3    -1  -626  imp:p,e=8
627     3    -1  -627  imp:p,e=8
628     3    -1  -628  imp:p,e=8
629     3    -1  -629  imp:p,e=8
c     detector70degree
c       711     3    -1  -711  imp:p=8
712     3    -1  -712  imp:p,e=8
713     3    -1  -713  imp:p,e=8
714     3    -1  -714  imp:p,e=8
715     3    -1  -715  imp:p,e=8
```

```
716     3    -1  -716  imp:p,e=8
717     3    -1  -717  imp:p,e=8
718     3    -1  -718  imp:p,e=8
719     3    -1  -719  imp:p,e=8
720     3    -1  -720  imp:p,e=8
721     3    -1  -721  imp:p,e=8
722     3    -1  -722  imp:p,e=8
723     3    -1  -723  imp:p,e=8
724     3    -1  -724  imp:p,e=8
725     3    -1  -725  imp:p,e=8
726     3    -1  -726  imp:p,e=8
727     3    -1  -727  imp:p,e=8
728     3    -1  -728  imp:p,e=8
729     3    -1  -729  imp:p,e=8
c     detector80degree
c       811     3    -1  -811  imp:p=8
c       812     3    -1  -812  imp:p=8
c       813     3    -1  -813  imp:p=8
c       814     3    -1  -814  imp:p=8
815     3    -1  -815  imp:p,e=8
816     3    -1  -816  imp:p,e=8
817     3    -1  -817  imp:p,e=8
818     3    -1  -818  imp:p,e=8
819     3    -1  -819  imp:p,e=8
820     3    -1  -820  imp:p,e=8
821     3    -1  -821  imp:p,e=8
822     3    -1  -822  imp:p,e=8
823     3    -1  -823  imp:p,e=8
824     3    -1  -824  imp:p,e=8
825     3    -1  -825  imp:p,e=8
826     3    -1  -826  imp:p,e=8
827     3    -1  -827  imp:p,e=8
828     3    -1  -828  imp:p,e=8
829     3    -1  -829  imp:p,e=8
c     detector90degree
c       911     3    -1  -911  imp:p=8
c       912     3    -1  -912  imp:p=8
c       913     3    -1  -913  imp:p=8
c       914     3    -1  -914  imp:p=8
c       915     3    -1  -915  imp:p=8
c       916     3    -1  -916  imp:p=8
c       917     3    -1  -917  imp:p=8
c       918     3    -1  -918  imp:p=8
919     3    -1  -919  imp:p,e=8
920     3    -1  -920  imp:p,e=8
921     3    -1  -921  imp:p,e=8
922     3    -1  -922  imp:p,e=8
923     3    -1  -923  imp:p,e=8
924     3    -1  -924  imp:p,e=8
925     3    -1  -925  imp:p,e=8
926     3    -1  -926  imp:p,e=8
927     3    -1  -927  imp:p,e=8
928     3    -1  -928  imp:p,e=8
```

```
929      3     -1  -929  imp:p,e=8
c
900      3     -1  -6    #5
     #011  #012  #013  #014  #015  #016  #017  #018  #019  #020
     #021  #022  #023  #024  #025  #026  #027  #028  #029
     #111  #112  #113  #114  #115  #116  #117  #118  #119  #120
     #121  #122  #123  #124  #125  #126  #127  #128  #129
     #211  #212  #213  #214  #215  #216  #217  #218  #219  #220
     #221  #222  #223  #224  #225  #226  #227  #228  #229
     #311  #312  #313  #314  #315  #316  #317  #318  #319  #320
     #321  #322  #323  #324  #325  #326  #327  #328  #329
     #411  #412  #413  #414  #415  #416  #417  #418  #419  #420
     #421  #422  #423  #424  #425  #426  #427  #428  #429
     #511  #512  #513  #514  #515  #516  #517  #518  #519  #520
     #521  #522  #523  #524  #525  #526  #527  #528  #529
     #611  #612  #613  #614  #615  #616  #617  #618  #619  #620
     #621  #622  #623  #624  #625  #626  #627  #628  #629
     #712  #713  #714  #715  #716  #717  #718  #719  #720
     #721  #722  #723  #724  #725  #726  #727  #728  #729
     #815  #816  #817  #818  #819  #820
     #821  #822  #823  #824  #825  #826  #827  #828  #829
     #919  #920
     #921  #922  #923  #924  #925  #926  #927  #928  #929
     imp:p,e=4
c       void
999     0       #5
     #011  #012  #013  #014  #015  #016  #017  #018  #019  #020
     #021  #022  #023  #024  #025  #026  #027  #028  #029
     #111  #112  #113  #114  #115  #116  #117  #118  #119  #120
     #121  #122  #123  #124  #125  #126  #127  #128  #129
     #211  #212  #213  #214  #215  #216  #217  #218  #219  #220
     #221  #222  #223  #224  #225  #226  #227  #228  #229
     #311  #312  #313  #314  #315  #316  #317  #318  #319  #320
     #321  #322  #323  #324  #325  #326  #327  #328  #329
     #411  #412  #413  #414  #415  #416  #417  #418  #419  #420
     #421  #422  #423  #424  #425  #426  #427  #428  #429
     #511  #512  #513  #514  #515  #516  #517  #518  #519  #520
     #521  #522  #523  #524  #525  #526  #527  #528  #529
     #611  #612  #613  #614  #615  #616  #617  #618  #619  #620
     #621  #622  #623  #624  #625  #626  #627  #628  #629
     #712  #713  #714  #715  #716  #717  #718  #719  #720
     #721  #722  #723  #724  #725  #726  #727  #728  #729
     #815  #816  #817  #818  #819  #820
     #821  #822  #823  #824  #825  #826  #827  #828  #829
     #919  #920
     #921  #922  #923  #924  #925  #926  #927  #928  #929
     #900
     imp:p,e=0
c       end     of      cell    cards

c       surface card
c       surface of      water
1   CZ          0.04
```

```
2   PZ       -0.45
3   PZ        0.45
6   SO          2
c      7CZ        0.02
c      detector0degree
11  S         0.1       0       0    0.005
12  S        0.15       0       0     0.01
13  S         0.2       0       0     0.01
14  S        0.25       0       0     0.01
15  S         0.3       0       0     0.01
16  S        0.35       0       0     0.01
17  S         0.4       0       0     0.01
18  S        0.45       0       0     0.01
19  S         0.5       0       0     0.01
20  S        0.55       0       0     0.01
21  S         0.6       0       0     0.01
22  S        0.65       0       0     0.01
23  S         0.7       0       0     0.01
24  S        0.75       0       0     0.01
25  S         0.8       0       0     0.01
26  S        0.85       0       0     0.01
27  S         0.9       0       0     0.01
28  S        0.95       0       0     0.01
29  S           1       0       0     0.01
c      detector10degree
111  S     0.098         0     0.017   0.005
112  S     0.148         0     0.026   0.01
113  S     0.197         0     0.035   0.01
114  S     0.246         0     0.043   0.01
115  S     0.295         0     0.052   0.01
116  S     0.345         0     0.061   0.01
117  S     0.394         0     0.069   0.01
118  S     0.443         0     0.078   0.01
119  S     0.492         0     0.087   0.01
120  S     0.542         0     0.096   0.01
121  S     0.591         0     0.104   0.01
122  S      0.64         0     0.113   0.01
123  S     0.689         0     0.122   0.01
124  S     0.739         0      0.13   0.01
125  S     0.788         0     0.139   0.01
126  S     0.837         0     0.148   0.01
127  S     0.886         0     0.156   0.01
128  S     0.936         0     0.165   0.01
129  S     0.985         0     0.174   0.01
c      detector20degree
211  S     0.094         0     0.034   0.005
212  S     0.141         0     0.051   0.01
213  S     0.188         0     0.068   0.01
214  S     0.235         0     0.086   0.01
215  S     0.282         0     0.103   0.01
216  S     0.329         0      0.12   0.01
217  S     0.376         0     0.137   0.01
218  S     0.423         0     0.154   0.01
```

```
219  S    0.47        0   0.171   0.01
220  S   0.517        0   0.188   0.01
221  S   0.564        0   0.205   0.01
222  S   0.611        0   0.222   0.01
223  S   0.658        0   0.239   0.01
224  S   0.705        0   0.257   0.01
225  S   0.752        0   0.274   0.01
226  S   0.799        0   0.291   0.01
227  S   0.846        0   0.308   0.01
228  S   0.893        0   0.325   0.01
229  S    0.94        0   0.342   0.01
c      detector30degree
311  S   0.087        0    0.05   0.005
312  S    0.13        0   0.075   0.01
313  S   0.173        0     0.1   0.01
314  S   0.217        0   0.125   0.01
315  S    0.26        0    0.15   0.01
316  S   0.303        0   0.175   0.01
317  S   0.346        0     0.2   0.01
318  S    0.39        0   0.225   0.01
319  S   0.433        0    0.25   0.01
320  S   0.476        0   0.275   0.01
321  S    0.52        0     0.3   0.01
322  S   0.563        0   0.325   0.01
323  S   0.606        0    0.35   0.01
324  S    0.65        0   0.375   0.01
325  S   0.693        0     0.4   0.01
326  S   0.736        0   0.425   0.01
327  S   0.779        0    0.45   0.01
328  S   0.823        0   0.475   0.01
329  S   0.866        0     0.5   0.01
c      detector40degree
411  S   0.077        0   0.064   0.005
412  S   0.115        0   0.096   0.01
413  S   0.153        0   0.129   0.01
414  S   0.192        0   0.161   0.01
415  S    0.23        0   0.193   0.01
416  S   0.268        0   0.225   0.01
417  S   0.306        0   0.257   0.01
418  S   0.345        0   0.289   0.01
419  S   0.383        0   0.321   0.01
420  S   0.421        0   0.354   0.01
421  S    0.46        0   0.386   0.01
422  S   0.498        0   0.418   0.01
423  S   0.536        0    0.45   0.01
424  S   0.575        0   0.482   0.01
425  S   0.613        0   0.514   0.01
426  S   0.651        0   0.546   0.01
427  S   0.689        0   0.579   0.01
428  S   0.728        0   0.611   0.01
429  S   0.766        0   0.643   0.01
c      detector50degree
511  S   0.064        0   0.077   0.005
```

```
512  S   0.096        0    0.115   0.01
513  S   0.129        0    0.153   0.01
514  S   0.161        0    0.192   0.01
515  S   0.193        0     0.23   0.01
516  S   0.225        0    0.268   0.01
517  S   0.257        0    0.306   0.01
518  S   0.289        0    0.345   0.01
519  S   0.321        0    0.383   0.01
520  S   0.354        0    0.421   0.01
521  S   0.386        0     0.46   0.01
522  S   0.418        0    0.498   0.01
523  S    0.45        0    0.536   0.01
524  S   0.482        0    0.575   0.01
525  S   0.514        0    0.613   0.01
526  S   0.546        0    0.651   0.01
527  S   0.579        0    0.689   0.01
528  S   0.611        0    0.728   0.01
529  S   0.643        0    0.766   0.01
c      detector60degree
611  S    0.05        0    0.087   0.005
612  S   0.075        0     0.13   0.01
613  S     0.1        0    0.173   0.01
614  S   0.125        0    0.217   0.01
615  S    0.15        0     0.26   0.01
616  S   0.175        0    0.303   0.01
617  S     0.2        0    0.346   0.01
618  S   0.225        0     0.39   0.01
619  S    0.25        0    0.433   0.01
620  S   0.275        0    0.476   0.01
621  S     0.3        0     0.52   0.01
622  S   0.325        0    0.563   0.01
623  S    0.35        0    0.606   0.01
624  S   0.375        0     0.65   0.01
625  S     0.4        0    0.693   0.01
626  S   0.425        0    0.736   0.01
627  S    0.45        0    0.779   0.01
628  S   0.475        0    0.823   0.01
629  S     0.5        0    0.866   0.01
c      detector70degree
712  S   0.051        0    0.141   0.01
713  S   0.068        0    0.188   0.01
714  S   0.086        0    0.235   0.01
715  S   0.103        0    0.282   0.01
716  S    0.12        0    0.329   0.01
717  S   0.137        0    0.376   0.01
718  S   0.154        0    0.423   0.01
719  S   0.171        0     0.47   0.01
720  S   0.188        0    0.517   0.01
721  S   0.205        0    0.564   0.01
722  S   0.222        0    0.611   0.01
723  S   0.239        0    0.658   0.01
724  S   0.257        0    0.705   0.01
725  S   0.274        0    0.752   0.01
```

```
726  S    0.291          0    0.799   0.01
727  S    0.308          0    0.846   0.01
728  S    0.325          0    0.893   0.01
729  S    0.342          0     0.94   0.01
c       detector80degree
815  S    0.052          0    0.295   0.01
816  S    0.061          0    0.345   0.01
817  S    0.069          0    0.394   0.01
818  S    0.078          0    0.443   0.01
819  S    0.087          0    0.492   0.01
820  S    0.096          0    0.542   0.01
821  S    0.104          0    0.591   0.01
822  S    0.113          0     0.64   0.01
823  S    0.122          0    0.689   0.01
824  S     0.13          0    0.739   0.01
825  S    0.139          0    0.788   0.01
826  S    0.148          0    0.837   0.01
827  S    0.156          0    0.886   0.01
828  S    0.165          0    0.936   0.01
829  S    0.174          0    0.985   0.01
c       detector90degree
c       101  S          0       0    0.05   0.005
c       102  S          0       0     0.1   0.005
c       103  S          0       0    0.15   0.005
c       104  S          0       0     0.2   0.005
c       105  S          0       0    0.25   0.005
919  S          0       0     0.5    0.01
920  S          0       0    0.55    0.01
921  S          0       0     0.6    0.01
922  S          0       0    0.65    0.01
923  S          0       0     0.7    0.01
924  S          0       0    0.75    0.01
925  S          0       0     0.8    0.01
926  S          0       0    0.85    0.01
927  S          0       0     0.9    0.01
928  S          0       0    0.95    0.01
929  S          0       0       1    0.01
c       end     of      surface cards

MODE    p       e
c       materialcard
c       Pr
c       Si:Al:Pr0.153:0.)
m1          14000  -0.153   13000  -0.081   59000  -0.445    8000  -0.322
c       W
m2          74000       1
c       water
c       H       :       2O      :               1
m3          1001        2    8016        1
SDEF    cell=5  pos=0  0  0     ERG=d1 PAR=3   rad=d2  ext=d3 axs=0 0 1
c       SDEF    cell=5  ERG=D1  PAR=3   rad=d2
SI1  A  0.017 0.172 0.265 0.395 0.574 0.766 0.877 0.946 1.026 1.188
        1.268 1.343 1.615 1.712 1.884 1.923 2.011 2.064 2.104 2.139 2.160
```

```
SP1  D  586   656   673   669   649   632   613   598   578   527
      497   464   311   244   121   95.2  43.4  19.8  7.32  1.19  0.0069
c  SI1 L 0.017 0.172 0.265 0.395 0.574 0.766 0.946 1.188 1.343 1.712 2.011 2.104
c  SP1 D 586   656   673   669   649   632   598   527   464   244   43.4  7.32
SI2           0    0.04
SP2          -21       1
SI3        -0.45    0.45
SP3          -21       0
c   elpt:e     0.01     0.1  0.1  $cell-bycutoff
c   phys:e    10       0       0       0       0       1       1       1      10 $bremsstoptions
*F8:P,E  11   12  13  14  15  16  17  18  19      20
       21   22  23  24  25  26  27  28  29
       111 112 113 114 115 116 117 118 119     120
       121 122 123 124 125 126 127 128 129
       211 212 213 214 215 216 217 218 219     220
       221 222 223 224 225 226 227 228 229
       311 312 313 314 315 316 317 318 319     320
       321 322 323 324 325 326 327 328 329
       411 412 413 414 415 416 417 418 419     420
       421 422 423 424 425 426 427 428 429
       511 512 513 514 515 516 517 518 519     520
       521 522 523 524 525 526 527 528 529
       611 612 613 614 615 616 617 618 619     620
       621 622 623 624 625 626 627 628 629
       712 713 714 715 716 717 718 719 720
       721 722 723 724 725 726 727 728 729
       815 816 817 818 819 820
       821 822 823 824 825 826 827 828 829
       919 920
       921 922 923 924 925 926 927 928  929
c      E0
c      F8:P          10
NPS     2.00E+09
DBCN    18J     1  $ITS-styindexing
PRDMP   1E7 1E8      0       4
PRINT
c PRINT   -10   -40   -50   -70   -98   -85   -86    -110    -140    -170    -130    -128
```

APPENDIX C

MATLAB INPUT DECK

```
[film,map] = imread('file_name.gif');
film = map(film);
[size1, size2] = size(film);
S_control = 203;
Odbox = log10(S_control./film);
A=X;
B=Y;
C=Z;
Odbox2=Odbox*Odbox;
Gybox=A*Odbox2 + B*Odbox +C;
C = contour(Gybox)k
Clabel(C);
Save test.txt Gybox –ascii;
C=plot3(Gybox);
```

APPENDIX D

MONTE CARLO FORTRAN PROGRAM

```
      real pi,re,L,kay,kradius
      real myu,ke2,myuc,myuph
! dimension flux(0:27),expo(0:27),fll(20),exl(20)
  INTEGER(4) iseed
  open(unit=7,file='cover7-3.out',status='unknown')

!   Global parameters


  imax=10000000
  idose=0
  iseed=5425001

    pi=3.141592654
!      radius of prostate
  kay=2.3

!      length of seed
      L=0.45
  doser0t0=30.0
  referdose=15.0

      do i=1,imax

      dose=0.0

!      step 1-1 : find radius of point
      call randomtime(iseed)
    ssai1=RAN(iseed)
    radius=ssai1**0.333333
      kradius=kay*radius
!! write(6,*) 'iseed,ssai1,radius,kradius'
!! write(6,*) iseed,ssai1,radius,kradius

!      step 1-2 : the angle(phi) of point
      call randomtime(iseed)
  ssai2=RAN(iseed)
  phi=2*pi*ssai2
!! write(6,*) 'iseed,ssai2,phi'
!! write(6,*) iseed,ssai2,phi

!      step 1-3 : the angle(theta) of point
      call randomtime(iseed)
  ssai3=RAN(iseed)
```

```
  theta=pi*ssai3
!!  write(6,*) 'iseed,ssai3,theta'
!!  write(6,*) iseed,ssai3,theta

!       step 1-4 : find x,y,z
        x=kradius*sin(theta)*cos(phi)
   y=kradius*sin(theta)*sin(phi)
   z=kradius*cos(theta)
!!  write(6,*) 'x,y,z'
!!  write(6,*) x,y,z

!!   if((z .le. 0.005) .and. (z .ge. -0.005)) then
!!   write(6,*) '******exceed dose *******',dosert, doser0t0'
!!   write(6,*) dosert, doser0t0
!!   write(7,*) 'x,y,z,dosert'
!!   write(7,*) x,y,z,dosert
!!   end if

!  if seed is vertical, axis=1.0(z parallel)
!  if seed is horizontal(y paralle), axis=2.0
!  if seed is horizontal(x paralle), axis=3.0

!!  ------------------------------------------------
        x0=-1.8
              y0=0.3
              z0=0.0
        axis=1.0

!!  write(6,*) 'dose1, dosert'
!!  write(6,*) dose, dosert

        if((z .eq. z0) .and. (y .eq. y0) .and.  &
   (x .eq. x0)) then
     dose=10000.0
!  idose=idose+1

   else

        call finddose(x,y,z,x0,y0,z0,L,idose, &
                dosert,doser0t0,axis,pi,dose,dist)

!!  write(6,*) 'dose2, dosert'
!!  write(6,*) dose, dosert


        endif
!! ---------------------------------------------------------
        x0=-1.2
         y0=0.3
         z0=0.0
        axis=1.0
        if((z .eq. z0) .and. (y .eq. y0) .and.  &
   (x .eq. x0)) then
```

```
     dose=10000.0
!  idose=idose+1

   else

       call finddose(x,y,z,x0,y0,z0,L,idose, &
                dosert,doser0t0,axis,pi,dose,dist)
       endif
!! ---------------------------------------------------------

    if(dose .gt. referdose) then
!!   write(6,*) '******exceed dose *******,dosert, doser0t0'
!!   write(6,*) dosert, doser0t0
!!   write(7,*) 'x,y,z, dosert'
!!   write(7,*) x,y,z,dosert
      idose=idose+1
    end if

!!   write(6,*) dist

!!   if((dist .le. 0.31) .and. (dist .ge. 0.29) .and. &
!!   (z .le. 0.1) .and. (z .ge. -0.1)) then
    if((z .le. 0.01) .and. (z .ge. -0.01)) then
!!   write(6,*) '******exceed dose *******,dosert, doser0t0'
!!   write(6,*) dosert, doser0t0
!!   write(7,*) 'x,y,dose'
    write(7,*) x,y,dose
    end if


      end do

      ratio=real(idose)/real(imax)

    write(6,*) 'idose, imax, ratio'
    write(6,*) idose, imax, ratio

    END PROGRAM



        subroutine randomtime(iseed)
        USE DFPORT
        INTEGER(4) iseed
        character*8 char_time
!         iseed = TIME( )
!         call TIME(char_time)
        xtime=0.0
        iseed=iseed+int(1000.0*secnds(xtime))
!!     write(6,*) 'secnds(xtime), int(1000.0*secnds(xtime)),iseed'
!1      write(6,*) secnds(xtime), int(1000.0*secnds(xtime)),iseed
!        print *, 'Integer: ', int_time, 'time: ', char_time
        END subroutine
```

```
      subroutine finddose(x,y,z,x0,y0,z0,L,idose, &
              dosert,doser0t0,axis,pi,dose,dist)
  real L

      if((z .le. z0+L/2) .and. (z .ge. z0-L/2) .and.  &
  (sqrt((x-x0)**2.0+(y-y0)**2.0) .le. 0.02)) then
    dosert=10000.0
!  idose=idose+1

  else

      dist=sqrt((x-x0)**2.0+(y-y0)**2.0+(z-z0)**2.0)

      if(axis .eq. 1.0) then
      angle=acos(abs(z-z0)/dist)
!!  write(6,*) 'seed is vertical, axis, angle,dist'
!!    write(6,*) angle

  else if(axis .eq. 2.0) then
      angle=acos(abs(y-y0)/dist)

  else if(axis .eq. 3.0) then
      angle=acos(abs(x-x0)/dist)

  end if

     if((angle .le. 0.001) .and. (angle .ge. 0.0)) then
     bgl=1.0/(dist**2.0-L**2.0/4)
    agl=1.0

    else


!        find angle-1, angle-2

        if(axis .eq. 1.0) then
        dist1=sqrt((x-x0)**2.0+(y-y0)**2.0+(z-(z0-L/2))**2.0)
        angle1=acos(abs(z-(z0-L/2))/dist1)

        dist2=sqrt((x-x0)**2.0+(y-y0)**2.0+(z-(z0+L/2))**2.0)
        angle2=acos(abs(z-(z0+L/2))/dist2)

!!   write(6,*) 'seed is vertical'
!!    write(6,*) 'angle1, angle2'
!!     write(6,*) angle1,angle2


    else if(axis .eq. 2.0) then
        dist1=sqrt((x-x0)**2.0+(y-(y0-L/2))**2.0+(z-z0)**2.0)
        angle1=acos(abs(y-(y0-L/2))/dist1)
```

```
        dist2=sqrt((x-x0)**2.0+(y-(y0+L/2))**2.0+(z-z0)**2.0)
        angle2=acos(abs(y-(y0+L/2))/dist2)

!!    write(6,*) 'seed is horizontal, y parallel'
!!         write(6,*) 'angle1, angle2'
!!       write(6,*) angle1,angle2

     else if(axis .eq. 3.0) then
        dist1=sqrt((x-(x0-L/2))**2.0+(y-y0)**2.0+(z-z0)**2.0)
        angle1=acos(abs(x-(x0-L/2))/dist1)

        dist2=sqrt((x-(x0+L/2))**2.0+(y-y0)**2.0+(z-z0)**2.0)
        angle2=acos(abs(x-(x0+L/2))/dist2)

!!    write(6,*) 'seed is horizontal, x parallel'
!!         write(6,*) 'angle1, angle2'
!!       write(6,*) angle1,angle2

     end if


      bgl=abs(angle2-angle1)/(L*dist*sin(angle))
      agl=abs(angle2-angle1)/(L*dist*sin(pi/2))

    end if

!!       write(6,*) 'agl,bgl'
!!    write(6,*) agl,bgl

      dosert=doser0t0*bgl/agl*1106.6*exp(-26.119*dist)
      dose=dose+dosert

!!    write(6,*) 'dose, dosert'
!!    write(6,*) dose, dosert


    end if
      return
    end subroutine
```

VITA

The author, Jae Won Jung was born in Hadong, Korea. He earned his B.S. (1992) and M.S. (1994) degree in the Department of Nuclear Engineering at Hanyang University. He then worked as a researcher and senior researcher in the Korea Institute of Nuclear Safety for almost nine years. He entered Texas A&M University in 2003, to pursue a Ph.D. degree in the health physics program. He earned his Ph.D. degree in Nuclear Engineering in May 2007. He can be reached at the Department of Nuclear Engineering, Texas A&M University, College Station, Texas 77843-3133 through Dr. W. Daniel Reece.